STUDIES OF MUMPS VIRUS RNA SYNTHESIS AND IMMUNOGENICITY

by

KELSEY ROSE BRIGGS

(Under the Direction of Biao He)

ABSTRACT

Mumps virus (MuV) is a highly contagious human pathogen in the *Paramyxoviridae* family. The hallmark symptom of mumps is the swelling of the parotid glands. Though clinical symptoms of mumps are often mild, severe neurological complications, such as meningitis and encephalitis, can occur (1). After the introduction of the mumps vaccine, cases dramatically decreased to less than 500 per year in the United States. However, there has been a resurgence of mumps in the last two decades, warranting a better understanding of the disease and virus (2). There are no approved anti-viral drugs available for mumps. Viral replication and transcription have become targets for therapeutics in recent years (3). This work seeks to better understand virus-host interactions and the role phosphorylation plays in RNA synthesis. It is well established that the MuV nucleoprotein (NP) and phosphoprotein (P) are highly phosphorylated by host kinases and that their phosphorylation status regulates viral transcription and replication (4, 5). However, many host kinase regulators remain unknown. In this study, we identify a novel virus-host interaction. We show that host kinase, ribosomal protein S6 kinase beta-1 (RPS6KB1), negatively regulates MuV growth via phosphorylation of the MuV phosphoprotein. We then provide novel evidence

that the MuV large (L) protein is phosphorylated during *in vitro* infection and identify four putative phosphorylation sites within the polyribonucleotidyltransferase domain of L. Our work provides insight into phosphorylation as a regulator of MuV growth. MuV outbreaks are occurring in vaccinated populations, and clinical isolates sequenced from these outbreaks belong to a divergent genotype (genotype G) compared to the vaccine strain (genotype A), which questions the efficacy of the mumps component of the measles, mumps, and rubella (MMR) vaccine. (2). We examine the immunogenicity and longevity of recombinant genotype G-based vaccines and show that a third dose of a genotype G-based vaccine increases neutralizing titers toward the circulating outbreak strain of MuV. We identify a host kinase important for MuV replication, elucidate MuV polymerase phosphorylation, and seek to advance the development of a next generation MuV vaccine.

INDEX WORDS: paramyxovirus, mumps virus (MuV), P protein, L protein, phosphorylation, RPS6KB1, vaccine

# STUDIES OF MUMPS VIRUS RNA SYNTHESIS AND IMMUNOGENICITY

by

KELSEY ROSE BRIGGS

BS, University of California, Santa Barbara, 2014

A Dissertation Submitted to the Graduate Faculty of The University of Georgia in Partial Fulfillment of the Requirements for the Degree

DOCTOR OF PHILOSOPHY

ATHENS, GEORGIA

2021

STUDIES OF MUMPS VIRUS RNA SYNTHESIS AND IMMUNOGENICITY

by

KELSEY ROSE BRIGGS

| | |
|---|---|
| Major Professor: | Biao He |
| Committee: | Melinda Brindley |
| | Wendy Watford |
| | Balázs Rada |
| | Paul Rota |

Electronic Version Approved:

Ron Walcott
Vice Provost for Graduate Education and Dean of the Graduate School
The University of Georgia
December 2021

ACKNOWLEDGEMENTS

First, I must thank Dr. Biao He for taking me in all those years ago. You immediately assigned me multiple challenging projects and always pushed me to be a better scientist. Thank you for trusting me with all that you did. Thank you to all the members of the He lab past and present for helping me throughout my career. Several past members took the time to help and train me whenever I needed it. Current members, you guys are a riot. I am always laughing in lab. Preetish and Kaito, you guys were the best undergrads I could have ever asked for and you both are going to do great things. Thank you to the entire lab for keeping me sane, especially during this past year.

Ash, you have been my desk buddy, bench buddy, animal work buddy, and lunch buddy since day 1. I'm so happy we joined the same lab; it would not have been the same without you. I can't thank you enough for all you have done for me over the years. You were always there to help with experiments, brainstorm problems and edit ALL of my stuff (except this don't read to close, it'll be littered with mistakes). I hope 20 years from now, I still call you for science advice.

Thank you to all of my committee members and all the members of their labs. Dr. Brindley and Dr. Watford you guys helped me so much over the years, always taking the time to answer all my questions because I never had any idea what I was doing. Dr. Rada, thank you for helping for the human samples. Dr. Rota,

I met you very late in grad school, but you were so positive and helpful during our meetings. Thank you to everyone on my committee.

Jeremy, thank you for not dying. That would have been a bummer. You have always been so supportive of grad school and my career, and I can't thank you enough for that. I love our little family and the home we've created. Yogi, Yzma, Grant, and Mickey make it a nut house, but I love every second of it.

To all of my beyond amazing friends, thank you for everything. I have made so many long-lasting friendships throughout my life (Westlake, San Diego, Santa Barbara) and have too many to list here. You know who you are. Thank you for always making an effort to see me when I was in town. Thank you for coming to visit me down in Georgia. Thank you for always checking in on me and reaching out to talk because I am so bad at it. To the Clique, I have never had such a random group of friends before. We are also different, but somehow it works. You guys are a second family to me. We have been through so much in the last 5 years, good and bad, and I can't wait to see where we all end up. Y'all showed up to support me for the 3MT, defense, and any other time I've ever asked. They said we would never last, that 'groups' always dissolve, but not us. We showed them.

Lastly, to my incredible family. I could not have done any of this without your unwavering support. You guys looked at me like I was crazy when I said I was going to go to grad school in Georgia, but none the less helped me move and made sure I could always come home when I wanted/needed to. You have always supported all of my hopes and dreams and I hope I made you proud.

TABLE OF CONTENTS

Page

LIST OF TABLES

Page

LIST OF FIGURES

Page

# CHAPTER 1

## INTRODUCTION

Mumps virus is a highly contagious human pathogen that causes inflammation of the parotid glands, fever, and headache. While many cases are asymptomatic or mild, severe complications can occur, which include meningitis, encephalitis, and deafness. Prior to mass vaccination in the 1960's, mumps was considered a common childhood disease, resulting in seroconversion of >90% of the population before age 15 (6). In the post-vaccine era, cases in the United States (U.S.) were reduced by 99% with two doses of the Measles, Mumps, and Rubella vaccine (MMR). However, in the past two decades, there has been a resurgence of MuV infections. These infections have occurred primarily in vaccinated populations, often on college campuses. The largest U.S. outbreak originated in Iowa in 2006 (IA, 06), which resulted in over 6500 diagnosed cases of MuV. Since 2006, there has been a resurgence of mumps , causing the number of cases in the U.S. to remain higher than in previous decades (2, 7).

Previously, we created a reverse genetics system based on a MuV virus from the IA, 06 outbreak to study it *in vitro* and *in vivo* (8). MuV is a member of the family *Paramyxoviridae*, in the genus *Rubulavirus*, and has a non-segmented, negative-stranded RNA genome of 15,384 nucleotides. The genome contains

seven genes that are transcribed into nine viral proteins (9, 10). The RNA genome serves as a template for replication of the viral RNA (vRNA) genome and mRNA synthesis, and it associates with nucleoproteins (NP) to form the helical ribonucleoprotein (RNP), which protects the genome from degradation. The RNP associates with the viral RNA-dependent RNA polymerase (vRdRp) complex to perform viral RNA synthesis. The replication machinery is essential for viral growth and RNA synthesis (9, 11).

The phosphoproteins (P) of paramyxoviruses are highly phosphorylated, and their phosphorylation status impacts vRNA and viral mRNA synthesis. Previous studies, with Parainfluenza Virus 5 (PIV5), Respiratory Syncytial Virus (RSV), and MuV have shown that mutating phosphorylation residues within P affects RNA synthesis (4, 12-14). It is thought that phosphorylation of the P protein is facilitated by host kinases, because paramyxovirus viral proteins lack inherent kinase enzymatic activity (9, 14). Furthermore, several paramyxovirus P proteins have been shown to interact with host kinases, including MuV P, which was shown to interact with human kinase Polo-like kinase 1 (PLK1) (15-18). Additional host kinases that are important for MuV P phosphorylation and RNA synthesis have yet to be discovered.

The L protein, or polymerase, is highly conserved amongst negative-sense RNA viruses (19). The structure of L contains five major conserved domains: RNA-dependent RNA polymerase (RdRp), polyribonucleotidyltransferase (PRNTase), connecting domain (CD), methyltransferase (MTase), and the C-terminal domain (CTD), each of which perform a specific role in RNA synthesis. These regions are

separated by two highly flexible and non-conserved hinge regions (H1 and H2) (20). L is responsible for initiation, elongation, and termination of RNA synthesis, in addition to adding the 5’ cap and 3’ poly(A) tail to transcribed viral mRNA (9, 10, 21). Much of the work on L has been with PIV5 or VSV, while identifying residues/regions in L that affect the growth of MuV has been understudied.

The most widely used MuV vaccine is based on the Jeryl Lynn (JL) strain, a genotype A virus. Over fifty years ago, the virus was isolated from a patient and serial passaged in embryonated hen’s eggs and chicken embryo cell culture to achieve attenuation (22, 23). While genotype A viruses have circulated in the past, currently, the most common strains in North America and many European countries are from genotype G (24). The drift away from genotype A MuV strains has brought into question the efficacy of the MuV vaccine and requires a better understanding of genotype G viruses. Previously, we generated a vaccine candidate based on the genotype G MuV IA, 06 virus, which was genetically modified to delete the SH gene and prevent transcription of the V protein (rMuV-ΔVΔSH). It was shown to be immunogenic in mice and have low neurovirulence (8, 25). This knowledge can be applied to next generation vaccines that can better protect against the circulating strains of MuV.

Understanding MuV viral replication and virus-host interactions can lead to the generation of antiviral treatments, while improving the current MuV vaccine strategy can lead to a decrease in world-wide cases. Together, this work will provide insight into MuV growth that will aid in the development of countermeasures to MuV infection.

## SPECIFIC AIMS

**Aim 1**. Identify and characterize host kinases that affect MuV replication and growth. A large-scale siRNA screen was used to identify potential kinases that affect MuV growth. RPS6KB1 was identified to have an effect on MuV growth. Using siRNA knockdown, inhibitors, and cells lacking RPS6KB1 the kinase's role during MuV infection was determined. The hypothesis for this aim is that RPS6KB1 negatively regulates MuV growth through phosphorylation of MuV P.

**Aim 1a.** Identification of host kinases that affect MuV growth using a large-scale siRNA screen

**Aim 1b.** Characterization of the role RPS6KB1 has on MuV replication and transcription

**Aim 1c.** Determine the mechanism of regulation on MuV RNA synthesis by RPS6KB1.

**Aim 2**. Examine MuV large protein function. To examine MuV L, a functional flag-tagged recombinant virus was generated. The tagged L was used to identify phosphorylation sites within MuV L. The working hypothesis for this aim that L is phosphorylated, and its phosphorylation status plays a role in RNA synthesis.

**Aim 2a.** Development and characterization of a tagged L protein

**Aim 2b.** Identification of phosphorylation sites within MuV L

**Aim 3**. Evaluate MuV genotype G-based vaccine candidates. The vaccine candidates were assessed for immunogenicity and longevity in a mouse model. The hypothesis is that a genotype G-based vaccine may protect against the circulating strain better than the current vaccine.

**Aim 3a**. Development and *in vitro* characterization of recombinant Jeryl-Lynn (rJL) vaccine candidates

**Aim 3b**. Immunogenicity and longevity of MuV vaccine candidates in mice

**Aim 3c**. Immunogenicity of a heterologous prime/boost strategy in mice

# CHAPTER 2

# LITERATURE REVIEW

## History and classification

The first description of an illness consistent with MuV symptoms dates to 5th century BCE Greco-Roman times. Hippocrates described it in his first book of *Epidemics* as an acute illness that caused parotitis and orchitis in both children and adults (26). In the late 18th century, a physician outlined the entire disease progression and first associated MuV with central nervous system (CNS) complications (27). During this time, the name “mumps” had been given to the disease, which is thought to mean “to sulk” or “to talk indistinctively” in old English or Scottish (27, 28). However, it would be another 150 years before the etiological agent causing mumps was discovered.

In 1934, Johnson and Goodpasture successfully proved that a virus was responsible for mumps. They first demonstrated that rhesus macaques developed similar mumps-like symptoms after being injected with filtered saliva from patients with mumps symptoms. Then they were able to fulfill Koch’s postulates by transferring infected saliva from rhesus macaques to children back to naïve rhesus macaques who then developed the disease, using bacteria-free conditions. In doing so, they conclusively showed that the disease agent was a virus, not

bacteria, and the causative agent of mumps (29). These studies, although unethical today, were critical for our understanding of MuV infection and pathogenesis and pioneered rhesus macaques as an animal model for mumps.

In 1945, MuV was successfully isolated and propagated in embryonated chicken eggs allowing researchers to characterize the virus (30, 31). This study also inadvertently showed that serial passaging MuV in eggs attenuated the virus, which would ultimately lead to a MuV vaccine, first licensed in 1967 (30-32). Finally, with the advancement of molecular cloning and sequencing, the MuV genome including the intergenic, leader, and trailer sequences were determined using mRNA isolated from MuV infected Vero cells, which allowed for the reverse genetics system to be developed (8, 33).

MuV has a nonsegmented, negative-stranded RNA genome of 15,384 nucleotides and is a member of the order *Mononegavirales* in the family *Paramyxoviridae* (9). The virus family includes several important human and animal pathogens such as measles, rinderpest virus, and canine distemper virus. As of 2021, MuV belongs to the genus *Orthorubulavirus* in the subfamily *Rubulavirinae*, along with Parainfluenza virus 5 (PIV5), its most closely related virus and the prototypic virus for the subfamily (9, 34). There are currently 12 different genotypes of MuV, which are assigned letters from A to N (excluding E and M), but there is only 1 recognized serotype (28). The genotypes are based on the sequences of the small hydrophobic (SH) gene, the most variable gene, and the haemagglutinin-neuraminidase (HN) gene (28, 35). As of 2014, 6 of the 12

genotypes (G, H, C, F, K, and D) were actively circulating in the human population (28).

**Mumps virus genome**

The MuV viral genome starts at the 3’ end with a 55-nucleotide long leader sequence and terminates at the 5’ end with a 24-nucleotide trailer region. The leader and trailer contain initiation and termination signals for the vRdRp. The genome encodes for all the MuV genes (3’-NP-V/P/I-M-F-SH-HN-L-5’) in succession using start/stop signals on either side of each gene. Each gene has an upstream gene start (GS) signal (3’) and a downstream gene end (GE) signal (5’), which are located in the short untranslated regions (UTRs) of the genome (33). Additionally, the UTRs contain a *cis*-acting intergenic (IG) region that is variable in length. Rubulaviruses typically vary in length and sequence while respiroviruses and morbilliviruses have more conserved IG sequences (9). Immediately downstream of the gene end is a poly(U) tract of variable length, which is responsible for the polyadenylation that occurs in mRNA synthesis. These regions are responsible for mRNA synthesis and polyadenylation signaling but are not transcribed or translated (9, 36).

The MuV genome consists of seven genes that encode for 9 viral proteins with RNA synthesis beginning at the 3’ end (10). The V/P/I gene encodes for 3 proteins that are produced via RNA editing. V, P, and I share the same N-terminal sequence, but have different C-terminal ends due to the frame shift. The V mRNA is the faithful transcript, while the insertion of 2 non-template guanine (G) residues at site 155 results in the P mRNA. I mRNA is made via insertion of 1 or 4 G residues

(37, 38). RNA editing occurs by slippage of the viral RNA dependent RNA polymerase (vRdRp) in a short G-rich coding region within the V open reading frame (38). Although the most common insertion is +1 G or +2 G for MuV, up to 6 Gs have been observed and do not appear to affect protein function (38, 39). Paramyxoviruses share RNA editing as a common feature but some viruses within the family have P as the faithful copy, rather than V (9). It is thought that the common ancestor to the *Paramyxoviridae* family had P as the faithful transcript, and the editing system switched to V at least four times in history to give rise to the genuses *Metaavulavirus, Orthorubulavirus, Salemvirus*, and *Ferlavirus* (40).

**Mumps viral proteins**

*Nucleocapsid protein (NP)*

The nucleocapsid protein or nucleoprotein (NP) is the most abundant protein produced in a MuV infection, it is 549 amino acids in length and roughly 61 kDa in size (41, 42). Initially, NP is found as a soluble monomer within the cell and P acts as a chaperone by binding to NP to prevent it from encapsidating cellular RNA in the cytosol (43). In the case of Orthorubulaviruses, it is thought that the amount of soluble NP bound to P triggers the switch from viral transcription to replication (38, 44, 45). The main function of NP is to encapsidate the viral RNA (vRNA), which forms the ribonucleoprotein (RNP). Each NP protein binds six nucleotides of RNA in a helical fashion for efficient RNA synthesis (46). The confirmation is effectively known as the “rule of 6” and dictates that all paramyxovirus genomes must be divisible by six (37, 46, 47). NP binds to both the viral genome and antigenome RNA during transcription and replication (9, 48, 49).

The RNP structure is nuclease resistant and protects the genome from degradation and from activation of host cell immune responses (50). NP has an N-terminal domain and a C-terminal tail. The N-terminal domain of MuV NP is responsible for RNA encapsidation and P binding, which differs from some other Paramyxoviruses that have their P binding site in the C-terminal region (41, 42, 51). The viral polymerase associates with NP and in turn the RNA template, through NP's interaction with P. The N-terminus of P uncoils the helical RNP that gives vRdRp access to the vRNA temple (50). Phosphorylation of NP has been shown to play a role in RNA synthesis and genome stability (5, 52).

*Phosphoprotein (P)*

The phosphoprotein (P) is produced by the insertion of two non-template guanine residues in the V/P/I ORF. The resulting protein is 391 amino acids long and 47 kDa in size (10). P is a cofactor in the vRdRp complex, making it essential for replication and transcription of the viral genome (9, 10). P interacts with L to help chaperone the polymerase to the RNP (21). P also interacts with nascent NP to keep it from encapsidating host RNA rather than viral RNA. Additionally, P acts as an anchor for NP and L in the vRdRp so that replication and transcription can occur (21, 50, 53). Although P has no intrinsic enzymatic activity, it is highly phosphorylated, and its phosphorylation status has been shown to regulate viral RNA synthesis (4, 16, 54).

The phosphoproteins of paramyxoviruses contain three domains, the N-terminal, oligomerization, and C-terminal domains. P self-associates via

oligomerization, which occurs through a centralized coiled-coil domain (55). MuV P has a unique structure differing from PIV5, the prototypic virus in the subfamily. The recent partial crystal structure of MuV P revealed that P is a tetramer with two pairs of dimers in antiparallel orientation. This unique structure positions two N-terminal and two C-terminal domains on each end the of oligomerization domain, instead of all 4 N-terminal or C-terminal ends on each side (21). This unique confirmation allows NP binding at both the N-terminal and C-terminal domain of the protein, which differs from other paramyxoviruses (50).

*V protein (V)*

The V protein is translated from the faithful transcript of the V/P/I gene. It has 224 amino acid residues and roughly 25 kDa in size (10). V shares the N-terminal sequence with P and I but has a unique C-term sequence that contains seven cysteine residues. The C-term domain of V is conserved among paramyxoviruses and plays a major role in viral pathogenesis and host evasion (9, 56). V is involved in virus and host modulation. The unique C-term of V can bind to the L protein to inhibit genome replication and transcription. It is thought that this prevents the virus from over replicating and alerting the immune system of its presence before it can establish a robust infection (57, 58). The mRNA of L has been shown to activate MDA5 (melano- differentiation-associated protein 5) and RNAse L, both of which activate the innate immune response, so V helps reduce the amount of viral RNA to prevent this detection (57-59). In addition, V binds to MDA5, which disrupts its folding and blocks its activation (60). V ubiquitinates the

transcription factors STAT1 and STAT3 causing them to be degraded, thereby reducing IFN and IL-6 gene expression (61-64). V also interacts with RACK1, a kinase that mediates the interaction between STAT1 and the IFN reception, to reduce IFN expression early in infection before it can degrade STAT1 completely (63).

The PIV5 and MuV V proteins have both been detected in the virion allowing for an immediate modulation of host proteins upon entering a cell (58, 61, 65). A full-length MuV virus lacking the V protein was rescued demonstrating that V is a non-essential protein for MuV growth (61). However, the rMuVΔV virus was shown to be highly attenuated in the neonate neurotoxicity rat model that evaluates the level of hydrocephalus in infant rats, demonstrating it plays a major role in viral pathogenesis (25, 61, 66, 67).

*I protein (I)*

The MuV I protein is translated from a frame shift in the V/P/I gene ORF. It is 171 amino acid residues and 19 kDa in size. It shares the same N-terminal sequence as V and P but has a different C-terminus that is much smaller. Although, it has been detected in virus infected cells, it has not been detected in the virion, nor has the function been determined (37, 40).

*Matrix protein (M)*

The matrix protein (M) is 375 amino acids long, 40 kDa in size, and essential for viral assembly and budding (68, 69). The M protein assembles as a layer

beneath the membrane to provide structural support to the new virus particles by creating a surface of positively charged domains that interact with the negatively charged cell membrane (68, 70). M has been shown to interact with the cytoplasmic tail of paramyxovirus glycoproteins and the viral RNP to gather the viral proteins near the surface for assembly and budding (71-73). In addition, MuV virus-like particles (VLPs) required M, NP, and F for efficient production. F's interaction with M, over HN, was determined to be the major contributor to particle formation (69, 74). M also interacts with some host proteins, which assists in viral assembly and budding. The FPVI and FPIV motifs in M are essential for binding host proteins at the cell surface to assist in budding (69, 71, 74, 75).

*Fusion protein (F)*

The fusion protein (F) is a type I transmembrane glycoprotein that consists of 538 amino acids (76). The F protein facilitates virus-to-cell and cell-to-cell membrane fusion. F is synthesized as an inactive precursor ($F_0$) which is 74 kDa. A signal peptide directs the $F_0$ to the rough ER where it undergoes glycosylation (77). It then travels though the Golgi where the cellular endoprotease furin cleaves the $F_0$ at amino acid residues 98-102 into the F1 and F2 subunits (76, 78). The resulting subunits are linked by a disulfide bond forming a heterodimer, which is the active conformation of the protein. The cleavage of $F_0$ exposes a hydrophobic domain in the N-terminus of the F1 subunit that comprises the fusion peptide (79). Hydrophobic residues in the form of heptad repeats are conserved among fusion proteins of paramyxoviruses. Heptad repeats 1 and 2 (HR1 and HR2) have been

found in the MuV F protein and are known to be involved in joining viral and cellular membranes because of their high affinity for cellular membranes (80-82).

*Small hydrophobic protein (SH)*

The small hydrophobic protein (SH) is the smallest protein in MuV. It's 57 amino acids long and 6 kDa in size (83). While all the paramyxovirus SH proteins are a type 1 membrane protein and have several hydrophobic residues, the sequences and orientations are not conversed within the family *Paramyxoviridae*. For example, MuV SH has its C-terminal domain in the cell cytoplasm, while PIV5 SH has its N-terminal domain in the cytoplasm (84). MuV phylogenetics use the SH protein to distinguish between strains and genotypes because of this heterogeneity (28, 35, 85). Serendipitously, we know that SH is a non-essential protein for MuV growth because a point mutation in the IG region before SH in the classical Enders and Rubini MuV strains prevented expression of the SH protein (86). Other studies showed that inserting the PIV5 SH into MuV yielded a viable virus and suggested they share a similar role (87).

Although variable in sequence, the SH protein has a similar role of host-cell immune modulation and is a non-essential protein for paramyxoviruses (87, 88). SH blocks TNF-α (tumor necrosis factor alpha) signaling in infected cells, which would induce apoptosis, increase TNF-α levels, and activate NFκB (a transcription factor for pro-inflammatory genes). In doing so, it prevents cell death and dampens immune responses that would control the spread of the virus (8). The RdRp domain of L has been shown to activate NFκB, but SH is able to down regulate its

expression and reduce expression of pro-inflammatory genes (89). A MuV virus lacking SH, rMuVΔSH, was shown to be partially attenuated using the neonate rate neurotoxicity model, demonstrating its role in viral pathogenesis (8).

*Haemagglutinin-neuraminidase protein (HN)*

The hemagglutinin-neuraminidase (HN) protein is 582 amino acids in length and 80 kDa in size. It is a type II transmembrane glycoprotein with the N-terminal containing a 30 amino acid cytoplasmic tail. HN has a hydrophobic transmembrane domain and a large globular head that makes up the C-terminal domain (84, 90, 91). Once in the membrane of cells, the HN protein first dimerizes by disulfide bonds and then is thought to form a tetramer by non-covalent interactions (92-94). Viral attachment is facilitated by the HN protein. HN recognizes sialylated glycoconjugates allowing it to bind the sialic acid receptor on the cell surface (90, 91). HN also is essential for the activation of F so that fusion of the membranes can occur (95). HN has neuraminidase activity to neutralize sialic acid receptors on the progeny virions to minimize viral aggregations during egress that would limit viral spread (90, 95).

*Large protein (L)*

The large (L) protein is the largest of the MuV proteins at 2,261 amino acids in length. It is the last protein to be transcribed and translated, making it the lowest in abundance (38). L is a multi-functional enzyme that contains the catalytic centers required to perform both replication and transcription of the genome (Fig

2.3). L is essential for viral replication and mutations within L can be catastrophic to its function. P and L minimally make up the vRdRp complex, in which L transcribes and replicates the viral genome. Without P, L is unable to secure attachment to the RNP (96-99). L must be packaged into the virion to transcribe and replicate the negative sense genome (11). L has also been implicated in host pathogenesis. L mRNA of PIV5 was found to activate IFN-β through MDA5, a viral sensor (59). Additionally, in another paramyxovirus, J Paramyxovirus (JPV), three nucleotide differences in L resulted in attenuation in mice (100).

The L protein was traditionally broken into three large functional domains, denoted domains I-III, that were flanked by two flexible hinge regions. The large domains were conserved between non-segmented negative sense viruses (NNSVs), but the hinge regions were notably variable (20, 101). Sequence alignments identified six conserved regions (CRI-CRVI) within these domains, which were used to assign L's function in RNA synthesis (102, 103). Technological advancements allowed the structures of the L protein for parainfluenza virus 5 (PIV5), respiratory syncytial virus (RSV), and vesicular stomatitis virus (VSV) (101, 104, 105) to be solved, however the structure of MuV L remains elusive. With the structures, five smaller conserved domains were identified across NNSV L proteins consisting of the RNA-dependent RNA polymerase (RdRp), polyribonucleotidyltransferase (PRNTase), connecting domain (CD), methyltransferase (MTase), and the C-terminal domain (CTD) (9, 101, 102, 106).

The N-terminal portion of L forms the RdRp domain, which responsible for oligomerization with P, RNA binding, and phosphodiester bond formation, although

its entire role is unclear (101-103, 107). The C-terminal portion of the protein contains the rest of the domains. The PRNTase is responsible for adding the 5' cap to nascent mRNAs and contains a conversed priming loop that is thought to facilitate initiation of transcription (101, 108). The PRNTase domain can be split further into critical regions IV and V. mRNA capping has been associated with CRV, while CRIV's precise role is unknown. A study showed that several mutations in CRIV resulted defective RNA synthesis, but did not appear to affect vRdRp complex formation (109). The CD does not contain enzymatic activity but is required for proper function, it contains flexible regions that are thought to help in domain rearrangements (101). A study showed that VSV L could not tolerate any insertions in this region (106). The MTase domain performs a critical catalytic reaction by methylating the first nucleotide in the sequence and then methylating the cap. Its enzymatic activities are essential for efficient viral RNA translation into proteins (101, 110, 111). The CTD is structurally divergent among NNSVs, but they all contain a conserved guanylyl transferase (GTase) motif that is unique to viruses (101). L is a complex protein made up of several domains and its functions have not been entirely elucidated.

**Virus entry**

MuV enters the target cell through the interaction between HN and sialic acid, a receptor found on most host cells. It preferentially binds to α2,3-linked sialic acid, but can bind the α2,6 formation (112). A mutation in the Urabe AM9 vaccine in HN(E335K) was found to bind the α2,6-linked sialic acid over the α2,3. This mutation was originally thought to be involved in neurotoxicity, but it was later

disproven (113, 114). Binding of HN to sialic acid induces a conformational change in the F protein, which leads to fusion activity (95, 115). The exact mechanism and sites of interaction between F and HN are unknown, but fusion occurs in a pH-independent manor (116). Once fusion with the membrane occurs the MuV viral proteins, including the helical nucleocapsid containing the genome, is released into the cytosol (Fig 1) (11). Syncytia can be observed in a variety of cell lines upon MuV infection due to the F protein causing cell-to-cell fusion (117-119).

**Viral transcription and replication**

The MuV replication machinery, NP, P, and L, must be packaged into the virion so that they can initiate primary transcription of the genome. Upon entry into the host cell, they are delivered to the cytoplasm and start viral RNA synthesis (Fig 2.1). The RNA genome associates with NP to form the RNP. P interacts with the RNP and shuttles it to L to form the active vRdRp. The vRdRp uses the RNP as a template for both replication and transcription (9, 11). Initially, transcription occurs to produce more viral proteins. The vRdRp attaches to the leader (Le) sequence and scans the genome until it reaches the first GS site upstream of the NP protein. It is thought that the GS site contains the signals for capping and methylation, which is carried out by the auxiliary domains of the L protein (120-122). After transcription of NP, polyadenylation occurs by stuttering over the poly(U) tract in the GE site (33, 38). The final mRNA product has a methylated and capped 5’ end, a transcribed NP gene, and a polyadenylated 3’ tail. The transcripts are then translated by host ribosomes into proteins.

It this thought that paramyxoviruses use a mechanism called start-stop transcription, which creates a transcriptional gradient. This model suggests that after transcribing NP, the vRdRp can either continue scanning the genome for another GS site or disengage from the genome. If the vRdRp disengages, it must restart at the Le sequence, which causes the genes at the 3' end to be more abundant the genes at the 5' end (123-125). A recent study, using high-throughput sequencing, was able to experimentally show the transcriptional gradient of MuV (Enders strain). There was a noticeable difference in the number of V/P/I mRNAs found in MuV compared to PIV2, PIV5, and PIV3. Unlike the other viruses, the MuV V/P/I mRNAs did not follow the predicted reduction based on the theoretical transcriptional gradient, there was substantially more mRNA than expected. Interestingly, after V/P/I the gradient decreased as expected due to a larger drop between V/P/I and M mRNAs (38).

The switch from transcription to replication is poorly understood. Additionally, it is unclear whether a single polymerase complex transitions between replication and transcription or if different complexes perform each role independently (126, 127). Although the structure of MuV L is unknown, the structure of the PIV5 P+L complex was recently solved using cryo-electron microscopy. In this study, they propose a model for transcription and replication and show the potential conformational changes that occur to accommodate each. The major difference between the complexes is the position of the MTase and CTD domain (Fig 2.3). In transcription, the MTase and CTD domain are positioned directly above the PRNTase domain so methylation of the cap can occur, while in

replication it positioned further away (101). While their model is supported by several earlier hypotheses, more experiments are required to prove the mechanism. Moreover, although PIV5 and MuV are closely related, their P structures are different, therefore the polymerase structure may also have key differences.

For rubulaviruses, it is generally accepted that replication occurs after sufficient amounts of soluble NP is produced since it is required to encapsidate the newly formed genomes and anti-genomes (44, 45, 128, 129). During replication, the vRdRp attaches to the Le and replicates the entire genome, ignoring all UTR regions. This creates a positive sense antigenome, which then acts as a template for more viral genome. The vRdRp attaches to the complement of the trailer region (TrC), which contains an antigenome promoter to initiate synthesis of new negative-sense viral genomes (33, 126). The newly synthesized genomes are encapsidated by NP to avoid degradation in the cell.

**Virion assembly, budding, and egress**

Viral glycoproteins are translated and modified by the cell and then transported to the plasma membrane, while the newly synthesized genome is encapsidated by the nucleoprotein. These processes occur simultaneously within the cell and the M protein functions to gather them together (9). M interacts with the RNP, which is also associated with P and L, and the cytoplasmic tails of F and HN to assemble them at the plasma membrane. F has been shown to be the key contributor to virion egress, while HN is primarily for entry (Fig 2.1) (69, 115, 130).

However, HN's neuraminidase activity does prevent self-aggregation of progeny virions, which is important for efficient spread of the virus (76, 77, 90).

## Phosphorylation in transcription and replication

### *Nucleoprotein phosphorylation*

The importance of NP phosphorylation has been shown in several negative sense non-segmented RNA viruses including measles virus (MeV), rabies virus (RABV), Marburg virus (MBGV), and MuV. In MeV, NP phosphorylation was important for genome stability and activation of transcription and replication. It was also preferentially bound to RNA to form the RNP, rather than the unphosphorylated form (52, 131, 132). In RABV, phosphorylated NP was found to increase transcription and replication over unphosphorylated NP in a minigenome system, suggesting phosphorylation of NP plays a regulatory role (Fig 2.2) (133). MBGV virions were found to only incorporate phosphorylated NP suggesting that only the phosphorylated NP can bind RNA to form the RNP (134).

MuV NP phosphorylation was detected in chick embryo cells in 1989, however its full role was not understood until several years later (135). A comprehensive study of MuV NP was performed using liquid chromatography-mass spectrometry (LC-MS) and mutational analysis. Nine putative phosphorylation sites in MuV NP were identified by LC-MS or *in silico* prediction software. The serine or threonine residues were mutated to alanine and their minigenome activity was determined. Four of the mutations resulted in lower minigenome activity, another four had WT-like activity and one mutation (S439A) had increased activity. A single mutation in MuV NP, S439A, resulted in a 90%

reduction of phosphorylated NP suggesting it is a major phosphorylation site during an infection. Since mutating the serine to an alanine resulted in increased minigenome activity, protein expression, and growth, it was hypothesized that the site is important for downregulated RNA synthesis. Although residue 439 was found to be the major phosphorylation site for MuV NP, other residues (25, 298, 520, etc.) were found to play a role in replication and transcription suggesting phosphorylation of NP can up- or downregulate MuV growth (5). Phosphorylation of MuV NP by a specific host kinase has yet to be identified.

*Phosphoprotein phosphorylation*

As the name suggests, the phosphoprotein is highly phosphorylated. In addition to being an essential cofactor of the vRdRp complex, P regulates RNA synthesis through its phosphorylation status. Phosphorylation of the P protein of many paramyxoviruses has been shown to play a role in regulating mRNA synthesis including, MeV, RSV, PIV5, and MuV. In addition, several host kinases have been shown to phosphorylate paramyxovirus P proteins such as, cellular casein kinase II (CKII), protein kinase c isoform zeta (PKC-ζ), protein kinase B (AKT), and polo-like kinase 1 (PLK1).

A study found that there was an inverse correlation between MeV P phosphorylation level and virus transcription levels. Increased phosphorylation of MeV P decreased transcriptional activity in a minigenome system. Specific sites were identified (S86 and S151) which had strong phosphorylation, but the phosphorylation could be blocked by RNP binding. MeV P was found to be

involved in viral RNA synthesis through P's phosphorylation status (132). CKII was later found to phosphorylate residues S86, S151, and S180 in MeV P using $P^{32}$-labeling (136). Canine distemper virus, a closely related virus to MeV, was also found to have its P protein phosphorylated by CKII and PKC-ζ (137).

RSV P is heavily phosphorylated, and two main clusters (S-116/117/119 and S-232/237) were identified to contain phosphorylated residues, but all were found to be dispensable for viral replication (18, 138-140). One study observed a decrease in phosphorylated P and NP-P interactions when the residues were mutated to an alanine, but it did not ablate virus replication. This supports the notion that P phosphorylation plays a regulatory role (141). RSV contains an additional RdRp cofactor, M2-1, and a study found that phosphorylation at T108 in RSV P mediated the interaction between P and M2-1 in the RdRp in a minigenome system (12). A recent report mutated all 41 possible serine and threonine residues in RSV P and observed their outcome in a minigenome assay. Eight mutations significantly reduced minigenome activity compared to wildtype RSV P, only four of the mutations (T151A, S156A, T160A, and S23A) were rescuable, suggesting the other four residues (T210, S203, T188, and T105) are essential for RSV replication and transcription (142). RSV P residue S237 was found to be phosphorylated by CKII (18, 143, 144).

PIV5 P phosphorylation has been found to both upregulate and downregulate PIV5 gene expression (13, 17, 145). A report that used mass spectrometry analysis identified residue T286 in PIV5 P as a phosphorylation site. The mutational analysis found that T286 plays a positive role in PIV5 replication

and transcription (145). Another study identified PIV5 P residue S157 is an important phosphorylation site for regulating RNA synthesis. The mutation S157F elevated viral gene expression suggesting it negatively affects PIV5 growth (13). A later study identified that PLK1 was responsible for phosphorylating PIV5 P residue S308 after associating with S157. They found that inhibiting PLK1 increased PIV5 gene expression, while PLK1 overexpression decreased PIV5 gene expression. They observed increased gene expression, induction of cell death, and cytokine expression in a recombinant PIV5 virus lacking the PLK1 binding site, which suggests PIV5 limits viral RNA synthesis to avoid triggering host innate responses (17). AKT, another serine/threonine kinase was found to have the opposite effect on PIV5, it was shown to up-regulate gene expression via phosphorylation of PIV5 P (15).

A comprehensive analysis of MuV P phosphorylation was performed to identify potential phosphorylation sites using mass spectrometry and a minigenome system. All 64 serine and threonine residues within MuV P were mutated to alanine and examined. A cluster of residues (T145/S146/T147/T150) was found to reduce minigenome activity compared to the WT control. Another residue T101 when mutated to alanine significantly enhanced minigenome activity. A recombinant MuV virus containing T101A was found to have increased growth, protein expression, and decreased phosphorylation. These results suggest T101 negatively regulates MuV virus RNA synthesis through phosphorylation at this site (4). MuV P was found to bind to PLK1 at sites 146-148 and phosphorylate P residues S292 and S294. The presence of NP induced a band shift of

phosphorylated P, which indicates it enhances P phosphorylation via PLK1. This suggests that NP can regulate RNA synthesis through phosphorylation of P (16).

*Large protein phosphorylation*

The phosphorylation status of L is unknown and highly debated. It remains possible that no L phosphorylation occurs during RNA synthesis, however there is a body of evidence indicating otherwise. There are two main hypotheses concerning the phosphorylation status of NNS L proteins. The first suggests that L has its own kinase activity, while the second hypothesis suggests that all L-associated kinase activity comes from host kinases (89). A study using VSV determined that L contains a serine/threonine kinase domain using chemical studies involving ATP-binding (146). While another group using VSV, determined all kinase activity observed during an infection was cellular rather than viral using fast protein liquid chromatography (FPLC) (147). Sendai virus (SeV) L was found to phosphorylate both P and NP using chromatography and purified NP, P, and L proteins (148). But, another report with RSV L demonstrated L could not phosphorylate P in vitro (140). Several conflicting reports emerged in the 1990's, but since then there have been few studies examining the phosphorylation of or by a NNS L protein.

However, there has been some progress in other virus families. A recent study using influenza virus, a member of the *Orthomyxovirus* family, found that a subunit of its viral polymerase (PB1) contained several phosphorylation sites. Orthomyxoviruses lack polymerase co-factors, like Paramyxoviruses' P, which use

phosphorylation to regulate RNA synthesis. They found that PB1 contained several phosphosites capable of regulated RNA synthesis. Another study with norovirus (NoV), a single-stranded, positive-sense RNA virus, reported that its vRdRp (NS7 protein) was phosphorylated by host kinase AKT (149). AKT has been implicated in several viral infections (15, 89, 149-152) PIV5 L, specifically the RdRp domain, was shown to activate the phosphorylation of AKT through a direct interaction suggesting it contains intrinsic kinase activity (89).

Phosphorylation of MuV L has not been formally examined. The lack of immunological reagents for L and low abundance during an infection has made the detection of L phosphorylation an on-going challenge.

**Transmission, pathogenesis, and treatment**

MuV is transmitted though inhalation or oral contact of infected respiratory droplets (29, 153). It is assumed, but not formally confirmed, that MuV first infects the upper respiratory tract before disseminating to other tissues (1). MuV has an incubation period of 12 to 25 days with an average of 16-18 days, where upon the hallmark symptom of parotitis typically occurs and lasts for 2-5 days (2, 153). However, asymptomatic infections are thought to occur in one-third to one-half of infections, so many cases go undiagnosed. Humans have been shown to secrete virus in their saliva one week prior to symptoms and up to one week after. Virus has also been detected in saliva of asymptomatic carriers (1, 153-155). Parotitis (swelling of parotid gland), orchitis (swelling of male testis), and deafness were the primary symptoms for diagnosis before laboratory diagnostics became available (26, 27, 29). RT-PCR and IgM ELISA assays are now typically used to detect MuV

in samples, especially in atypical or mild manifestations of the disease (28, 156, 157). In humans with symptoms, virus can be isolated from saliva, cerebrospinal fluid, urine, and on rare occasions blood (154, 155).

Humans are thought to be the only natural host of MuV, however a recent study identified a “mumps-like” virus in bats (158). Original pathogenesis studies were performed in non-human primates using an unnatural route of infection, so the full scope of its pathogenesis is still unknown (29, 153). A study from 2013, was able to show a more relevant disease progression using Rhesus Macaques. The non-human primates were infected via intranasal or intratracheal route, rather than the original study in which injection to the Stetson’s duct was used. Swelling of the parotid glands occurred 2-3 weeks post infection simulated disease progression in humans, however no signs of fever or neurological symptoms were observed (159). MuV is thought to be a mild and self-limiting disease with the most common symptoms being headache, fever, malaise, and parotitis (153). However, more severe complications can occur as the virus spreads. Virus readily disseminates to the kidney, but rarely causes disease in the organ. Yet, there have been some reported cases of severe interstitial nephritis (160-162). MuV has also been reported to cause pancreatitis and carditis in some cases (163, 164). Mastitis and oophoritis has been reported in post-pubertal woman and can use premature menopause or infertility (165-167). Orchitis occurs in 10-20% of post-pubertal males and virus has been recovered from semen and testis suggesting it’s a direct site of replication. Orchitis can cause temporary sterility or a decrease in fertility, but it is rarely permanent (168-170). Transplacental transmission of MuV has been

shown in non-human primates and supported by the detection of virus from spontaneous abortions during maternal mumps (171-174). The full pathogenesis of MuV in the reproductive tract and in pregnancy is still being investigated.

The most severe symptoms can occur when MuV invades the central nervous system (CNS), which is thought to be in as many as half of cases based on cerebrospinal fluid samples. Symptomatic CNS infection occurs in 5-10% of cases that manifest with meningitis and <0.5% with encephalitis. Almost all MuV related deaths are due to encephalitis (175-178). Deafness is reported in 4% of MuV cases. Loss of hearing typically occurs in one ear, but it can occur in both. In the pre-vaccine era, MuV was the most frequent cause of acquired unilateral hearing loss in children (179-182). MuV can cause a wide variety of symptoms, both mild and severe, which ultimately leads to a case fatality ratio of 1.6-3.8/10,000 people (1, 2).

Currently there is no approved antiviral treatment for MuV. In some cases, treatment can be administered to help alleviate symptoms. MuV-specific immunoglobulins have been administered in the past, but had little to no success (183). There are several anti-paramyxovirus therapeutics in pre-clinical studies that may show to be effective in the future (3). Until then, the best preventative of mumps is through vaccination.

**Vaccination and epidemics**

Prior to mass vaccination in the 1960's, mumps was considered a common childhood disease, resulting in seroconversion of >90% of the population before age 15 (6). In the U.S., mumps is part of the childhood vaccination program as a

component of the measles, mumps, and rubella (MMR) or measles, mumps, rubella, and varicella (MMRV) vaccine (2). Children are initially immunized between 12-15 months of age and then boosted between ages 4-6 (178). This immunization schedule has reduced MuV cases in the U.S. by 99% (Fig 2.4) (2). Similarly, MuV immunization programs have been implanted in roughly 60% of countries belonging to the WHO (28).

All currently approved mumps vaccines are live attenuated vaccines from various origins. The most commonly used strain of mumps vaccines is Jeryl Lynn (JL) (or a JL- derived strain), which was isolated from a virologist's daughter (named Jeryl Lynn) and belongs to genotype A. The virus was attenuated through serial passage in embryonated hen's eggs and chick embryo cell culture. It was licensed for human use in 1967 and became part of the MMR vaccine in 1971 (Fig 2.4) (23). The JL component of the MMR vaccine is comprised of at least two closely related viruses, the major component ($JL^5$) and the minor component ($JL^2$) at a 5:1 ratio (184, 185). Other vaccines, outside of the U.S., have been attenuated in the same fashion with limited success. The Leningrad-3 and L-Zagreb were created by the former Soviet Union and belong to genotype N (28, 186). Urabe AM9 was developed into a vaccine in Japan in 1967 and belongs to genotype B (28, 187). These vaccines had a high incidence of aseptic meningitis of 20-100 cases per 100,000 people, while JL has a rate of <1 per 100,000 people (188-191). Today, the Leningrad-3 and L-Zagreb strains have limited or no use and the Urabe AM9 vaccine was pulled from the market in the early 1990's (28). Other vaccines,

such as the Rubini strain from genotype A, were removed from market for having low vaccine efficacy (192).

After the introduction of the vaccine there was a dramatic decrease in the number of MuV cases, but in the last 15 years the number of mumps cases have significantly increased. In 2006, many large outbreaks occurred, the first of which was on a college campus in Iowa, resulting in the resurgence of mumps in the U.S. This resurgence has lead to several years of numerous mumps cases including: 2010, 2016, 2017, and 2019 (2). These outbreaks typically occur in young adults living in confined quarters (college campuses, detention centers, sports teams), rather than children. Additionally, they often occur in areas of high vaccine coverage. The outbreak-associated strain isolated in 2006 was found to be from genotype G, while the vaccine strain is from genotype A (Table 2.1). Genotype G viruses primarily circulate in North America and much of Europe, and they have been the cause of several outbreaks since the early 2000s (24, 28). Outbreaks have been observed in several other countries where the circulating strain does not match the vaccine strain. For example, Argentina, who uses JL (A) has outbreaks from genotype K and D viruses (24, 193). South Korea used Urabe AM9 (B) until 1997, then switched to JL (A), but the current outbreak strain(s) are from genotype H and I (24, 194). China did not introduce a vaccine program for MuV until 2008 and continues to have endemic mumps. There vaccine strategy administers 1 dose at 18-24 months, rather than the typical 2 dose regiment. They currently use S79 (A) but have primarily genotype F outbreaks (24, 195, 196).

These worldwide outbreaks have raised concerns about the efficacy of the available mumps vaccines.

Measuring the MuV vaccine efficacy is challenge because of the lack of correlates between immune response and level of protection (1, 24). The Centers for Disease and Prevention (CDC) estimates the mumps component of the MMR reduces risk of mumps by 78% with one dose and 88% after 2 doses. A measure of IgG antibodies post vaccination is the typical serological measure used to determine efficacy, a >2-fold increase in IgG titers is considered a positive seroconversion (2, 197). However, there is a poor correlation between IgG concentrations and neutralization titers, inferring that IgG titers do not accurately measure immunity (198). A study using human samples after a third dose of the MMR found a poor correlation between MuV specific NP and HN IgG antibody titers and plaque reduction neutralization (PRN) titers, meaning antibody titers could not be used to infer a predictive PRN titer. Although more labor-intensive than an ELISA, PRN assays are thought to be a better indicator of immunity because they show levels of neutralizing antibodies rather than total antibody titers (199, 200). Neutralizing antibodies are thought to be essential for protection against mumps, but still there is no predictive neutralization titer that confers protection. There is limited data on mumps-specific cellular immunity and the degree to which T-cell immunity protects against mumps is unknown. A study compared T-cell responses in individuals who were fully vaccinated versus individuals who had naturally acquired immunity and found similar levels of mumps specific $CD4^+$ T cells, but the naturally acquired group produced more IFN-γ when

stimulated with mumps antigens. However, this study was able to detect a T-cell response ten years post vaccination (201). Another study measured the mumps antigen-specific IFN-γ response from fully vaccinated individuals 21 years after their second dose of MMR. They found that the individuals who were seronegative for mumps antibodies had a detectable T-cell response, suggesting the vaccine-induced T-cell memory response is more long-lived than the B-cell memory (202). In recent years, studies looking at mumps specific $CD4^+$ and $CD8^+$ epitopes have found that there may be differences between epitope affinity in naturally acquired and vaccinated individuals (203, 204). More research is required to fully understand the mumps T-cell response after infection and immunization.

There are thought to be four main causes of mumps outbreaks in vaccinated populations. Primary vaccine failure due to lack of vaccination or a sufficient antibody response following vaccination is thought to contribute to outbreaks. This was observed in Ireland in the late 1990s, so they adjusted the timing of the second dose of MMR, from 10-14 years to 4-5 years (2, 205). Another probable cause is waning immunity, which is a decline in protection over time. This has been observed in numerous outbreaks across the globe (194, 206-209). A mathematical model estimated that the MuV vaccine efficacy declines by 25% starting 7.9 years post vaccination and continues to decline over time (210). Immune escape is another factor, variation between the vaccine strain and outbreak strains result in reduced cross-neutralization leading to lower vaccine efficacy. Studies have provided evidence that immunization with JL results in lower neutralizing titers against other MuV genotypes (211, 212). One study showed that serum from

children immunized with 2 doses of the MMR had lower neutralizing titers against non-genotype A viruses, such as genotype G and H. However, this study argued against immune escape because all serum samples were able to neutralize the heterologous viruses to some degree (208, 213). In addition, mouse studies have shown that immunizing with JL results in lower neutralizing titers to a genotype G virus (22, 25). The last contributor to mumps outbreaks is thought to be a lack of natural boosting, which has only become a factor in the post-vaccine era. As herd immunity increases, the incidence of mumps decreases, and individuals are not exposed to low levels of circulating virus as they would be, which would act to boost their memory response (2, 24). With a large spread of neutralizing titers found within individuals considered to be immune and no correlates for protection, determining the cause of MuV outbreaks continues to be a challenge.

Although breakthrough infections are occurring worldwide, one study found that patients infected with MuV after two doses of MMR had milder symptoms and lower viral shedding. They performed a large-scale study comparing confirmed mumps patients who were unvaccinated to patients who had previously received two doses of the MMR vaccine. The vaccinated patients had a higher incidence of asymptomatic infection or a mild localized infection and shed lower amounts of virus in their saliva. The unvaccinated patients typically had detectable virus in their urine, an indicator of systemic viremia, and shed virus for longer. This study suggests that although the MMR may not provide sterilizing immunity it may prevent severe life-threatening mumps cases (214).

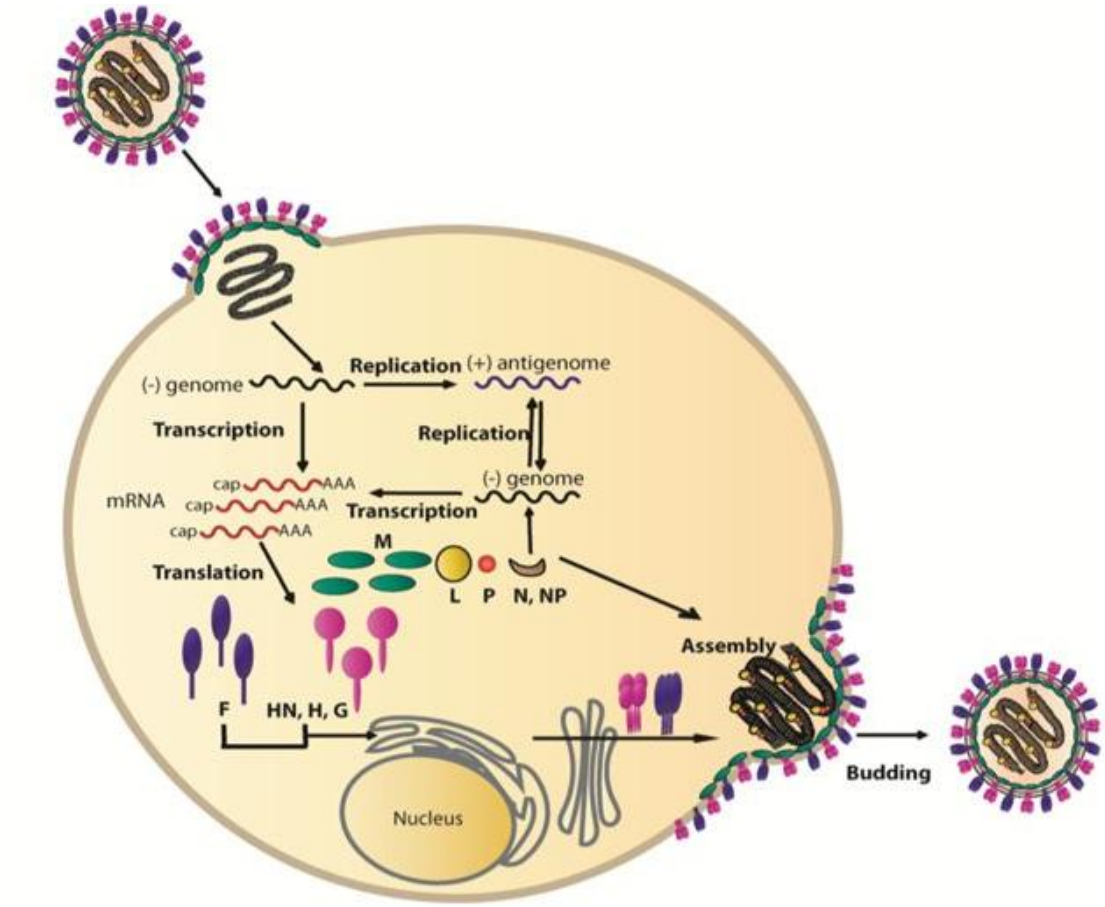


**Figure 2.1. Schematic illustration of the life cycle of paramyxoviruses.** The virion enters the cell via attachment by the haemagglutinin-neuraminidase (HN) protein, which causes a conformational change in the fusion (F) protein. Once fusion with the host membrane occurs the viral proteins and RNA genome are released into the cytoplasm. The RNA genome is encapsidated by the nucleoprotein (NP) to form the helical ribonucleoprotein (RNP) and acts as a template for replication of the viral genome and mRNA synthesis. The RNP associates with the phosphoprotein (P) and large protein (L) to form the viral RNA-dependent RNA polymerase (vRdRp) complex. Transcription occurs using the

genome as a template for mRNA production. In replication, the vRdRp first synthesizes an antigenome to use as a template for more viral genomes (11). The matrix (M) protein associates with the replication machinery and glycoproteins near the cell surface before budding from the cellular membrane. Adapted from Najjar *et al.* 2014. (215).

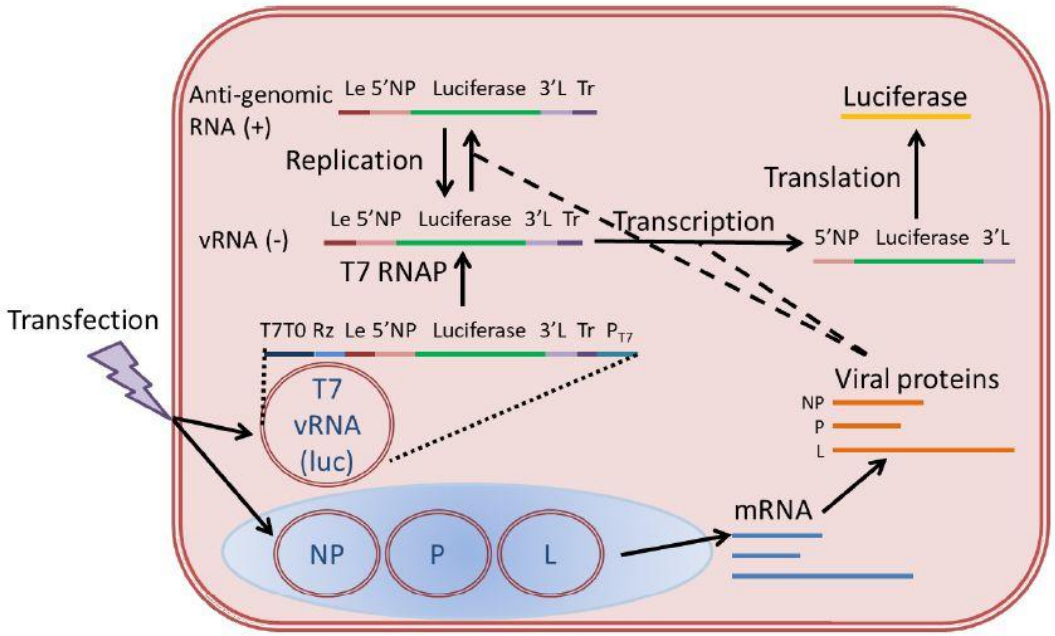


**Figure 2.2. MuV minigenome system.** Minigenome systems are used to examine the effects of the MuV replication machinery, NP, P, and L, on MuV RNA synthesis. Mutations can made and tested in any of the proteins to examine the effect on replication. The minigenome plasmid contains the MuV 3' leader and 5' trailer sequences flanking a *Renilla* luciferase open reading frame (ORF) under a T7 promoter. When transfected into BSRT7 cells the T7 polymerase will generate an RNA template that can be recognized by the mumps replication machinery. Plasmids containing MuV NP, P, and L are co-transfected with the minigenome plasmid to produce the viral proteins. NP, P, L recognize the leader sequence of the RNA template and transcribe the Renilla luciferase ORF, which can be translated by host machinery. Firefly luciferase is used as a transfection control. The amount of each luciferase produced it quantified using a luminometer (4).

Adapted from the Dissertation of Zengel, J., The roles of phosphorylation in mumps virus RNA synthesis and replication, 2017. (216).

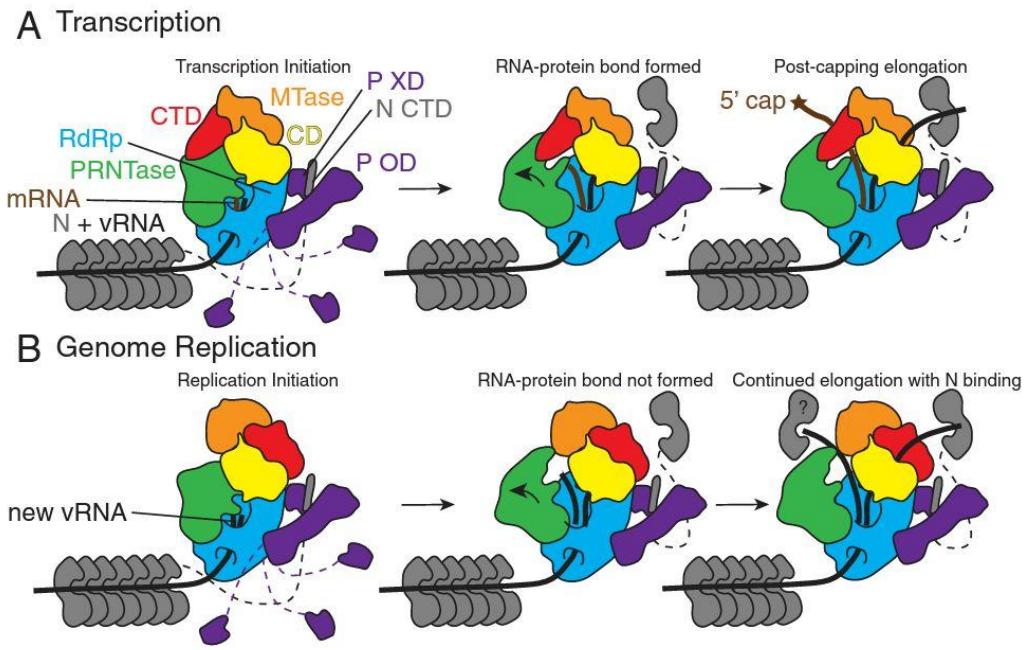


**Figure 2.3. L structure and model of transcription and genome replication rearrangement.** Proposed model of L domain rearrangement during transcription and replication based on VSV and PIV5 L structures (101, 217). L is comprised of five conserved domains: RNA-dependent RNA polymerase (RdRp), polyribonucleotidyltransferase (PRNTase), connecting domain (CD), methyltransferase (MTase), and C-terminal domain (CTD). The vRdRp cofactor, P, has three domains: N-terminal domain (not pictured), the central oligomerization domain (P OD), and C-terminal X domain (P XD). The vRNA is encapsidated by NP before and after elongation. P shuttles monomers of NP from the original vRNA to nascent RNAs. **(A) Transcription.** The MTase and CTD are located directly above the PRNTase domain so efficient capping and methylation can occur. **(B) Replication.** MTase and CTD are positioned further away from PRNTase. Adapted from Abdella *et al.* 2020. (101).

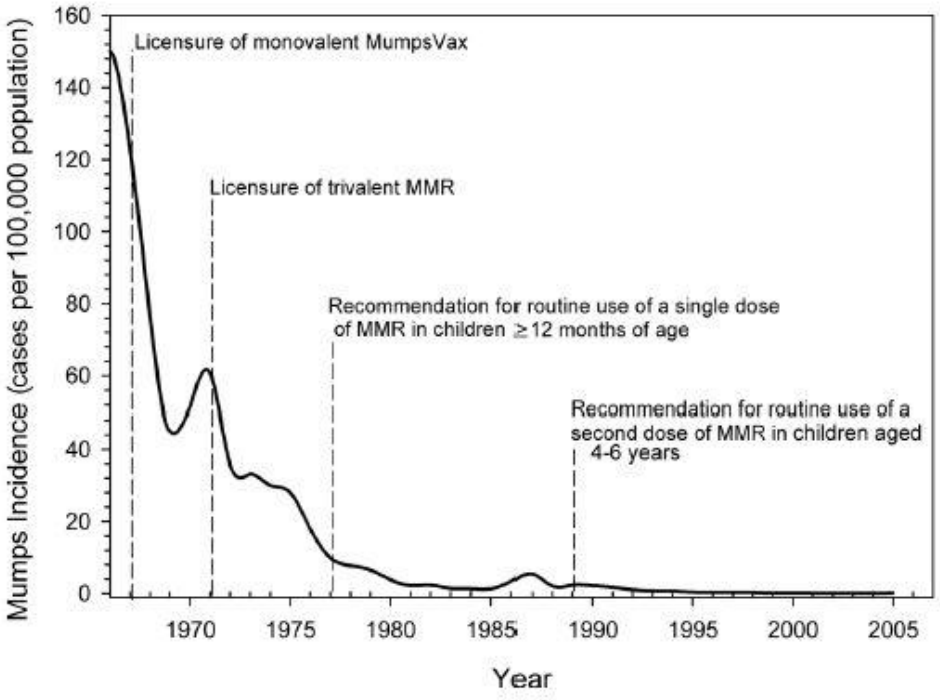


**Figure 2.4. Mumps incidence in the United States after vaccine licensure.** The number of mumps cases per 100,000 people from 1967 to 2006. Cases declined following the licensure of the monovalent MumpsVax in 1967 and continued to decrease after the licensure of the trivalent measles, mumps, and rubella (MMR) vaccine in 1971. MMR vaccination became routine in 1977 and in 1989 a second dose was added to the regiment. Cases remained below 500 a year in the United States until 2005-2006. Adapted from Dayan *et al.*, 2008 (218).

| Outbreak year(s) & study | Location | Number of reported cases | Patients who received 1 doses of MMR* | Patients who received 2 doses of MMR* | Patients who received 3 doses of MMR*# | Mumps virus genotype recovered |
|---|---|---|---|---|---|---|
| 2006-2007 Marin *et al.* (7) & Dayan *et al.* (219) | Iowa & midwestern states; college campuses | 6584 total; highest incidence 18-24 age group | 24.8% total | 62.5% total; 84% in 18-24 age group | N/A | G, H (1 imported case from Bulgaria) |
| 2009-2010 Nelson *et al.* (220) | Guam; community & schools | 505 total; 169 ages 9-14 years | 3.0% in 9-14 age group* | 95.8% in 9-14 age group | 17% (1 out of 6 school-age students) | G |
| 2009-2010 Barskey *et al.* (221) | New York & New Jersey; Jewish community | 3502 total; 884 ages 13-17 years | 14% total; 8% in 13-17 age group | 76% total; 89% in 13-17 age group | NR | G |
| 2015-2016 Shah *et al.* (222) | Iowa; University affiliates | 453 total; 301 university students | 0.7% of university students | 86% of university students | 12% of university students | G |
| 2016-2017 Fields *et al.* (223) | Arkansas; Marshallese community | 2954 total; 1676 ages 5-17 | 8% total; 3% in 5-17 age group | 63% total; 92% in 5-17 age group | NR | G |
| 2019 Donahue *et al.* (224) | Nebraska; guests at a wedding | 62 total, age range 6-59 years (Ave. 33 years) | 8% | 61% | 5% | G |

**Table 2.1. Mumps resurgence in the United States after 2006.** Some of the major outbreaks that have occurred in the U.S. from 2006-2020. Several patients (confirmed or suspected cases) received greater than 1 dose of the measles, mumps, and rubella (MMR) vaccine. *; Only verified vaccination status presented

in table. #; When administered in outbreak setting. NR; not reported. N/A; not applicable.

# CHAPTER 3

# REGULATION OF MUMPS VIRUS REPLICATION AND TRANSCRIPTION BY KINASE RPS6KB1

Briggs K, Wang L, Nagashima K, Zengel J, Tripp RA, He B. 2020. Regulation of Mumps Virus Replication and Transcription by Kinase RPS6KB1. Journal of Virology 94:e00387-20. Reprinted here with permission of the publisher.

**ABSTRACT**

Mumps virus (MuV) caused the most viral meningitis before mass immunization. Unfortunately, MuV has re-emerged in the United States in the past several years. MuV is a member of the family *Paramyxoviridae*, in the genus *Rubulavirus*, and has a non-segmented, negative-stranded RNA genome. The viral RNA-dependent RNA polymerase (vRdRps) of MuV consists of the large protein (L) and the phosphoprotein (P), while the nucleocapsid protein (NP) encapsulates the viral RNA genome. These proteins make up the replication and transcription machinery of MuV. The P protein is phosphorylated by host kinases, and its phosphorylation is important for its function. In this study, we performed a large-scale siRNA screen targeting host kinases that regulated MuV replication. The human kinase RPS6KB1 was identified to play a role in MuV replication and transcription. We have validated the role of RPS6KB1 in regulating MuV using siRNA knockdown, an inhibitor, and RPS6KB1 knockout cells. We found that MuV grows better in cells lacking RPS6KB1, indicating that it downregulates viral growth. Furthermore, we detected an interaction between the MuV P protein and RPS6KB1, suggesting that RPS6KB1 directly regulates MuV replication and transcription.

**IMPORTANCE**

Mumps virus is an important human pathogen. In recent years, MuV has reemerged in the United States with outbreaks occurring in young adults who have been vaccinated. Our work provides insight into a previously unknown Mumps

virus-host interaction. RPS6KB1 negatively regulates MuV replication, likely through its interaction with the P protein. Understanding viral-host interactions can lead to novel antiviral drugs and enhanced vaccine production.

## INTRODUCTION

Mumps virus (MuV) is a human pathogen that causes an acute infection resulting in symptoms like parotitis, fever, and nausea. Additionally, it is highly neurotropic and has been shown to invade the central nervous system (CNS) Prior to mass vaccination in the late 1960s, MuV was the leading cause of aseptic meningitis, encephalitis, and deafness in children (10). Mass vaccination dramatically reduced MuV infections across the United States. However, there has been a recent resurgence in MuV infections that has occurred mostly in vaccinated populations. In 2006, there was an outbreak within college campuses in Iowa (IA) that resulted in over 6500 diagnosed cases of MuV. Since 2006, there have been several years with over 1000 diagnosed cases in the U.S. In 2016 and 2017, there were over 6000 cases, rivaling that of the IA outbreak (2, 7). Currently, there are no antiviral drugs approved for MuV infections. Understanding the interactions of host and viral proteins, using the currently circulating 2006 MuV Iowa outbreak strain, will aid in developing new treatments.

MuV is a member of the family *Paramyxoviridae*, in the genus *Rubulavirus*, and has a non-segmented, negative-stranded RNA genome of 15,384 nucleotides (9, 10). The genome contains seven genes that are transcribed into nine viral proteins in the order 3’-NP-V/I/P-M-F-SH-HN-L-5’, with RNA synthesis beginning

at the 3’ end. The RNA genome serves as a template for replication of the vRNA genome and mRNA synthesis, and it associates with nucleoproteins (NP) to form the helical ribonucleoprotein (RNP), which protects the genome from degradation. The RNP associates with the phosphoprotein (P) and the large protein (L) to form the viral RNA-dependent RNA polymerase (vRdRp) complex. The L protein is responsible for initiation, elongation, and termination of RNA synthesis, in addition to adding the 5’ cap and 3’ poly(A) tail to transcribed viral mRNA. The P protein interacts with NP in the RNP, as well as free NP, and is essential for the formation of the vRdRp (9, 10, 21).

The P proteins of paramyxoviruses are highly phosphorylated, and their phosphorylation status impacts vRNA and viral mRNA synthesis. Previous studies, with parainfluenza virus 5 (PIV5), respiratory syncytial virus (RSV), and MuV have shown that mutating residues within P affects RNA synthesis (4, 12-14). It is thought that phosphorylation of the P protein is achieved by host kinases, because paramyxovirus viral proteins lack inherent kinase enzymatic activity (9, 14). Furthermore, several paramyxovirus P proteins have been shown to interact with host kinases, including MuV P, which was shown to interact with human kinase Polo-like kinase 1 (PLK1) (15-18). Additional host kinases that are important for MuV P phosphorylation and RNA synthesis have yet to be discovered.

In this work, we used a siRNA screen to identify host kinases that are involved in MuV replication and examined the effect of one specific kinase, RPS6KB1, on MuV replication.

## MATERIALS AND METHODS

### Cells.

293T cells were maintained in Dulbecco's modified Eagle medium (DMEM) with 5% fetal bovine serum (FBS) and 1% penicillin-streptomycin (P/S) (Mediatech Inc., Manassas, VA). Vero and HeLa cells were maintained in DMEM supplemented with 5% FBS and 1% P/S. BSR-T7 cells were maintained in DMEM supplemented with 5% FBS, 1% P/S, 10% tryptose phosphate broth (TPB), and 400 µg/ml G418 sulfate antibiotic (Mediatech Inc.). Hap1 cells (Horizon Discovery, Cambridge, United Kingdom) were maintained in Iscove's Modified Dulbecco's Medium (IMDM) supplemented with 10% FBS and 1% P/S. All cell lines were incubated at 37°C with 5% CO2.Cells were passed at an appropriate dilution 1-2 days prior to use in order to achieve 80% - 90% confluence upon infection or 60% - 80% confluence upon transfection. 293T and BSR-T7 cells were used for transfection experiments, Hela cells were used for transfection and then infection experiments, and Hap1 and Vero cells were used for infection experiments.

### Plasmids and Transfections.

Plasmids were constructed using standard molecular cloning techniques and are available upon request (8). A flag tag was added to the 3' end of recombinant RPS6KB1, which was cloned into the pCAGGS expression vector, along with MuV NP, P, and L genes. Plasmids containing firefly luciferase (pFF-luc) and the MuV minigenome (pBH526/pMG-Rluc) containing *Renilla* luciferase under the T7 promoter were used in the MuV minigenome assays (4).

JetPRIME was used to transfect cells with plasmids and INTERFERin was used to transfect cells with siRNA according to the manufacturer's protocols (Polyplus Transfection Inc., New York, NY).

**Viruses and Infections.**

As previously described, Wild-type MuV (WT MuV) and a recombinant MuV virus expressing *Renilla* luciferase (rMuV-rLuc) were propagated from an early passage and sequenced to confirm that no mutations occurred (5, 8). In brief, a T150 flask of 90-100% confluent Vero cells was infected at a MOI of 0.01 for 1 hour. The inoculums were then replaced with fresh DMEM supplemented with 2% FBS and 1% P/S and virus was propagated for 2-3 days. The viruses were collected after syncytia formed, and plaque assays were performed to determine titer (4, 5). Viral infections were performed at a multiplicity of infection (MOI) of 0.01, 0.1, 1, or 3. Inoculums were prepared in DMEM supplemented with 2% FBS and 1% P/S and incubated on cells for 1-2 hours. The inoculums were then replaced with fresh DMEM supplemented with 2% FBS and 1% P/S. Hap1 cells were inoculated with IMDM supplemented with 10% FBS and 1% P/S.

**siRNA screen and Cytotoxicity assay.**

A library of 720 siRNA pools targeting protein kinase families (Dharmacon siARRAY siRNA Library; Human Genome, G-003505, Thermo Fisher Scientific, Lafayette, CO) were utilized. Using DharmaFECT 1 transfection reagent (Dharmacon) and following the manufacturer's instructions, Vero-E6 cells (96-well format) were reversely transfected with siRNAs at a 50nM final concentration. Each 96-well plate had additional control wells with a non-target control siRNA

(siCONTROL non-target siRNA, Dharmacon), siRNA targeting AKT1, TOX control siRNA, and wells without any siRNA. At 2 days post-transfection, cells were infected with rMuV-rluc or rPIV5-rLuc virus at a MOI of 1 or 2, respectively. The transfected/infected cells were lysed for renilla luciferase assay at 1-day post-infection.

Cytotoxic effects of siRNAs on cells were determined using ToxiLight® BioAssay Kit (Lonza). Supernatants of gene-silenced cells were harvested at 2 days post-transfection and before infection and assayed for adenylate kinase (AK) release according to the manufacturer's protocol.

***Renilla* luciferase and cytotoxicity assays.**

Two different MISSION predesigned siRNAs (Sigma-Aldrich, St. Louis, MO) were transfected into 60-80% confluent HeLa cells using INTERFERin (Polyplus Transfection Inc.) to a final concentration of 5 nM. Non-target control (NT), also purchased from Sigma-Aldrich, was used as the control. The catalog numbers for the predesigned siRNAs are as follows: RPS6KB1 (NM_003161), MAP3K6 (NM_004672), MYO3B (NM_001083615), UMPK (NM_016308), and AK7 (NM_152327). Individual sequences are available upon request. Twenty-four hours later, cells were infected with a recombinant MuV expressing *Renilla* luciferase protein (rMuV-rluc) at a MOI of 0.1. After another 24 hours, cells were lysed in 100 µl of 5X *Renilla* luciferase lysis buffer (Promega, Madison, WI) by vigorous shaking. 40 µl of lysate from each well was used to run the *Renilla* luciferase assay according to the manufacturer's protocol, and light intensity was detected using a GloMax 96 Microplate Luminometer (Promega). Three replicates

of each sample were compared to the non-target control, which was used to normalize the activities. The lysates of each replicate were combined and collected for western blot analysis.

LY2584702 Tosylate Inhibitor (Selleck Chemicals, Houston TX), a RPS6KB1 inhibitor, was dissolved in DMSO to make a 10 mM stock solution. HeLa cells were infected in triplicate with rMuV-rluc for 1 hour in a 12-well plate. During this time, the inhibitor was diluted 2-fold starting at 10 µM. After infection, the diluted inhibitor, plus media, was added back to the cells for 24 hours. The *Renilla* luciferase assay was performed as described above.

To determine if the siRNAs and RPS6KB1 inhibitor had any negative effects on HeLa cells, the CellTiter-Glo Luminescent Cell Viability Assay (Promega) was used. siRNAs were transfected, and the inhibitor was added as described above. After 24 or 48 hours, cells were lysed with 100 µl of CellTiter-Glo reagent (Promega) according to the manufacturer's protocol. Sample lysates were ran straight and diluted 10-fold in triplicate. Either the non-target control NON-TARGET CONTROL or 0.1% DMSO was used as the control, and values were normalized to these values.

**Multi-step and single-step growth curve.**

Wild-type (WT) or RPS6KB1-knockout (RPS6KB1-KO) Hap1 cells were seeded in a 6-well plate in triplicate. Upon confluency, cells were either infected with a MOI of 0.01 (multi-step) or a MOI of 5 (single-step). Media was collected from each well at 0, 24, 48, 72, 96, 120, 144, and 168 HPI for the multi-step, and

at 0, 12, 24, 36, 48, 60 for the single-step growth curves. Virus titers were determined in Vero cells by plaque assays as previously described (61).

**Immunoblotting.**

Cell lysates were mixed with 2X Laemmli sample buffer with β-mercaptoethanol (Bio-Rad Laboratories, Inc., Hercules, CA) and heated at 95°C for 5 min. Samples were resolved in 10% SDS-PAGE and transferred to a polyvinylidene difluoride membrane (GE Healthcare, Piscataway, NJ). Immunoblotting, using monoclonal MuV protein-specific antibodies, was performed as previously described (8). The membrane was incubated with mouse anti-MuV-NP antibody (1:2500 dilution) and mouse anti-MuV-P antibody (1:2000 dilution), followed by incubation with Cy3-conjugated goat anti-mouse IgG secondary antibody (1:2500 dilution) (Jackson ImmunoResearch, West Grove, PA), and imaged using a Typhoon 9700 imager (GE Healthcare Life Sciences, Piscataway, NJ).

To compare the viral protein expression levels in infected cells, Hap1 cells were mock infected or infected with WT MuV (IA, 06) at a MOI of 0.01. At 0, 12, 24, 36, 48, 60, 72, and 96 HPI, cells were prepared and resolved as described above. Immunoblotting was performed with primary antibodies mouse anti-MuV-NP and rabbit anti-Actin antibody at a 1:2500 dilution (Sigma-Aldrich, St. Louis, MO), followed by Cy3-conjugated goat anti-mouse IgG secondary antibody and Cy3-conjugated goat anti-rabbit IgG secondary antibody at 1:2500 dilutions (Jackson Immuno-Research).

**Minigenome and dual-luciferase assays.**

BSR-T7 and Hap1 cells in 24-well plates were transfected with pCAGGS-NP (25 ng), pCAGGS-L (500 ng), pMG-RLuc (100 ng), pFF-Luc (1 ng), and various amounts (20, 40, 80, or 160 ng) of pCAGGS-P. For inhibition of RPS6KB1, BSR-T7 cells were either treated with 1 µM of the RPS6KB1 inhibitor (Selleck Chemicals), or 0.1% DMSO. For over-expression of RPS6KB1, BSR-T7 cells were transfected with a vector control or a plasmid containing RPS6KB1 at 100 ng per well. pCAGGS vector with GFP was used to confirm the transfection. After 24 hours, cells were lysed in 100 µl passive lysis buffer (Promega, Madison, WI) and vigorously shaken for 20 min to permit full lysis. Clear lysate (40 µl) from each well was used to carry out the dual-luciferase assay according to the manufacturer's protocol (Promega), and light intensity was detected using a GloMax 96 Microplate Luminometer (Promega). Relative luciferase activity was defined as the ratio of *Renilla* luciferase (R-Luc) to firefly luciferase (FF-Luc) activity. Three replicates of each sample were used to compare the peak activity of each P concentration with or without RPS6KB1.

**Flow Cytometry.**

WT and RPS6KB1-KO Hap1 cells in 10-cm dishes were infected with WT MuV at a MOI of 0.1 in quadruplicate. At 24 HPI, cells were trypsinized and resuspended in 1% formaldehyde in PBS for 1 hour at 4°C. They were then washed with PBS, resuspended in 70% ETOH, and incubated overnight at 4°C. Cells were stained with anti-mouse MuV-NP antibody at 1:100 dilution in 1% BSA PBS for 1 hour at 4°C. Cells were then washed 3X with PBS and resuspended in

APC goat anti-mouse IgG secondary antibody (BioLegend, San Diego, CA) at 1:100. Cells were washed with PBS another 3X and resuspended in 1 mL PBS**.** Flow cytometry was performed using a LSRII flow cytometer (BD Biosciences, San Jose, CA) and analyzed using BD FACSDiva Software Version 8.0.1 (BD Biosciences). The mean fluorescence intensity of MuV NP was calculated for each replicate of infected and uninfected cells.

**qRT-PCR.**

WT and RPS6KB1-KO Hap1 cells were infected with WT MuV at a MOI of 5 in triplicate in a 12 well plate. Total RNA was collected at 2 and 24 HPI using the RNeasy mini kit (Qiagen, Waltham, MA). cDNA was generated via reverse transcription with Super Script III reverse transcriptase (Invitrogen, Frederick, MD). mRNA was generated with Oligo(dT)15 (Invitrogen), and genomic RNA was generated with a vRNA-specific primer flanking the MuV-F gene. Synthesized cDNAs were used as templates for quantitative real-time PCR (qRT-PCR). A MuV-HN specific FAM-tagged probe (Applied Biosystems, South San Francisco, CA) and TaqMan Gene Expression Master Mix (Applied Biosystems) were used according to the manufacturer's protocol. Real-time PCR was completed using a StepOnePlus RT PCR system (AB Biosciences, Foster City, CA). Threshold cycle (C*t*) values were normalized to the genomic RNA values when the inoculum was removed at 2 HPI.

**Radiolabeled IP.**

To examine the phosphorylation status of MuV-P, HeLa andHap1cells were used. HeLa cells were transfected with siRNA and then infected as described

above. Hap1 cells were infected or mock infected when confluent at a MOI of 0.1 and 3. 24 HPI, cells were starved in DMEM lacking cysteine-methionine and then labeled with 72.7 µCi/ml 35S-EasyTag Express $^{35}$S protein label (PerkinElmer, Waltham, MA) for 6 to 8 hours or starved with DMEM lacking sodium phosphate and then labeled with 100 µCi 33P-radionuclide orthophosphoric acid (PerkinElmer, Waltham, MA) for 6-8 hours. The cells were then lysed with whole-cell extraction buffer (WCEB) (50 mM Tris-HCl [pH 8.0], 280 mM NaCl, 0.5% NP-40, 0.2 mM EDTA, 2mM EGTA, and 10% glycerol) with a mixture of protease inhibitors as previously described (89).The lysate was split into two tubes and immunoprecipitated (IP) using recombinant protein G-Sepharose 4B conjugated beads and either a mouse monoclonal anti-MuV-P or anti-MuV-NP antibody. After washing 3X with WCEB, the beads were mixed with 2X Laemmli sample buffer with β-mercaptoethanol (Bio-Rad Laboratories, Inc., Hercules, CA) and heated at 95°C for 5 min. Samples were resolved with 10% SDS-PAGE. Phosphorylation of the P protein was calculated by densitometry analysis of the 33P/35S ratio using ImageQuant TL software (GE Healthcare Life Sciences).

**IP.**

To detect the interaction between MuV-P and RPS6KB1, 293T cells were transfected with 4 µg of pCAGGS-P, 4 µg of pCAGGS-RPS6KB1-Flag (pKB25), and 2 µg of pCAGGS-NP. pCAGGS-GFP was used to normalize the amount of DNA per 10-cm dish. 24 hours post-transfection, cells were lysed in 1 ml WCEB with a mixture of protease inhibitors. The lysates were immunoprecipitated overnight at 4°C using recombinant protein G-Sepharose 4B conjugated beads

and either mouse monoclonal anti-MuV-P or anti-Flag (M2 clone; Sigma-Aldrich, St. Louis, MO) antibodies. After washing 3X with WCEB, samples were resuspended in 2X Laemmli sample buffer with β-mercaptoethanol (Bio-Rad Laboratories, Inc., Hercules, CA) and heated at 95°C for 5 min. Immunoblotting was performed as described above. The membrane was blotted with anti-MuV-P or anti-Flag, followed by incubation with a conjugated HRP rat anti-mouse IgG antibody (Abcam, Cambridge, MA). After extensive washing, the blot was incubated with SuperSignal West Pico PLUS Chemiluminescent Substrate (ThermoFisher Scientific, Waltham, MA) for 5 minutes and then exposed on a Gel Doc RX+ imaging system with Image Lab for analysis (Bio-Rad Laboratories, Inc.).

**Statistical analysis.**

Statistical analyses were performed using GraphPad Prism version 6.00 for Windows (GraphPad Software, San Diego, CA). Student *t* test and One-way ANOVA were used to calculate P values when comparing two groups. When performing multiple comparisons, the Holm-Šidák method, with an alpha of 5%, was used to determine statistical significance.

## RESULTS

### Identification of host kinases that are important for MuV replication.

To identify host kinases that are important for MuV replication, a siRNA screen was performed using a library of 720 different siRNAs targeting human protein kinases. Vero-E6 cells were reverse transfected with 4 different siRNAs per kinase in 96-well plates that also contained a positive, negative, and TOX

control. Using a Z-score analysis, we found several candidates that upregulated or downregulated viral replication. In addition to MuV, a closely related virus in the same genus, Parainfluenza virus 5 (PIV5), was also screened. Interestingly, there were many differences in the kinases that play a role in their replication. Of the top 50 repressors, only 5 were similar between PIV5 and MuV, all of which were chosen for further study. Of the top 50 enhancers, 18 were similar between PIV5 and MuV, but only 4 were chosen for further study and are not discussed in this work. The candidates were chosen for further study because of their observed role in MuV, PIV5, or both. Notably, many of these candidates have been previously implicated in interacting with other viruses (15). To validate the siRNA screen, new siRNAs targeting different sequences of the kinase mRNA transcripts from the screen were used. UMPK and AK7, upon further validation, had no significant effect on MuV replication. A few candidates were shown to significantly increase MuV luciferase activity when knocked down including MYO3B, MAP3K6, and RPS6KB1. siRPS6KB1 consistently increased MuV activity the most compared to the other siRNA-inhibited kinases (Fig. 3.1A). A western blot was performed to examine the amount of RPS6KB1 siRNA-knockdown compared to the non-target control (NT). It was found that the siRNA-knockdown was approximately 40% percent of the control (Fig. 3.1B). The cellular toxicity of all the siRNA-inhibited kinases were assayed by measuring the amount of ATP produced. RPS6KB1 reduced cellular viability less than 10% compared to the non-target control and was not found to be significant (data not shown). siRNA-inhibited RPS6KB1 was not cytotoxic to HeLa cells and increased MuV-luciferase activity compared to the

non-target control. Upon further investigation, RPS6KB1 had no significant effect on PIV5 growth, despite the screening results, and no further testing occurred (data not shown).

**MuV grew to a higher titer in cells lacking RPS6KB1.**

To examine the growth rates of MuV in cells lacking RPS6KB1, siRNAs against RPS6KB1 were used. MuV grew to a higher titer in RPS6KB1 siRNA-treated cells compared to the non-target control at 24 HPI (Fig. 3.2A). To examine MuV growth over a longer period, Hap1 cells lacking RPS6KB1 (RPS6KB1-KO) were infected with MuV at a low (0.1) and high (3) MOI. MuV consistently grew to a higher titer in the RPS6KB1-KO cells compared to WT Hap1 cells (WT) at both MOIs, suggesting RPS6KB1 has a negative effect on MuV growth (Fig. 3.2B, 3.2C).

**Viral protein expression is increased in cells lacking RPS6KB1.**

RPS6KB1-specific siRNAs were used to examine MuV viral protein expression in cells. Lysates were collected and immunoblotted with monoclonal anti-MuV-NP (Fig. 3.3A). At 24 HPI, the NP protein density was greater in the siRPS6KB1-transfected cells than the non-target control (Fig. 3.3B). Cells were subjected to various concentrations of a RPS6KB1-specific inhibitor and then infected with rMuV-rluc to measure the luciferase production 24 HPI. Luciferase activity was increased using as little as 0.3 μM of the inhibitor at both a low (0.1) and high (3) MOI (Fig. 3.3C,D). To examine viral protein expression in cells lacking RPS6KB1, WT and RPS6KB1-KO Hap1 cells were infected at a low MOI. Lysates from infected cells were taken at various time points and immunoblotted for anti-

MuV-NP and anti-actin as a loading control (Fig. 3.3E). The relative NP densities were calculated, and MuV protein expression was slightly higher in the RPS6KB1-KO Hap1 cells starting at 24 HPI and gradually increased over time (Fig. 3.3F). To confirm that the Hap1 cells lacking RPS6KB1 caused an increase in MuV protein expression at an early timepoint, flow cytometry was performed. WT and RPS6KB1-KO Hap1 cells were infected with MuV and then stained for anti-MuV-NP. MuV grown in RPS6KB1-KO Hap1 cells had a greater mean fluorescence intensity (MFI) than MuV grown in WT Hap1 cells (Fig. 3.3G). MuV viral protein expression is increased in cells with inhibited or knocked out RPS6KB1.

**MuV minigenome activity is increased in the absence of RPS6KB1.**

To determine if RPS6KB1 plays a role in viral RNA synthesis, a minigenome system was used. BSR-T7 cells were transfected with the minigenome plasmids with varying concentrations of MuV-P plasmid. Multiple concentrations of MuV-P plasmid were transfected to find the optimal minigenome activity in the presence of the inhibitor and to examine if different amounts of MuV-P plasmid would affect the phenotype. The cells were then either mock treated or treated with the RPS6KB1 inhibitor. MuV minigenome activity was significantly increased at all concentrations of transfected MuV-P plasmid in the presence of the RPS6KB1 inhibitor (Fig 3.4A). A minigenome assay was also performed in Hap1 cells. The transfection efficiency of the Hap1 cells was much lower than the BSR-T7 cells, causing the overall minigenome activity to be lower. Regardless, the same trend was observed, and MuV minigenome activity was significantly increased in RPS6KB1-KO cells compared to WT Hap1 cells (Fig 3.4B). To determine if over-

expression of RPS6KB1 would diminish minigenome activity, varying amounts of MuV-P plasmid and a plasmid containing RPS6KB1 (pRPS6KB1) were transfected into BSR-T7 cells. MuV minigenome activity was reduced in the cells over-expressing RPS6KB1, suggesting RPS6KB1 plays a negative role in MuV RNA synthesis (Fig 3.4C).

**Viral replication and transcription are increased in cells lacking RPS6KB1.**

To investigate the role RPS6KB1 has on viral RNA synthesis, real-time PCR was used to compare levels of viral mRNA and genomic RNA (vRNA) in Hap1 cells. The cells were infected with MuV at high MOI to measure a single round of MuV RNA synthesis. Total RNA was extracted from infected WT and RPS6KB1-KO Hap1 cells. MuV genomic vRNA was increased in RPS6KB1-KO cells compared with WT Hap1 cells (Fig 3.5A). In addition, MuV mRNA was increased, which is consistent with increased protein expression (Fig 3.5B, 3.3). There was an increased viral mRNA-to-genomic vRNA ratio in the RPS6KB1-KO cells compared to WT Hap1 cells (Fig 3.5C). This suggests that RPS6KB1 plays a role in transcription by negatively regulating the viral RNA synthesis machinery.

**MuV has reduced P phosphorylation in cells lacking RPS6KB1**.

To determine if RPS6KB1 plays a role in MuV-P phosphorylation, cells were transfected with siRNA and then infected with MuV. Cells were labeled with $^{35}S$ or $^{33}P$, and then immunoprecipitated with monoclonal anti-MuV-P or monoclonal anti-MuV-NP. $^{35}S$-labeled P protein was increased in the RPS6KB1 siRNA-transfected cells compared to the non-target control. Interestingly, MuV-NP was coimmunoprecipitated with MuV-P in the RPS6KB1 siRNA transfected cells, which

was not observed in the non-target control. Additionally, more MuV-P was coimmunoprecipitated in the RPS6KB1 siRNA treated cells with the anti-MuV-NP antibody (Fig 3.6A). These results are consistent with the previous findings that MuV protein expression is increased in cells lacking RPS6KB1 (Fig 3.6B). MuV-P phosphorylation was significantly decreased in the RPS6KB1 siRNA-transfected cells, which suggests RPS6KB1 phosphorylates MuV-P (Fig 3.6C). The slight reduction in phosphorylation is feasible because MuV-P has several phosphorylation sites that all undergo phosphorylation changes during an infection and proteins were only radio-labeled for 6-8 hrs (4). The results indicate that RPS6KB1 phosphorylates MuV-P, which interferes with transcription and replication, causing a negative effect on MuV growth.

**RPS6KB1 interacts with MuV P.**

To examine if RPS6KB1 has a direct effect on MuV-P, cells were transfected with different combinations of MuV-P, MuV-NP, pCAGGS-GFP, and a plasmid encoding RPS6KB1 with a Flag-tag (pKB25). Lysates were immunoprecipitated with either a monoclonal anti-MuV-P or monoclonal anti-Flag antibody and then immunoblotted. The cells that were transfected with MuV-P + MuV-NP + pKB25 and immunoprecipitated/immunoblotted with their reciprocal antibody each showed a band at the corresponding size (Fig. 3.7A, 3.7B). For example, when an anti-MuV-P antibody was used for immunoprecipitation, the RPS6KB1-flag protein was detected with an anti-flag antibody in the immunoblot (Fig. 3.7A). The cells transfected with MuV-P + pKB25 alone also showed the correct corresponding bands, suggesting that MuV-P and RPS6KB1 interact

independently of MuV-NP (Fig. 3.7A, 3.7B). Interestingly, compared to lysate from cells transfected with P+pKB25+NP, lysate from cells transfected with P + pKB25 immunoblotted for less MuV-P when immunoprecipitated with anti-flag (Fig 3.7B). However, this was not seen when anti-MuV-P antibody was used for the immunoprecipitation and anti-flag was immunoblotted for (Fig. 3.7A).

To confirm that the interaction was not due to the presence of the recombinant protein with a flag-tag, another immunoprecipitation was performed using cellular RPS6KB1. Cells were transfected with MuV-P and MuV-NP and immunoprecipitated/immunoblotted for MuV-P or RPS6KB1. When anti-RPS6KB1 was immunoprecipitated, MuV-P was coimmunoprecipitated in samples containing MuV-P + MuV-NP and MuV-P + vector suggesting the proteins are interacting, while the MuV-NP + Vector did not show the interaction. The immunoprecipitation of RPS6KB1 was able to pull down MuV-P, however the reciprocal immunoprecipitation (IP: MuV-P, IB: RPS6KB1) did not pull down RPS6KB1 (Fig. 3.7C). Lastly, we confirmed that the interaction occurs during a MuV infection. Vero cells were infected with MuV and after 1 hr, the media was replaced with media containing 1 uM of LY2584702 (tosylate) inhibitor or fresh media. The cells were lysed and immunoprecipitated/immunoblotted for either MuV-P or RPS6KB1. MuV-P was coimmunoprecipitated when RPS6KB1 was immunoprecipitated, while the reciprocal did not appear on the blot (Fig. 3.7D). The inhibitor did enhance the amount of MuV-P and decrease the amount of RPS6KB1 on the immunoblots but did not enhance the interaction as predicted. These results show that

RPS6KB1 and MuV-P interact during transfection and infection, suggesting that RPS6KB1 negatively regulates MuV-P through a direct interaction.

## DISCUSSION

In this study, we performed a large-scale siRNA screen to identify host kinases that affect MuV growth. We found several candidates that enhanced the growth of MuV using a recombinant MuV expressing *Renilla* Luciferase. After assessing the top fifty candidates from the screen, some candidates were chosen for further analysis. Validation of the screen with some of the candidates showed that while the results were not consistent between different cell types or pools of siRNA, RPS6KB1 was consistent throughout these validation steps. Interestingly, in the initial siRNA screen, siRPS6KB1 had a much larger effect on PIV5 than it did on MuV. Upon further investigation with new siRNA against RPS6KB1 and Hap1 cells lacking RPS6KB1, the impact of RPS6KB1 on PIV5 was not consistent. This indicates the importance of validating initial screening results. Although PIV5 and MuV are closely related viruses, the host kinase mechanisms in which they use to replicate within a cell differ somewhat. This was different from previously two other kinases, PLK1 and AKT, which were found to regulate both PIV5 and MuV through similar mechanisms (15-17).

Ribosomal protein S6 kinase beta-1 (RPS6KB1 (referred to in this work), S6K1, p70S6K1) is a member of the AGC subfamily of serine/threonine protein kinases and is encoded by the human gene *Rps6kb1*. The gene mainly encodes two isoforms of the protein, p70 and p85, p70 which localizes to the cytoplasm, is

considered the major isoform and essential for cell cycle progression. RPS6KB1 promotes protein synthesis, cell survival, and growth, and regulates the DNA damage response (225-228). Recently, it has been observed that hyperphosphorylation and/or overexpression of RPS6KB1 is common in many types of cancer, and therefore it has become a target for anti-cancer treatments (229, 230). RPS6KB1 was shown to be essential for optimal viral infection in CD4+ T cells by CCR5-tropic human immunodeficiency virus 1 (HIV1), but a direct phosphorylation of an HIV1 protein was not tested (231). Interestingly, Kaposi's sarcoma-associated herpesvirus (KSHV) encodes a viral protein kinase that is homologous to cellular RPS6KB1, and it was shown that deleting the kinase inhibited the virus lytic replication (232). Lastly, one study found that using Rapamycin, an inhibitor against the mammalian target of rapamycin (mTOR) kinase, which has been shown to phosphorylate RPS6KB1, reduced Rift Valley Fever Virus (RVFV) titers *in vitro* and increased survivability of mice *in vivo* (233). To the best of our knowledge, this is the first time that RPS6KB1 has been shown to interact with MuV P protein and act as a negative regulator of viral replication and transcription.

We examined the effect of RPS6KB1 on MuV growth rates and protein expression using siRNA and an inhibitor. We found that using either mechanism of inhibition was sufficient to increase protein expression and growth rates in a variety of cell lines. Confirmation of this phenotype was performed using a RPS6KB1 knockout Hap1 cell line. While siRNA and inhibitors lose their efficiency over a few days, the cell line has the advantage to allow us to examine the growth

effect for up to seven days post-infection. Furthermore, the modest effect of inhibiting or knocking-out RPS6KB1 was likely due to phosphorylation of P by additional kinases.

The role of RPS6KB1 on replication and transcription was confirmed using a minigenome system, in which viral RNA synthesis could be dissected without involving viral entry and egress. Minigenome activity was increased in the presence of the RPS6KB1-specific inhibitor and in cells lacking RPS6KB1, and both viral vRNA and mRNA synthesis was increased in cells lacking RPS6KB1. Our findings suggest RPS6KB1 negatively regulates the production of new genomic RNA and viral mRNAs causing a decrease in titer and protein expression.

Next, we examined the role of phosphorylation on MuV and found that RPS6KB1 phosphorylates MuV-P. Cells transfected with RPS6KB1-specific siRNA showed a significant decrease in MuV-P phosphorylation, while MuV-NP phosphorylation seemed unaffected. Similar results were observed when the RPS6KB1-specific inhibitor was used (data not shown). Radiolabeling experiments were also performed in the Hap1 cells, but not enough viral protein was produced in the labeling period to produce quantifiable data (data not shown). However, we expect a greater effect would have been seen in the RPS6KB1 knockout cells. Interestingly, cells with reduced RPS6KB1 seem to have increased MuV-P and MuV-NP interactions suggesting that RPS6KB1 may interfere with MuV viral RNA polymerase complex formation or binding of MuV-P to MuV-NP, although this needs to be further explored.

Lastly, we examined the interaction between RPS6KB1 and MuV and found that it binds to the MuV-P protein. The P-RPS6KB1 interaction was examined in three different systems to ensure the validity of the interaction. First, a recombinant RPS6KB1 protein containing a flag tag was transfected into cells along with MuV-P and NP, and the interaction was observed using either anti-MuV P or anti-Flag. To confirm that MuV-P was binding to RPS6KB1 and not the Flag tag, we performed another immunoprecipitation using cellular RPS6KB1. Since most cell culture lines are cancer cell lines, RPS6KB1 is naturally upregulated and highly expressed in many lines making it easy to detect by western blot (225). One pitfall of using cellular RPS6KB1 is that the anti-MuV-P antibody does not coimmunoprecipitate the cellular RPS6KB1form, but the anti-RPS6KB1 antibody does coimmunoprecipitate MuV-P. Although MuV-NP is not required for the P-RPS6KB1 interaction, it appears to enhance the interaction. This also occurs with another kinase that negatively regulates MuV growth, PLK1 (11). Lastly, we confirmed the interaction occurs during a viral infection in cell culture. In our previous work, it was noted that the addition of a kinase inhibitor may help prolong the interaction with its counterpart, so the RPS6KB1-specific inhibitor was added post-infection to determine whether it enhanced the interaction (16). The presence of the inhibitor, however, did not seem to have any effect on the RPS6KB1-P interaction. Taken together, we speculate that RPS6KB1 negatively regulates MuV growth by binding to MuV-P and effecting subsequent phosphorylation.

We speculate that RPS6KB1 phosphorylates MuV by binding to the P protein. However, the site(s) of the interaction has not yet identified. Since

RPS6KB1 is an AGC kinase it has conserved binding motif, R/L-X-R-X-X-S/T, which is found in MuV-P in two locations in the MuV-P N terminal domain (NTD) and partially found (R-X-X-S/T) once in the C terminal domain (CTD) (234). Future studies will focus on elucidating interactions between RPS6KB1 and P, as well as the role of NP in this interaction.

Understanding the mechanism by which a host kinase can regulate viral replication is a useful tool and has translational applications. Kinases that positively regulate viruses can be used as potential antiviral drugs, many of which are already FDA approved and used as cancer treatments, while kinases that negatively regulate viral replication can be used to enhance viral vaccine yields in cell culture. To the best of our knowledge, this is the first time RPS6KB1 has been shown to negatively regulate a virus. We speculate that MuV uses RPS6KB1 to downregulate its viral transcription and replication to prevent overproduction of viral proteins and progeny virions within a host, which would activate the innate immune system and eventually clear of the infection. MuV uses the MuV-V protein in tandem with host kinase phosphorylation to balance its replication within a host. Since RPS6KB1 could be knocked-out in a Hap1 cell line, it suggests that other cell lines could also have RPS6KB1 knocked-out. As MuV growth is highly regulated by type I IFNs, developing a RPS6KB1 knockout in an IFN-deficient cell line, such as Vero cells, would be beneficial (235). A cell line lacking RPS6KB1 may enhance the growth of MuV for vaccine production.

**ACKNOWLEDGMENTS**

We appreciate the helpful discussion and technical assistance from members of Biao He's laboratory and to Ashley Beavis for her inciteful discussions and critical reading of the manuscript. This work was supported by a grant from National Institutes of Health (R01AI 097368) and endowment of Fred C. Davison Distinguished University Professor in Veterinary Medicine to B.H.

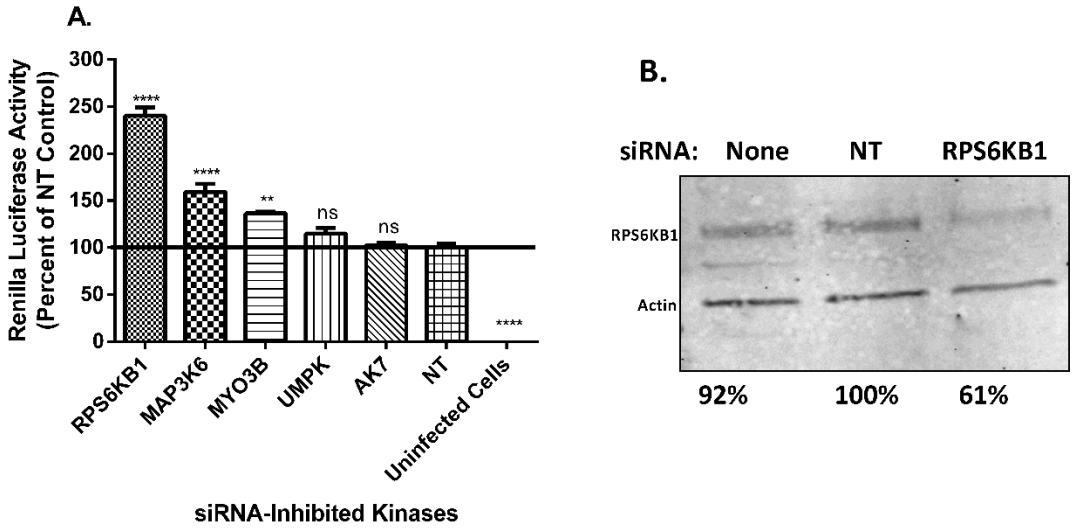


**Figure 3.1. Examination of kinases on MuV replication.** (A) Effects of siRNA targeting kinases on MuV replication. HeLa cells were transfected with 2 different siRNAs targeting different sequences of each kinase mRNA transcript. The next day, cells were infected with rMuV-rluc at a MOI of 0.1. 24 HPI, cells were lysed, and luciferase was measured. Values were normalized to the non-target control (NT). (B) Detection of RPS6KB1 using western blot analysis. Lysates from the luciferase assay were collected, replicates were combined, and mixed with loading buffer before being resolved by SDS-PAGE and immunoblotted using an anti-RPS6KB1 and anti-actin antibody. The values were normalized to the non-target control. Error bars represent standard error (SEM) with 3 replicates each, individual experiments were performed 3 independent times. P values were calculated by one-way ANOVA* $P < 0.05$, ** $P < 0.01$, *** $P < 0.001$, **** $P < 0.0001$

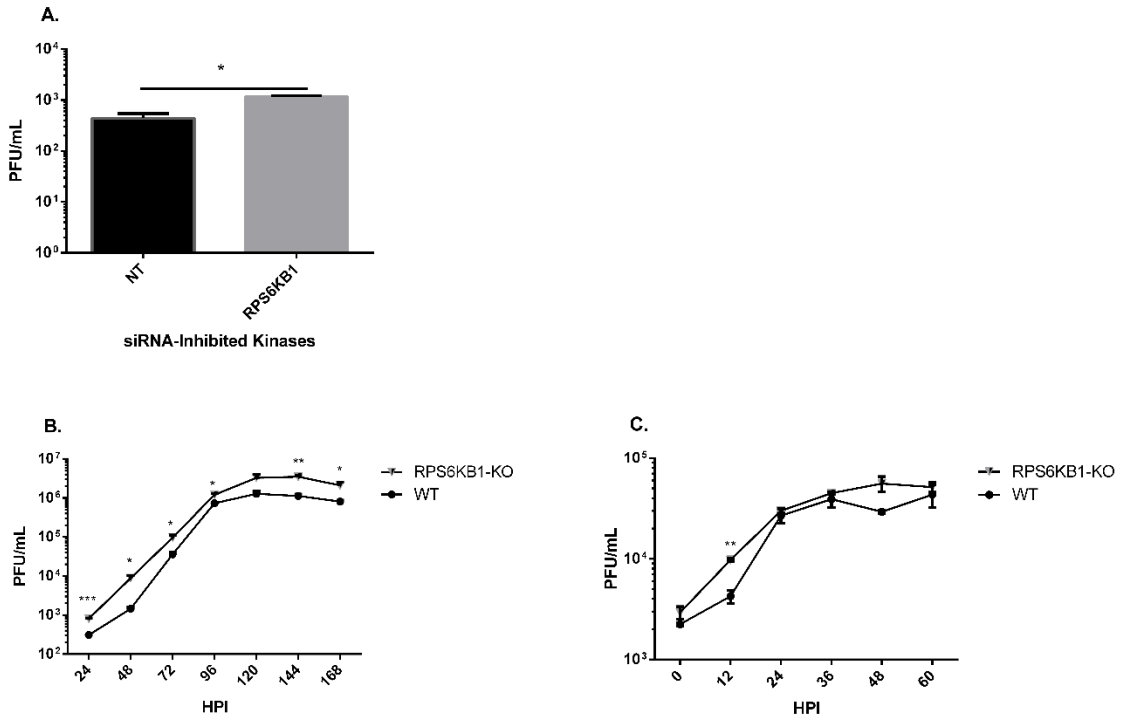


**Figure 3.2. Growth rates of MuV in cells with a RPS6KB1 deficiency**. (A) Growth of MuV in siRNA-knocked down RPS6KB1 HeLa cells. Cells were transfected with RPS6KB1 specific siRNAs, as previously described, and then infected with MuV at a MOI of 0.1. Media was collected 24 HPI, and plaque assays were performed to determine viral titers. (B) Multi-step growth curve of MuV in wildtype (WT) and RPS6KB1 knockout (RPS6KB1-KO) Hap1 cells. Cells were infected at a MOI of 0.1, and media was collected every 24 hrs for plaque assay. (C) Single-step growth curve of MuV in WT and RPS6KB1-KO Hap1 cells. Cells were infected at a MOI of 3, and media was collected every 12 hrs for plaque assay. P values were calculated using Multiple T tests. * $P < 0.05$, ** $P < 0.01$, *** $P < 0.001$. Error bars represent SEM of data from 3 replicates. Individual experiments were performed 3 times.

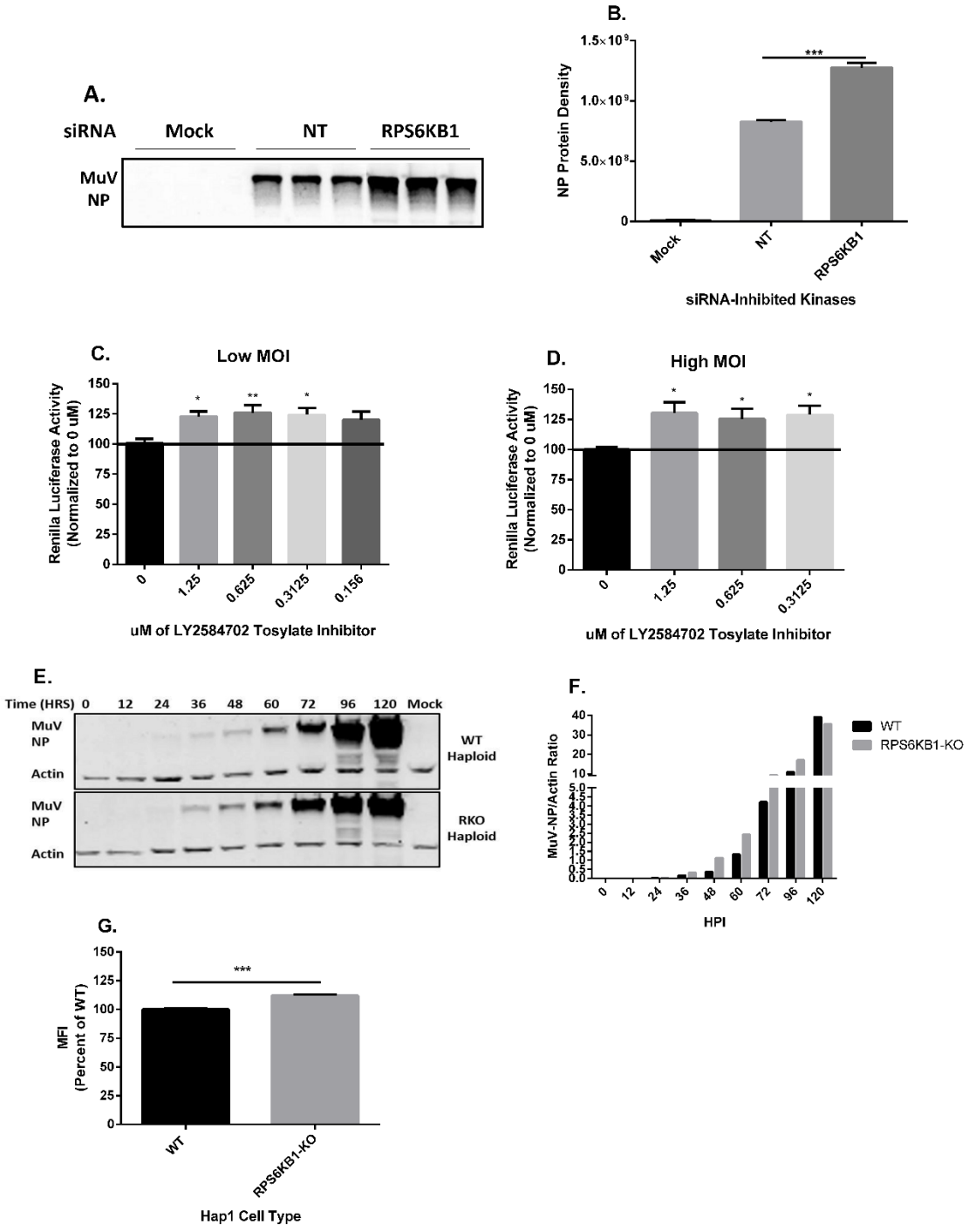


**Figure 3.3. Effects of inhibiting RPS6KB1 on MuV protein expression**. (A) Detection of MuV NP protein expression in siRNA-transfected HeLa cells at 24

HPI. HeLa cells were transfected with siRNA, then infected at MOI 0.1 with MuV 24 hours post-transfection in triplicate. Lysates were resolved by SDS-PAGE and immunoblotted using a monoclonal anti-MuV-NP antibody. A representative blot is shown. (B) Summary of quantified NP protein density from WB. (C,D) Luciferase activity of MuV using LY2584702 Tosylate Inhibitor, a RPS6KB1 specific inhibitor, in HeLa cells at a MOI of 0.1 (low) and 3 (high) respectively. Cells were infected, 1 HPI the media was replaced with differing concentrations of the inhibitor. At 24 HPI, cell lysate luciferase activity was quantified and normalized to the luciferase activity of cells treated with 0 uM inhibitor. Error bars represent SEM of data from 4 replicates. (E) Detection of MuV NP expression in WT and RPS6KB1-KO Hap1 cells. Cells were infected MuV at a MOI of 0.1 Lysates were collected at each timepoint, resolved by SDS-PAGE and both MuV NP and actin were immunoblotted for. Actin served as a loading control. A representative blot is shown. (F) Summary of quantified NP protein density from WB. The relative NP protein density was calculated by taking the ratio of NP to actin, and the graphed to compare protein expression between WT and RPS6KB1-KO Hap1 cells. Values represent one experiment of three independent experiments. (G) Flow cytometry analysis of WT and RPS6KB1-KO Hap1 cells infected with MuV at a MOI of 0.1. 24 HPI, cells were fixed and stained with an anti-MuV-NP antibody to measure the mean fluorescence intensity (MFI) of infected cells. Values were standardized to the infected WT Hap1 cell values. Error bars represent SEM of data from 4 replicates. P values were calculated by one-way ANOVA or Student *t* test. * $P < 0.05$, ** $P < 0.01$, *** $P < 0.001$. Individual experiments were performed 3 times.

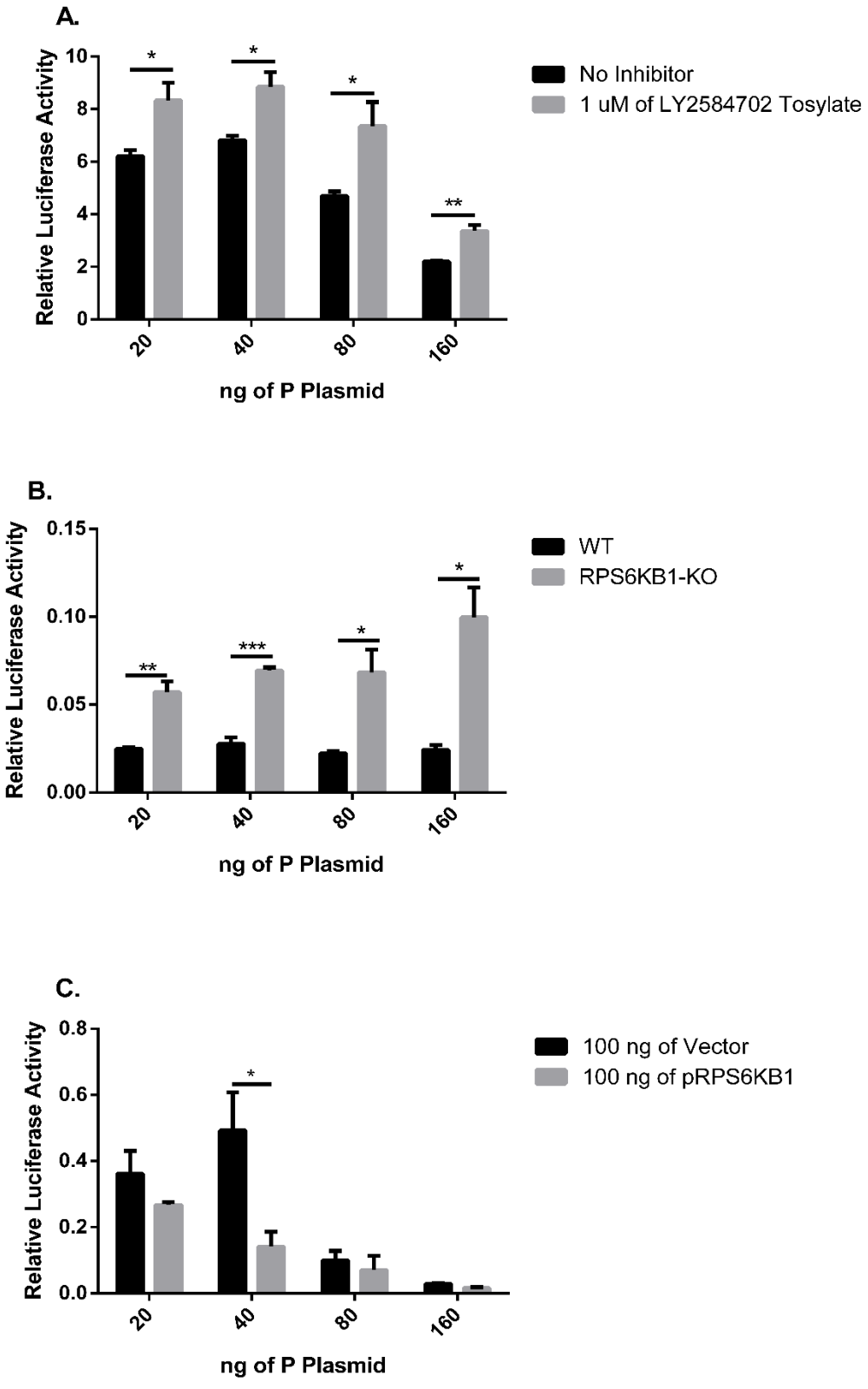
A.
Relative Luciferase Activity
10
8
6
4
2
0
*
*
*
**
20
40
80
160
ng of P Plasmid
No Inhibitor
1 uM of LY2584702 Tosylate
B.
Relative Luciferase Activity
0.15
0.10
0.05
0.00
**
***
*
*
20
40
80
160
ng of P Plasmid
WT
RPS6KB1-KO
C.
Relative Luciferase Activity
0.8
0.6
0.4
0.2
0.0
*
20
40
80
160
ng of P Plasmid
100 ng of Vector
100 ng of pRPS6KB1

**Figure 3.4. MuV Minigenome activity in the absence of RPS6KB1**. (A) MuV minigenome activity in the presence of an RPS6KB1 inhibitor. BSR-T7 cells were either mock treated or treated with 1 uM of a RPS6KB1 specific inhibitor, LY2584702 Tosylate. (B) MuV minigenome activity in RPS6KB1-KO Hap1 cells compared to WT Hap1 cells. (C) MuV minigenome activity with over-expressed RPS6KB1. 100 ng of a vector control or plasmid containing RPS6KB1 were transfected into BSR-T7 cells. The ratio of *Renilla* luciferase to firefly luciferase activity was calculated and graphed. Multiple concentrations of the MuV-P plasmid were transfected (20, 40, 80, and 160 ng/well) to obtain optimal minigenome activity. P values were calculated using Multiple T tests. * $P < 0.05$, ** $P < 0.01$, *** $P < 0.001$. Error bars represent SEM of data from 3 replicates. Individual experiments were performed 3 times.

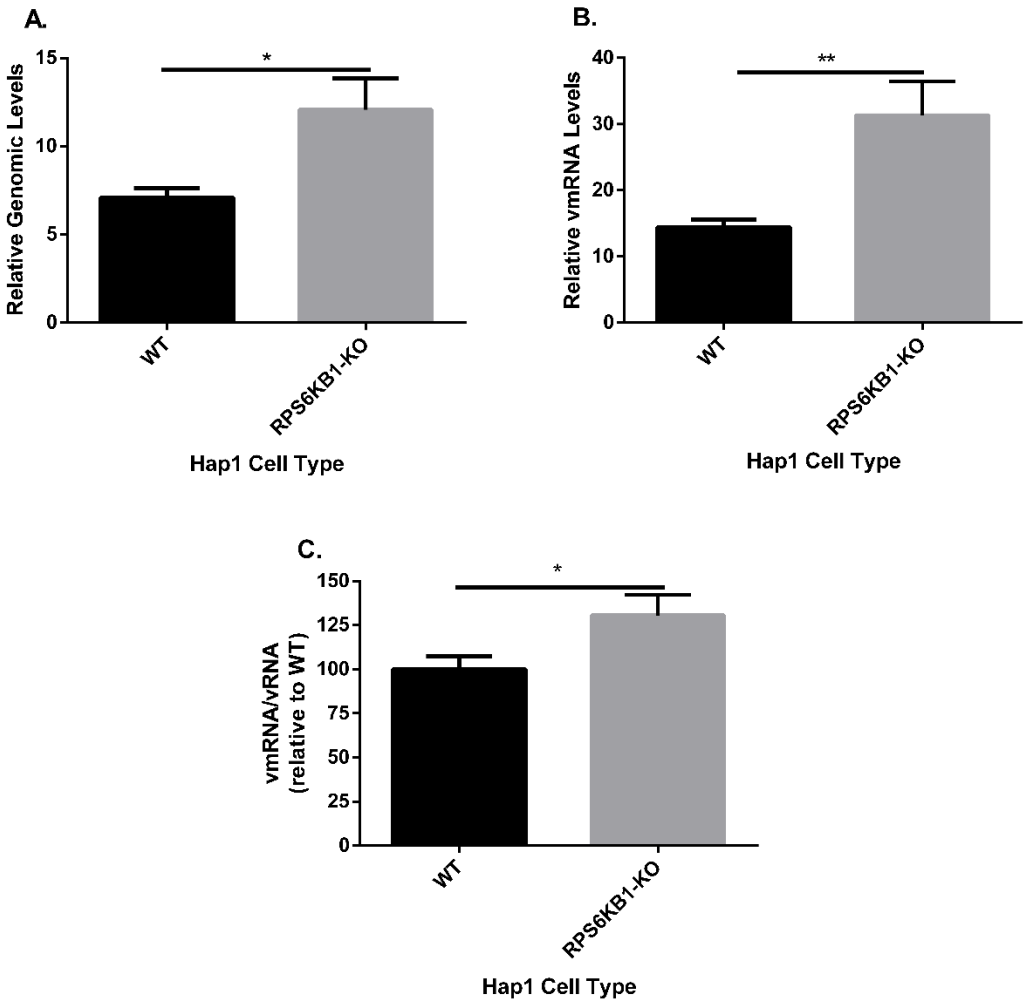


**Figure 3.5. Viral RNA synthesis in cells with RPS6KB1 deficiency.** Cells were infected at a MOI of 5 and total RNA was collected from 4 independent samples at 2 and 24 HPI. (A) Genome replication of MuV (vRNA) in WT and RPS6KB1-KO cells. Genome-specific primers were used to detect genomic RNA. (B) MuV viral mRNA. Oligo(dT) primers were used to generate mRNAs. (C) Relative vmRNA to genomic RNA. The ratio of vmRNA to genomic vRNA was calculated and then normalized to the WT Hap1 control. A MuV-F specific probe was used for real-time PCR after cDNA synthesis. Values were calculated after normalization to genomic

RNA levels at 2 HPI. P values were calculated using Multiple T tests. * $P < 0.5$, ** $P < 0.01$. Error bars represent SEM of data from 4 replicates from 3 individual experiments.

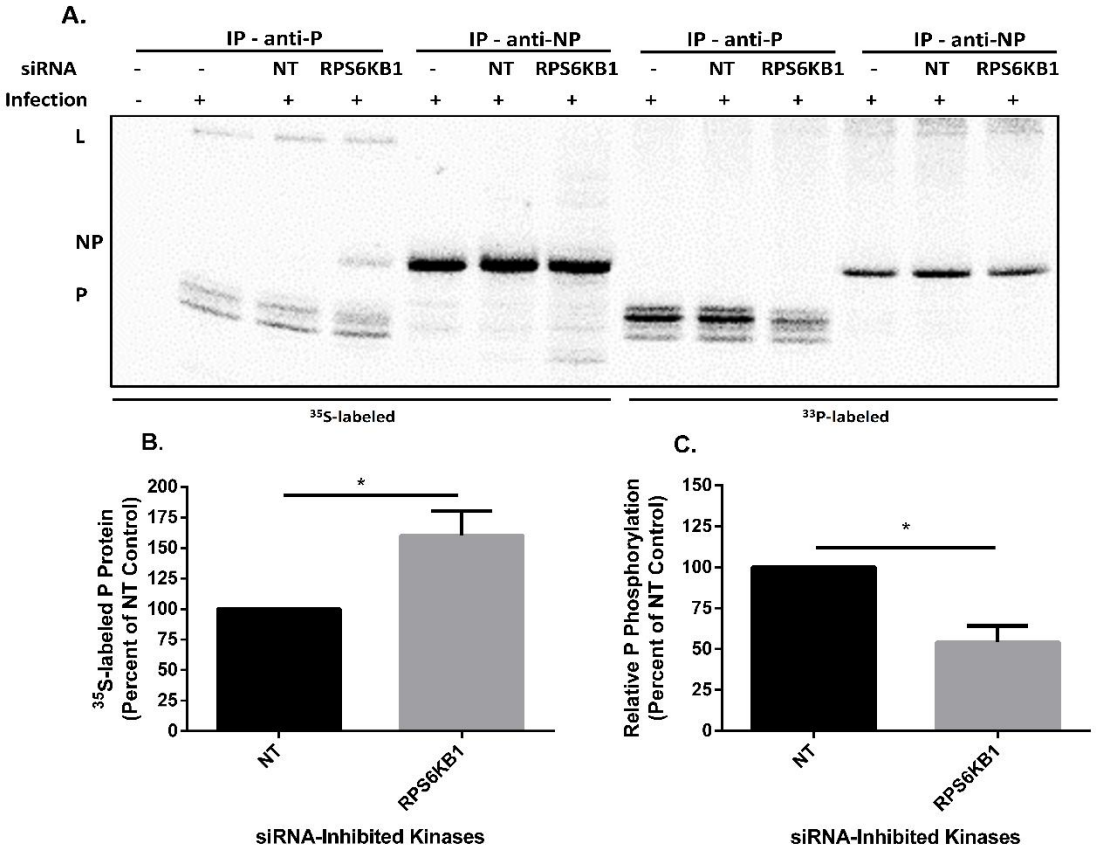


**Figure 3.6. MuV-P and -NP Phosphorylation in cells with a RPS6KB1 deficiency.** (A) Representative radio blot. HeLa cells were transfected with siRNA, infected with MuV at a MOI of 0.1, and then labeled with $^{35}S$ or $^{33}P$ for 6-8 hrs. Cell lysates were immunoprecipitated with monoclonal anti-MuV-P or anti-MuV-NP antibody and resolved by SDS-PAGE gel. (B) Total P protein quantification. $^{35}S$ labeled P protein from infected HeLa cells. Values were standardized to the non-target control. (C) Relative phosphorylation level of P in infected cells. The relative level was calculated as a ratio of phosphorylated protein ($^{33}P$) to total protein ($^{35}S$) and standardized to the non-target control. P values were calculated using Student's t test. * $P < 0.5$, ** $P < 0.01$. Error bars represent SEM of data from 3 individual experiments.

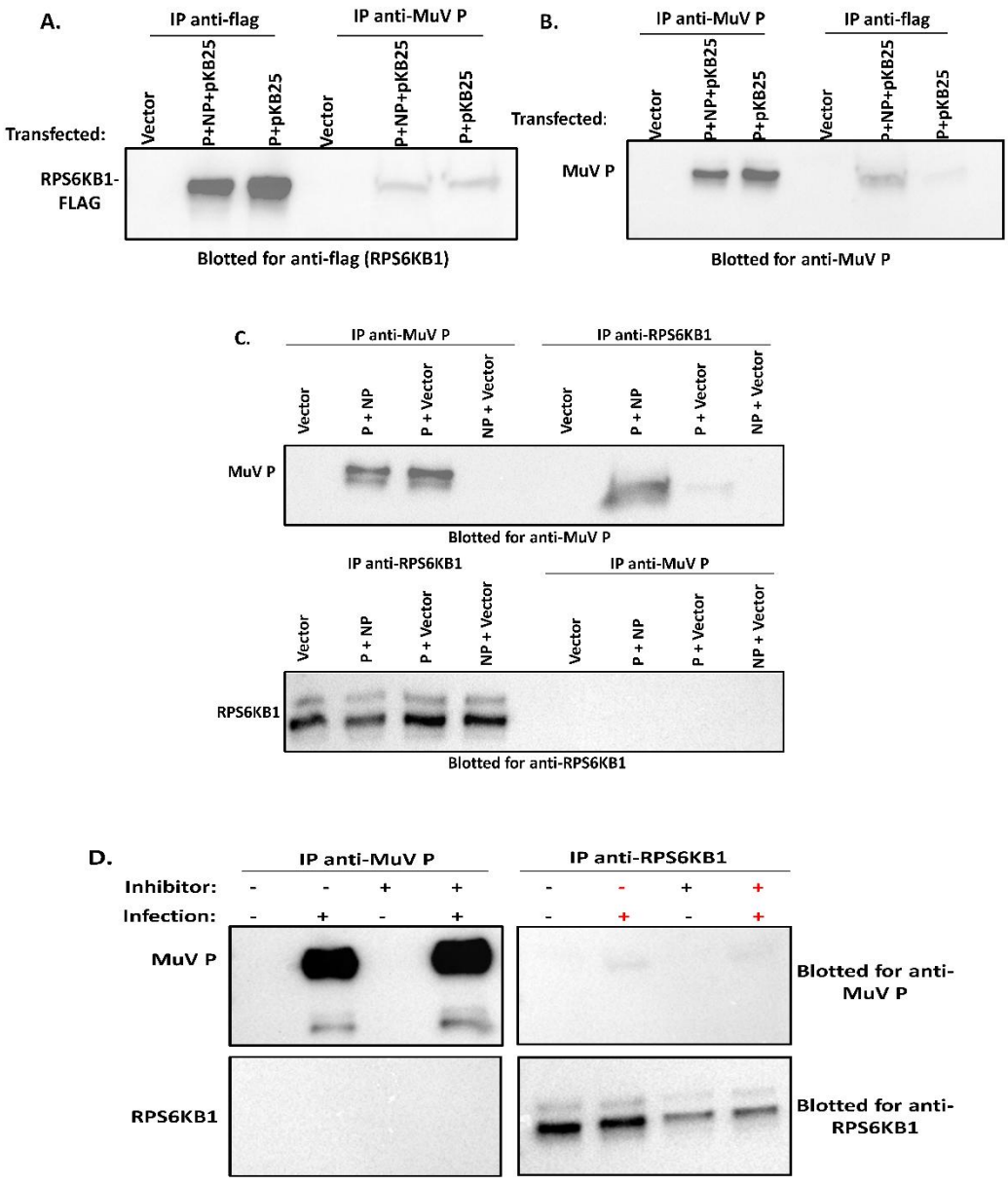


**Figure 3.7. MuV P and RPS6KB1 interact.** (A-B) 293T cells were transfected with plasmids containing MuV-P, MuV-NP, and RPS6KB1-Flag (pKB25). The cells were lysed and then immunoprecipitated with either monoclonal anti-MuV-P or monoclonal anti-Flag. (A) Lysates were blotted for anti-flag. (B) Lysates were blotted for anti-MuV-P. (C) 293T cells were transfected with plasmids containing

MuV-P and/or MuV-NP. The cells were lysed and then immunoprecipitated and immunoblotted with either monoclonal anti-MuV-P or monoclonal anti-RPS6KB1. (D) Vero cells were infected with MuV at a MOI of 0.1, after 1 hr the inoculum was replaced with media containing 1 uM of LY2584702 Tosylate Inhibitor or fresh media. 24 HPI, cells were lysed and immunoprecipitated and immunoblotted with either monoclonal anti-MuV-P or monoclonal anti-RPS6KB1. Each experiment was performed 3 independent times, a representative blot is shown for each.

# CHAPTER 4

# IDENTIFICATION OF PHOSPHORYLATION SITES IN THE LARGE PROTEIN OF MUMPS VIRUS

## ABSTRACT

Mumps virus (MuV) is a human pathogen that causes an acute infection with the hallmark symptom as the enlargement of the parotid gland. Mumps is highly neurotropic, therefore, severe complications including meningitis and encephalitis, can occur. While vaccination against mumps effectively reduces cases, outbreaks still occur. MuV is a paramyxovirus with a negative-sense nonsegmented RNA genome. The viral RNA genome is encapsidated by the nucleoprotein (NP) to form the helical ribonucleoprotein (RNP), which serves as a template for transcription and replication. The viral RNA-dependent RNA polymerase (vRdRp) minimally made up of the phosphoprotein (P) and large (L) protein, is responsible for transcription and replication of the viral genome. To investigate the function of MuV L, we developed a tool to study the protein during an infection. Using an internal flag tag in MuV L, we identified four putative phosphorylation sites using liquid chromatography mass spectrometry (LC-MS/MS). We mutated the sites to alanine and examined L-S1087A,T1088A in a minigenome system. We found that L-S1087A,T1088A had decreased minigenome activity, suggesting they play an important role in MuV RNA synthesis.

## INTRODUCTION

Mumps virus (MuV) is a highly contagious human pathogen. The hallmark symptom of MuV is the enlargement of the parotid gland, however severe complications can occur (6, 10). Symptoms range from asymptomatic to severe encephalitis, but the most common symptoms include fever, headache, and

muscle aches. Symptoms typically appear 16-18 days after infection and can last for up to two weeks (2). In the pre-vaccine era, MuV was the leading cause of viral meningitis and encephalitis due to its highly neurotropic nature. After the introduction of the MuV vaccine in the late 1960's, cases dramatically decreased (6). Currently, the best prevention for MuV is the Measles, Mumps, and Rubella (MMR) vaccine, which is given in early childhood. Unfortunately, MuV has reemerged in the last few decades. Several outbreaks have occurred worldwide, with a large proportion of them occurring in vaccinated populations (2, 213). There is no approved treatment for mumps beyond supportive care (2). Understanding MuV replication is critical for developing antiviral treatments.

MuV is a non-segmented, single-stranded negative-sense (NNS) RNA virus in the family *Paramyxoviridae* and order *Mononegavirales.* The genome has 7 genes that encode for 9 viral proteins (3'-NP-V/P/I-M-F-SH-HN-L-5') with RNA synthesis beginning at the 3' end. Paramyxoviruses use a mechanism known as start-stop transcription, which creates a transcriptional gradient of the viral mRNAs produced, therefore genes near the 3' end of the genome are transcribed more frequently than the genes at the 5' end (9, 38). The RNA genome serves as a template for both viral genomic RNA and viral mRNA synthesis and is encapsulated by nucleoprotein (NP), creating the helical ribonucleoprotein (RNP), which protects the genome from degradation. The phosphoprotein (P) helps shuttle the RNP to the RNA-dependent RNA polymerase (vRdRp), which minimally consists of the P and large (L) proteins. The complex can than initiate transcription using the viral genome as a template to produce more viral protein. For

paramyxoviruses, it is hypothesized that the switch from transcription to genome replication is driven by the accumulation of NP protein because large amounts are required to protect the viral genome (3, 101, 236, 237). During genome replication, an antigenome copy of the genome is generated, which serves as a template for more genomic RNA (11). While it is known that transcription and replication are two distinct processes, the initiation and regulatory mechanisms are poorly understood.

The polymerase, or L protein, in the order *Mononegavirales* is highly conserved. It is a multi-functional enzyme that contains catalytic centers required to perform both replication and transcription of the viral genome and has auxiliary functions like mRNA capping and methylation (10, 238). Its enzymatic activities are essential for virus replication and have recently become a large target of anti-viral drugs (101, 110, 111). Early studies using sequence alignment identified six conserved regions (CR), which contain critical motifs for NNS polymerases (19, 102, 103). CRI mainly contains hydrophobic regions and has been shown to be involved in oligomerization of P and L (96, 97, 102). CRII is rich in charged, basic amino acids and forms a KEKE-K motif (102). CRIII has several charged amino acids and a conserved GDN motif (101, 102, 239). CRIV is conserved with invariant proline residues but does not have a known function (102). CRV contains the motif, $GXXT_nHR$, which mediates the unique viral capping of mRNA (101, 217, 240). CRVI has a methyltransferase motif, K-D-K-E, which is responsible for methylating the first nucleotide product and residue N7 of the cap (102, 241, 242).

Although the structure of MuV L is unknown, L structures have been solved for respiratory syncytial virus (RSV), vesicular stomatitis virus (VSV), and parainfluenza virus 5 (PIV5) allowing for a more thorough examination of the protein and its function. More recent structural studies had identified five conserved domains (Figure 4.1). They are the RNA-dependent RNA polymerase domain (RdRp), which contains CRI-III, and is responsible for P/L oligomerization, RNA binding, and phosphodiester bond formation. This domain makes up the N-terminal portion of the protein and is responsible for the polymerase activity (101, 217, 239). The polyribonucleotidyltransferase domain (PRNTase) contains region CRIV and CRV and is responsible for addition of the 5' cap to nascent viral mRNAs (101, 240). The connecting domain (CD) is not known to have any enzymatic activity but is critical for proper function. Although is it less conserved than the other domains, mutational studies have shown that insertions in this region result in no L activity (106). The methyltransferase domain (MTase) contains CRVI and is responsible for methylating the cap (101, 102). While the last domain, the C-terminal domain (CTD), contains a conserved guanylyl transferase (GTase) motif, it is the least conversed domain and structurally divergent (241).

Structural analyses of multiple NNS polymerases have shed light on L's role in RNA synthesis, but other functions have not been thoroughly investigated. plays a role in pathogenesis in New Castle Virus (NCV) and J paramyxovirus (JPV) (100, 243, 244). Additionally, we previously found that PIV5 L mRNA can activate IFN-β through MDA5, a viral sensor (59). These studies suggest that in addition to RNA synthesis, L has other unknown functions.

*In vitro* studies of L with full-length viruses have traditionally been challenging because of its low abundance and lack of immunological reagents (101, 104, 245). Different methods have been employed to study the function of L. For example, Matsumoto *et al.*, used a minigenome system to identify four key amino acids in L that are involved in nucleotidyl transfer using a PIV5 minigenome, while Munday *et al.* used enhanced green fluorescent protein (EGFP)-tagged L and P proteins to identify RSV-host interactions via *in vitro* transfections (238, 246). Other studies have mutated different regions of L and observed the growth phenotype in a full-length MuV virus but lack protein-based studies of L (111). Attempts at adding an N-terminal or C-terminal to MuV L have failed to produce a functional L protein (unpublished data). Two different morbilliviruses, measles virus (MeV) and rinderpest virus (RPV), tolerate a tag or GFP protein in a flexible region upstream of the MTase domain within L. Both viruses were rescued using with an internal tag/protein and had detectable L protein by western blot analysis and immunofluorescence (20, 247).

While much of the work on L has been with PIV5 or VSV, identifying residues/regions in L that affect the growth of MuV has been largely neglected. This work emulates the internal tag strategy and rescues a full-length MuV virus to examine L function. Additionally, this work identifies 4 putative phosphorylation sites within MuV L and tests their function in a minigenome system.

## MATERIALS AND METHODS

### Cells

293T cells were maintained in Dulbecco's modified Eagle medium (DMEM) with 5% fetal bovine serum (FBS) and 1% penicillin-streptomycin (P/S) (Mediatech Inc). Vero cells were maintained in DMEM supplemented with 5% FBS and 1% P/S. BSR-T7 cells were maintained in DMEM supplemented with 5% FBS, 1% P/S, 10% tryptose phosphate broth (TPB), and 400 µg/ml G418 sulfate antibiotic (Mediatech Inc.). Cells were passed at an appropriate dilution 1-2 days prior to use in order to achieve 80% - 90% confluence upon infection or 60% - 80% confluence upon transfection. 293T and BSR-T7 cells were used for transfection experiments, Vero cells were used for infection experiments.

### Construction of L-H2(flag) construct

The insertion of an internal flag tag was adapted from Duprex *et al.*, who inserted a tag into the flexible hinge two (H2) region of measles virus (20). The placement of the flag tag was determined using sequence alignments of various negative sense RNA polymerases to determine the hinge region of each, including Measles virus, mumps virus, PIV5, and VSV. The flag tag was inserted after amino acid 1723 in the H2 region of MuV L using PCR and Gibson assembly. The fragments were subsequently cloned into the pCAGGS expression vector, and a full-length plasmid contained the MuV genome.

### Rescue of virus

To produce the recombinant viruses, the MuV-specific reverse genetics system previously established in the lab was used (8, 25, 61). In brief, the full-

length genome plasmid and plasmids encoding for the MuV replication machinery (pCAGGS containing NP, P, L, or T7) was transfected into 293T cells using lipofectamine 3000 reagents (Thermo Fisher Scientific). At 24 hours post transfection (HPT), the 293T's were co-cultured with fresh Vero cells at a 1:2 ratio. The rescue was monitored until syncytia formed, and the media was collected, and plaque purified. A large stock of each virus was propagated in Vero cells and sequenced to verify the viruses.

**Minigenome assay**

BSR-T7 cells in 24-well plates were transfected with pCAGGS-NP (25 ng), pCAGGS-P (40 ng) pMG-rLuc (100 ng), pFLuc (1 ng), and the various pCAGGS-L constructs (500 ng). A ΔL negative control was used and pCAGGS-GFP was used instead of pCAGGS-L. After 24 or 48 hours, cells were lysed in 100 µl passive lysis buffer (Promega) and vigorously shaken for 10 min to permit full lysis. Lysates (50 µl) from each well were used to carry out the dual-luciferase assay according to the manufacturer's protocol (Promega), and light intensity was detected using a GloMax 96 Microplate Luminometer (Promega). Relative luciferase activity was defined as the ratio of *Renilla* luciferase (R-Luc) to firefly luciferase (FF-Luc) activity. Three replicates of each sample were used to compare the peak activity of WT-L with each of the mutant Ls. JetPRIME was used to transfect cells with plasmids according to the manufacturer's protocols (Polyplus Transfection Inc.)

**Growth curves**

Vero cells were infected in triplicate with the MuV L constructs at a low (0.01) and high MOI (1). Low MOI timepoints were taken every 24 hours for 7 days

and high MOI timepoints were taken every 12 hours for 60 hours. At each timepoint samples were mixed with 10X sucrose phosphate glutamate (SPG), and flash frozen to preserve titers. Plaque assays were performed on all samples in Vero cells to determine viral titers. After 7 or 8 days, cells were fixed with 2% formaldehyde and stained with crystal violet to count the plaques.

**qPCR**

Vero cells were infected at a high MOI with the L-H2(flag)-L1759S or L-H2(flag) virus, and a mock-infection was used as a negative control. RNA extractions on the cells were performed at 2, 24 and 48 HPI for each virus. cDNA was generated via reverse transcription using Super Script III reverse transcriptase (Invitrogen). mRNA cDNA was be generated using Oligo(dT)15 (Invitrogen) to amplify all mRNA sequences in the sample, and genomic RNA cDNA was generated using a vRNA-specific primer for the MuV F gene. Synthesized cDNAs were used for quantitative real-time PCR (qPCR), and a MuV HN primer/probe was used to assess viral mRNA and vRNA. Values were normalized to the genomic vRNA at 2 HPI. The ratio of mRNA to vRNA at 24 HPI was calculated.

**Immunoblot**

Cell lysates were mixed with 2X Laemmli sample buffer with β-mercaptoethanol (Bio-Rad Laboratories, Inc) and heated at 95°C for 5 min. Samples were resolved in 10% SDS-PAGE and transferred to a polyvinylidene difluoride membrane (Bio-Rad Laboratories, Inc). Immunoblotting, using monoclonal MuV protein-specific antibodies, was performed as previously described (8). The membrane was incubated with mouse anti-MuV-NP antibody

(1:2500 dilution), mouse anti-MuV-P antibody (1:2000 dilution), or mouse anti-Flag™ antibody (1:2000) Flag (M2 clone; Sigma-Aldrich, St. Louis, MO), followed by incubation with Cy3-conjugated goat anti-mouse IgG secondary antibody (1:2500 dilution) (Jackson ImmunoResearch, West Grove, PA), and imaged using a Typhoon 9700 imager (GE Healthcare Life Sciences). Rabbit anti-Actin (1:2500) (Sigma-Aldrich) was used to blot for actin as a loading control.

**Immunoprecipitation & LC-MS/MS**

Immunoprecipitation of MuV L was performed by infected Vero cells at a high MOI with rMuV-L-H2(flag). At 48 HPI, cells were lysed in 1 ml WCEB with a mixture of protease inhibitors. The lysates were immunoprecipitated overnight at 4°C using recombinant protein G-Sepharose 4B conjugated beads with mouse anti-Flag™ Flag (M2 clone; Sigma-Aldrich). Lysates were washed 3X with WCEB buffer and 2X with PBS to remove excess buffer than resuspended with 2X Laemmli sample buffer with β-mercaptoethanol (Bio-Rad Laboratories) and heated at 95°C for 5 min. The samples were run on a 10% acrylamide gel by SDS-PAGE and stained using Coomassie blue G250 following the manufacturer's instructions. The L band was excised and frozen at -80ºC until use.

The excised L band was sent to the Mass Spectrometry and Proteomics W.M. Keck Foundation Biotechnology (Yale University, New Haven, CT) for processing and analysis. In brief, the protein was digested with trypsin (71% coverage), enriched for phosphoproteins on a $TiO_2$ column (11% coverage), both the enrichment and flow through were analyzed using liquid chromatography-tandem mass spectrometry (LC-MS/MS). Analysis was performed using a

MASCOT search (Matrix Science) against the NCBInr database and the MuV L-H2(flag) sequence provided. Phosphorylated peptides were considered significant with a random probability score of less than 5%, when possible, the PhosphorRS score was used to determine which residue (if multiple S/T) was phosphorylated. The phosphorylation sites were confirmed using NetPhos 3.1 (https://services.healthtech.dtu.dk/service.php?NetPhos-3.1).

**Immunofluorescence**

Colocalization of MuV P and L during an infection was observed by infected 12-well Vero plates with either WT MuV, rMuV-L-H2(flag) and rMuV-L-H2(flag)-L1759S. A mock infected was used as a negative control. Cells were infected at a high MOI for 24 and 48 hours. Each well contained a microscope coverslips. They were fixed with 2% formaldehyde and permeabilized with 0.1% triton for 20 min each. Blocking was performed using 3% BSA in PBS for 20 minutes. A mouse anti-MuV-P antibody and rabbit anti-Flag antibody were incubated on each sample for 1 hour in 1% BSA in PBS. Cells were washed with 3% BSA in PBS to remove excess primary antibody and incubated with Cy3-conjugated goat anti-rabbit IgG and FITC-conjugated goat anti-mouse for 1 hour. After the secondary incubation, the cells were washed 3X with 3% BSA in PBS and 2X with PBS. The coverslips were removed and mounted onto microscope slides using ProLong® Diamond Antifade Mountant with DAPI (Life technologies) and left to dry overnight. The next day the slides were imaged using a Nikon A1 confocal microscope.

## RESULTS

### Development and expression of MuV L containing an internal flag tag

MuV L is a 2,261 amino acid long protein. Traditional methods to develop an L antibody were unsuccessful. Additionally, epitope tags on the amino-terminal or carboxy-terminal end of the protein sequence resulted in a nonfunctional L protein (data not shown). To study MuV L function, we inserted a 1X flag tag (DYKDDDDK) into the H2 region of the L protein (Fig 4.1). Two NotI sites were introduced on each side of the tag for cloning purposes. An extra nucleotide (T) was added to the 3' end of the insert to follow 'rule of six' (Fig 4.2A) (248). To determine the optimal location for the insert, the MuV L protein sequence was aligned with MeV L (with and without internal tag) and the insert was placed after MuV L residue S1723 (20). Alignments were performed using tree-based consistency objective function for alignment evaluation (T-coffee) alignment and a sequence alignment by Sidhu *et al.* 1992 (19). Gibson cloning was used to assemble the L protein in a pCAGGS expression vector. Plasmids were confirmed by sequencing (Fig 4.2B).

To test the expression of the L-H2(flag) construct, an IFA and western blot were performed. 293T cells were transfected with either a plasmid containing WT L, L-H2(flag) or RPS6KB1-flag as a positive control. After 48 hours, cells were lysed and resolved by SDS-PAGE. A mouse anti-flag antibody was used to detect L protein expression. L, by way of the flag tag, was detected in the L-H2(flag) sample, but it was not detected in WT L or the mock (Fig 4.3A). 293T cells were transfected with either WT L or L-H2(flag), and at 48 hours post transfection, cells

were fixed and stained with a mouse anti-flag antibody and a CY3-conjugated anti-mouse secondary to detect L expression. L positive cells were observed by microscopy (Fig 4.3B). To ensure the flag tag did not disrupt L function, a previously-developed minigenome system was used (4). BSRT7 cells were transfected with pCAGGS-NP, pCAGGS-P, pMG-rLuc under T7, pCAGGS-fLuc, and either pCAGGS-WT L, pCAGGS-L-H2(flag) or no L (ΔL). The ratio of *Renilla* luciferase to firefly luciferase (transfection control) was calculated and graphed. L-H2(flag) had similar luciferase activity to WT L, suggesting the inserted flag tag did not hinder L function (Fig 4.3C).

**PIV5 L containing an internal flag tag has no minigenome activity**

The same strategy that was used to develop a MuV L containing an internal flag tag was used for PIV5 L. To test expression of the PIV5 L-H2(flag), 293T cells were transfected with either empty pCAGGS or two different L-H2(flag) plasmids (pKB33-4 and pKB33-8), and at 48 hours post transfection, cells were fixed and stained with a mouse anti-flag antibody and a CY3-conjugated anti-mouse secondary to detect L expression. L positive cells were observed by microscopy (Fig 4.4A). To test that the flag tag did not disrupt L function, a minigenome assay was performed. The ratio of *Renilla* luciferase to firefly luciferase (transfection control) was calculated and graphed. Transfection of either PIV5 L-H2(flag) plasmid resulted in no minigenome activity, suggesting the flag tag hinders proper L function (Fig 4.4B).

**Generation and characterization of recombinant MuV**

After confirming L-H2(flag) was expressed and functional, a plasmid containing the full-length MuV genome with L-H2(flag) was generated. The reverse genetics system previously developed by our lab was used to rescue the recombinant virus (8). The MuV-L-H2(flag) virus was plaque purified, sequenced, and propagated as described in the Materials and Methods. To determine if the MuV-L-H2(flag) virus had a growth defect, single-cycle and multi-cycle growth curves were performed. Vero cells were infected with WT MuV or MuV-L-H2(flag) at a low (0.01) and high (1) multiplicity of infection (MOI) and viral production was monitored overtime at the indicated time points (Figure 4.5). At a low MOI, MuV-L-H2(flag) lagged slightly in growth until 72 HPI (Fig 4.5A). At a high MOI, MuV-L-H2(flag had decreased viral titers at 24, 36, and 60 HPI (Fig 4.5B). While the growth was slightly decreased at a high MOI, the MuV-L-H2(flag) virus had a similar growth phenotype to WT MuV, and therefore can be used for downstream MuV L analysis.

To confirm MuV L could be detected during an infection, western blotting and IFA were performed. Vero cells were infected with WT MuV and MuV-L-H2(flag) at a high MOI. Cells were lysed at 48 HPI, and lysates were resolved by SDS-PAGE or fixed at 48 HPI and incubated with antibodies. A mouse anti-MuV P antibody and rabbit anti-Flag antibody were used for protein detection. Both WT MuV and MuV-L-H2(flag) expressed MuV P, but only the MuV-L-H2(flag) had detectable L protein (Fig 4.6A,B). This data confirms that the insertion of a flag tag

in the H2 region of MuV L results in a functional virus and expresses detectable L protein.

**Determination of phosphorylation sites in L by mass spectrometry and *in silico* modeling**

To identify phosphorylation sites within MuV L during an infection, Vero cells were infected with MuV-L-H2(flag). Immunoprecipitation with an anti-flag antibody was performed as described in the Materials and Methods. The samples were resolved by SDS-PAGE and stained with Coomassie blue G250. The labeled L band was excised from the gel, subjected to trypsin digestion and $TiO_2$ phosphopeptide enrichment, and analyzed by LC-MS/MS. The total trypsin coverage was 71% and after enrichment, the coverage was 11% (Fig 4.7A). Four residues were identified as likely phosphorylated: S1087, T1088, T1090, and S1102, all of which are located within the PRNTase domain. Phosphosite analysis could not determine which residue, S1087 or T1088, was phosphorylated, resulting in the same probability score. Residue T1090 was identified in the trypsin flowthrough, but not in the enrichment flowthrough. S1102 was identified with 100% confidence in the enrichment sample (Fig 4.7B). These putative phosphorylation sites were confirmed using NetPhos 3.1 as described in the Materials and Methods. The values were ranked from 0-1, only residue S1087 was below the general cutoff value of 0.5 (Table 1). These results suggest that MuV L is phosphorylated during an infection.

**Assessment of L residues with a MuV minigenome system**

To examine the role of the putative serine and threonine L residues in replication and transcription, each residue was mutated to an alanine and cloned into a pCAGGS vector. The S1087 and T1088 residues were mutated together since the analysis could not discern which residue was phosphorylated. Additionally, since the sites are close together in the genome, another plasmid was constructed which includes all four sites mutated (Fig 4.7 & Table 4.1). Minigenome assays were performed to compare transcriptional activity. Only the L-S1087A,T1088A mutant could be assessed. All other mutations were under construction. BSRT7 cells were transfected with the necessary minigenome plasmids along with plasmids containing WT L or L-S1087A/T1088A. Luciferase activity was compared to WT L. The L-S1087A/T1088A mutations had significantly lower minigenome activity compared to the control. There was a 70-80% reduction in activity indicating these residues are important for efficient replication and transcription (Fig 4.8 & Table 4.1).

**DISCUSSION**

In this study, we developed an immunological tool to study the function of L during MuV infection *in vitro*. We employed a strategy first used by Duprex *et al.*, to insert a flag tag into the flexible hinge region of MuV L (Fig 4.2) (20). The H2 region of several L proteins have been shown to be highly flexible in structure and variable in sequence suggesting the region doesn't contain critical motifs (19). It is thought that the H2 region acts as a linker between major functional domains,

which is why it tolerates large insertions (19, 20). The H1 region, located between CRII and CRIII, did not tolerate any insertions for MeV, so we did not attempt to insert a flag tag into this region (20). Similar to Duprex *et al.*, we inserted the mCherry gene into the H2 region and were able to generate a recombinant virus. It did not appear to have any major defects and expressed mCherry protein supporting the conclusion that the H2 region of MuV is also a flexible linker region (data not shown).

The same strategy was employed to insert a flag tag in the H2 region of PIV5, the prototypical virus in the genus. The flag tag was expressed in the protein by IFA and WB, however there was no minigenome activity (Fig 4.4). The tag was inserted in the same location (middle of H2 region) of L as MuV, but it appears to have disrupted function. It is possible that adjusting the insertion location may result in a functional L, however the PIV5 H2 region is only 25 amino acids in length which hinders available cloning sites. MuV H2 region is 23 amino acids, and it was able to support an insertion. This data suggests that there is a structural difference between PIV5 and MuV L. We are currently investigating the differences between the C-terminal ends of both proteins. We plan to switch the H2-MTase-CTD of PIV5 with MuV (and vice versa) and determine if L is functional in a minigenome system. While we have an L structure for PIV5, we do not have one for MuV, and more investigation into the differences between them is required.

The L protein is challenging to investigate because it typically lacks immunological reagents, has multiple functional domains, is unstable without viral co-factors, and there is low expression during infection (10, 20, 21, 38, 101, 238,

246, 249). It is estimated that 1-2% of viral mRNA transcripts are L, which is very low by comparison to the other viral mRNAs (38). We showed that L could be detected, via flag tag, after transfection and infection, however protein expression was very low (Fig 4.3A, 4.6A). Western blotting for L was a challenge. Transfecting the maximum amount of plasmid per well was sufficient to detect L, but it appeared less stable than during an infection. We observed that L was detected by western blot more consistently after infection than transfection (Fig 4.6A). L protein was more readily observed by IFA, but only after 48 HPI (Fig 4.6B) (38). Further optimization of L detection by western blot will be beneficial for downstream experiments. Additionally, S35-labeled L protein was detected during an infection, but we could not detect phosphorylated L using P33 isotopes (data not shown). This is likely due to the low amounts of L protein labeled during the incubation period and the very few likely phosphosites within the protein. Optimization will be required to prove L is phosphorylated during an infection. A possible solution for better detection may be to use a 3X flag tag, rather than a 1X, since we know the L structure can accommodate larger insertions.

Since MuV L expression is low during an infection, we were surprised to find that it was detectable by LC-MS/MS (Fig 4.7A). The anti-flag antibody sufficiently immunoprecipitated enough MuV L for detection; however, some off-target proteins were detected in the excised band. This is likely due to the anti-flag antibody or protein G beads binding to other proteins since it also occurred in the mock infected cells (data not shown). It may be beneficial to remove off-target proteins from the sample and reanalyze L by LC-MS/MS to increase coverage.

MuV P and NP coverage was >90%, while MuV L coverage was only 71% (4, 5). Regardless of the lower coverage, we were confident the phosphopeptide enrichment would be successful.

To the best of our knowledge this is the first time an L protein has been subjected to LC-MS/MS analysis to identify phosphorylation sites within the protein. Excitingly, four putative residues within MuV L were identified (Fig 4.7B). Residues S1087/T1088, T1090, and S1102 are all located in the PRNTase domain of L. Residues S1087/T1088, T1090 are located at the end of CRIV, while S1102 is in between CRIV and CRV. Representative MuV viruses from multiple genotypes (G, A, F, C, and B) were aligned and the residues were 100% conserved between the virus strains (data not shown). Additionally, these sites are highly conserved between other non-segmented, negative sense RNA virus Ls indicating they may have a critical function for L (19, 101).

The phosphorylation status of MuV P and NP have been shown to regulate viral RNA synthesis (4, 5, 54). L is a multifunctional enzyme responsible for RNA synthesis, however its phosphorylation status is unknown. There are two main hypotheses concerning the phosphorylation status of L proteins. The first suggests that L has its own kinase activity, while the second hypothesis suggests that all L-associated kinase activity comes from host kinases, similar to NP and P phosphorylation (89). There are reports demonstrating that VSV L contains a protein kinase domain, and that Sendai virus (SeV) L phosphorylates both P and NP in vitro (146, 148). But another VSV L report suggested that all kinase activity

observed was cellular rather than viral (147). Yet another report with RSV L demonstrated L could not phosphorylate P *in vitro* (140).

Previous work in our lab demonstrated that PIV5 L was able to activate the phosphorylation of AKT1 through a direct interaction. AKT1 has also been implicated in MuV growth, inhibition of AKT1 led to decreased MuV titers, but the mechanism remains unknown (15). We found that the RdRp domain of PIV5 L containing CRI-CRIII was able to enhance the phosphorylation of AKT1. Our results lead us to hypothesize that PIV5 L encodes for an intrinsic kinase. It was hypothesized that L phosphorylates AKT1, which phosphorylates P, which is essential for efficient replication and transcription, however this could not be proven (89). CRII of PIV5 L was essential for phosphorylation of AKT1, which differs from the location observed in MuV L (Fig 4.7B). It is possible more phosphorylation sites are in MuV L than what was detected by mass spectrometry. NetPhos 3.1 predicted 30+ residues with greater than >0.9 confidence throughout the MuV L protein. It is also possible that the AKT1 binding and phosphorylation site in L are different as seen in other viral-host interactions, like PLK1 (16, 17).

While this work starts to examine the putative phosphorylation residues in L, much work is needed to determine if they play a major role in MuV growth. We suspect the L residues are phosphorylated during a MuV infection, however detecting phosphorylation of L by radiolabeling has thus far been unsuccessful and will need to be addressed. We are currently optimizing and exploring new technologies to help detect L phosphorylation. In this work, we mutated the putative sites to an alanine to examine the effect on a MuV minigenome system.

Only the L mutant containing S1087A,T1088A could confidently be examined using a minigenome assay. The mutation had significantly decreased minigenome activity compared to the control. The other L mutants will still need to be assessed. We suspect that they will result in significantly increased or decreased activity. The WT L backbone was used; these experiments should be repeated in the L-H2(flag) backbone so that L expression can be examined. Additionally, recombinant viruses, containing WT L and L-H2(flag) should be rescued with the single or multiple mutations to examine their effect on MuV growth. It is possible that if these sites are critical for virus function, the recombinant viruses will not rescue. This has been observed before with mutations in MuV P and NP (4, 5). Lastly, determining whether L contains intrinsic kinase activity or is phosphorylated by a host kinase will be crucial to our understanding of MuV L. NetPhos 3.1 predicted phosphorylation by cyclin dependent kinases could be responsible for the phosphorylation of T1088, while a protein kinase C kinase may be responsible or either T1090 or S1102. S1102 also had predicted phosphorylation by a protein kinase A or a S6 kinase. These families of kinases could be tested using the L mutants, but NP and P phosphorylation may also be affected, which may cloud the results. Lastly, to examine if L phosphorylates P and NP as reported in SeV, we could examine the effect of the L mutants on P and NP phosphorylation either by transfection or infection (148).

The function of CRIV in the PRNTase domain, which contains the putative phosphorylation sites, is currently unknown. Future work on these sites may elucidate the function of this conserved region. Taken together, this work provides

a necessary tool to study the function of MuV L during an infection and provides the first evidence that MuV L is phosphorylated during *in vitro* infection.

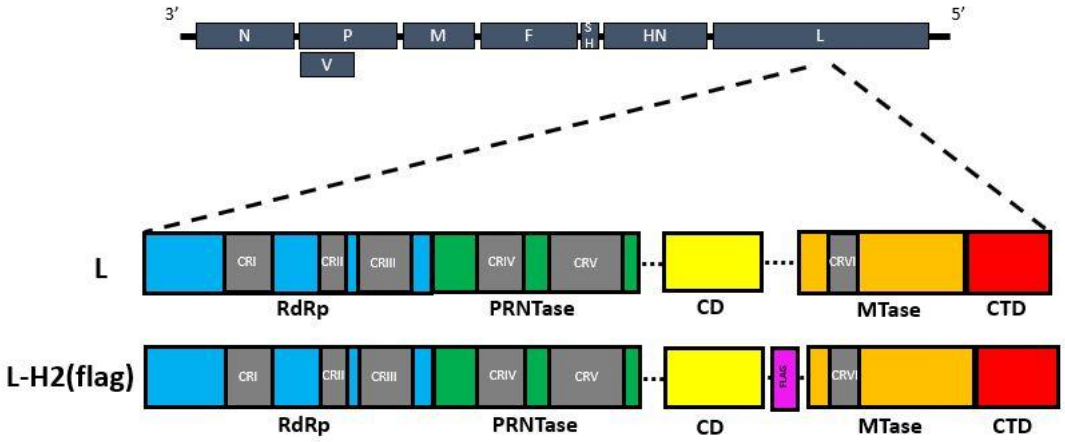


**Figure 4.1. Schematic of MuV L domains and location of flag insertion.** Construction of recombinant MuV virus and domains of MuV L. RNA-dependent RNA polymerase (RdRp) in blue contains the conserved regions (CR) CRI-III. Polyribonucleotidyltransferase (PRNTase) in green contains the CRIV and CRV. Connecting domain (CD) in yellow. Methyltransferase (MTase) in orange contains the CRVI. C-terminal domain (CTD) in red. A 1X flag tag (purple) was inserted into the H2 flexible region (dotted line), located between the CD and MTase domains of MuV L. L-H2(flag) was cloned into a pCAGGS expression vector and then a plasmid containing the full-length MuV genome.

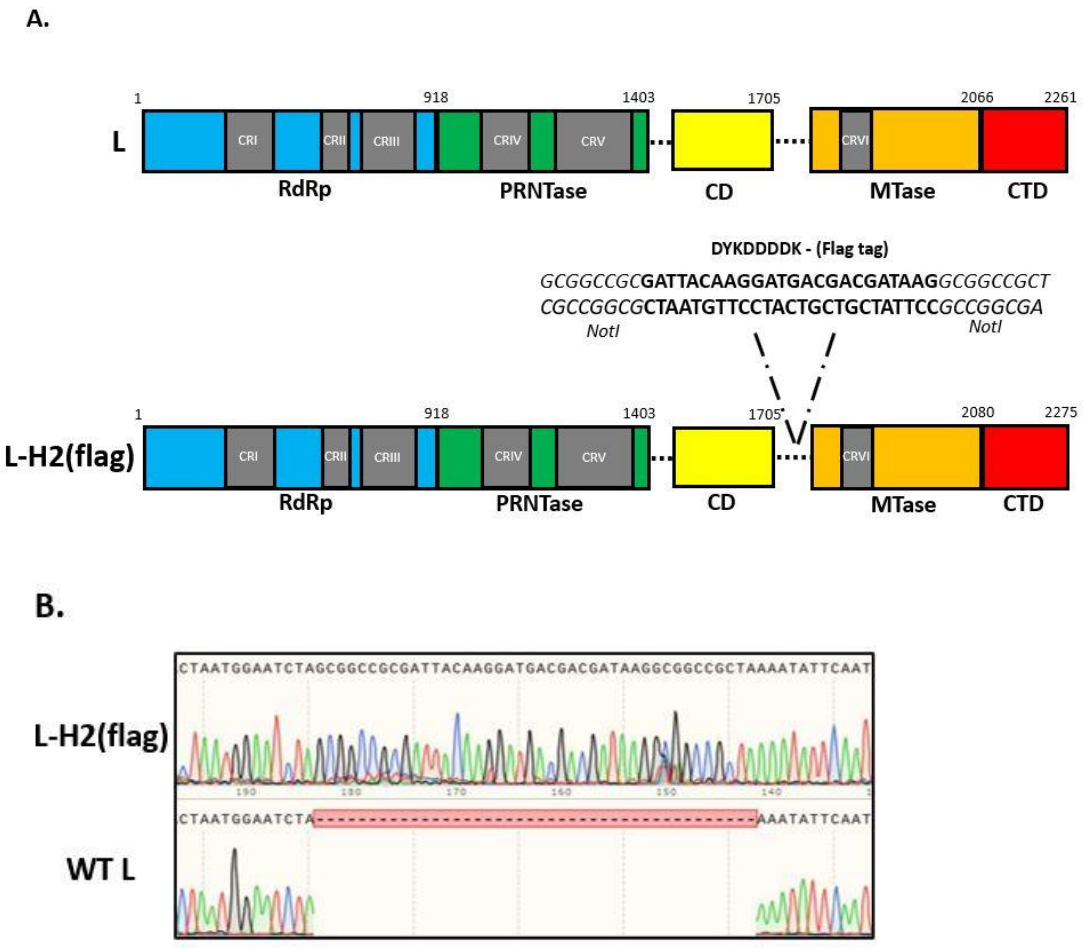


**Figure 4.2. Construction of flag tag in MuV L.** A 1X flag tag was inserted into the H2 region of MuV. The insertion was placed after the amino acid 1723 in the flexible region between the CD and MTase domains. NotI sites were added to both sides of the flag tag for cloning purposes and an additional nucleotide (T) was added to the end of the insert to follow rule of six. The L-H2(flag) was inserted into a pCAGGS expression vector and then a plasmid containing the full-length genome of MuV. **(A)** Schematic of whole insert in H2 region. The insert extended the L protein length by 14 amino acids resulting in a protein that is 2,275 amino acids long. **(B)** Sequencing of the plasmids containing WT L and L-H2(flag).

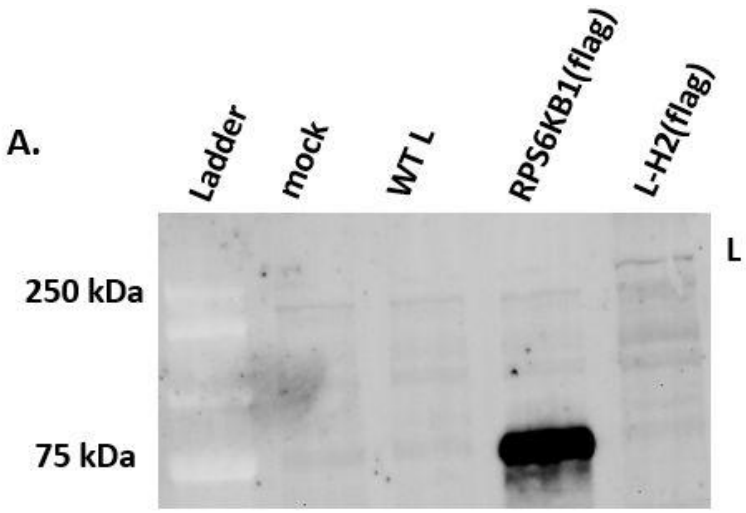
A.
Ladder
mock
WT L
RPS6KB1(flag)
L-H2(flag)
250 kDa
75 kDa
L

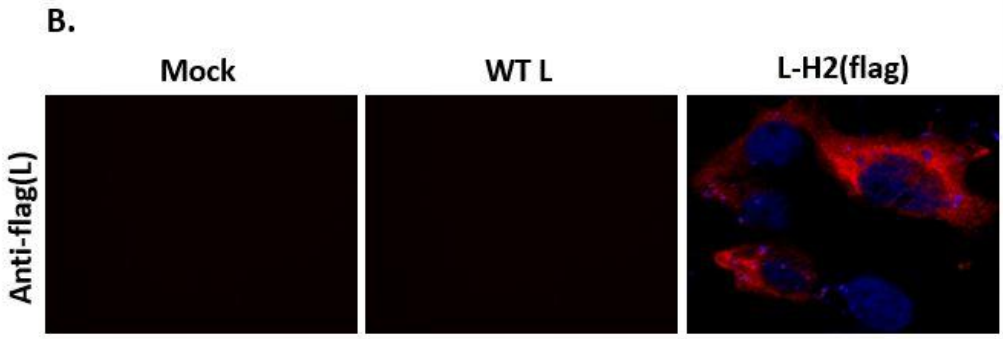
B.
Mock
WT L
L-H2(flag)
Anti-flag(L)

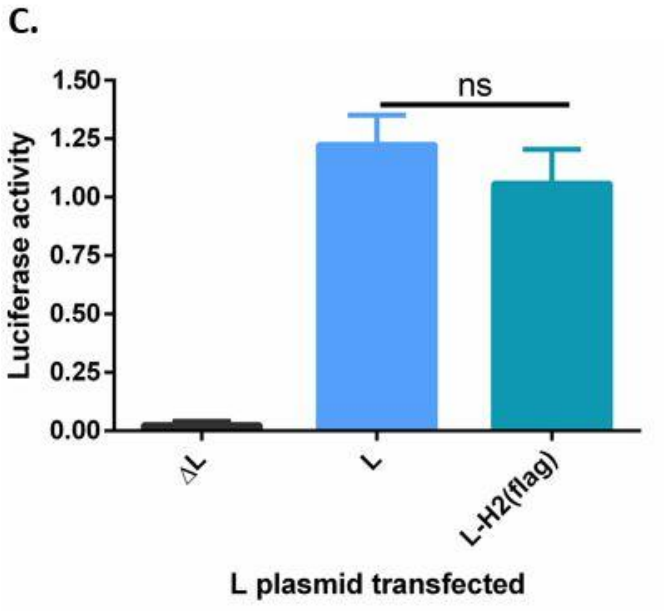
C.
ns
1.50
1.25
1.00
0.75
0.50
0.25
0.00
Luciferase activity
ΔL
L
L-H2(flag)
L plasmid transfected

**Figure 4.3. Confirmation of functional L-H2(flag) protein. (A)** Detection of MuV L after transfection by western blot. 293T cells were transfected with pCAGGS-WT L, pCAGGS-RPS6KB1-flag, and pCAGGS-L-H2(flag). Cells were lysed and resolved by SDS-PAGE. The immunoblot was stained with an anti-flag antibody to detect L. Mock transfected cells and pCAGGS-RPS6KB1-flag were used as a negative and positive control. **(B)** Detection of MuV L after transfection by IFA. 293T transfected cells were fixed and stained with an anti-flag antibody and a CY3-conjugated secondary (red) and then observed by fluorescence microscopy. **(C)** Minigenome activity of L-H2(flag). The mini genome assay was performed using plasmids that encode WT L and L-H2(flag). ΔL was used as a negative control. n=4; ANOVA with Dunnett's multiple comparison test; ns = non-significant, $p > 0.05$. Individual experiments were performed 3 times.

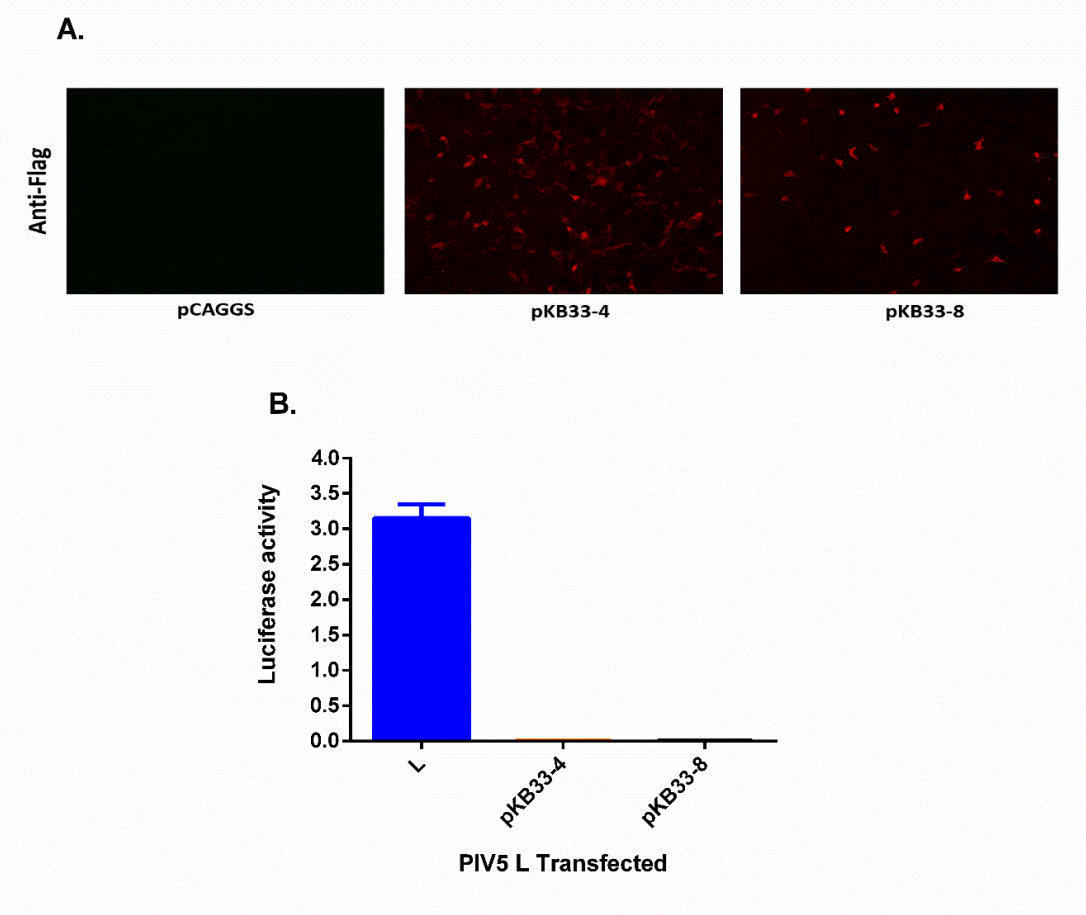


**Figure 4.4. PIV5 L containing internal flag tag is not functional. (A)** Detection of PIV5 L after transfection by IFA. 293T transfected cells were fixed and stained with an anti-flag antibody and a CY3-conjugated secondary (red) and then observed by fluorescence microscopy. **(B)** Minigenome activity of PIV5 L-H2(flag). The mini genome assay was performed using plasmids that encode WT L and two different PIV5 L-H2(flag) plasmids (pKB33-4 and pKB33-8).

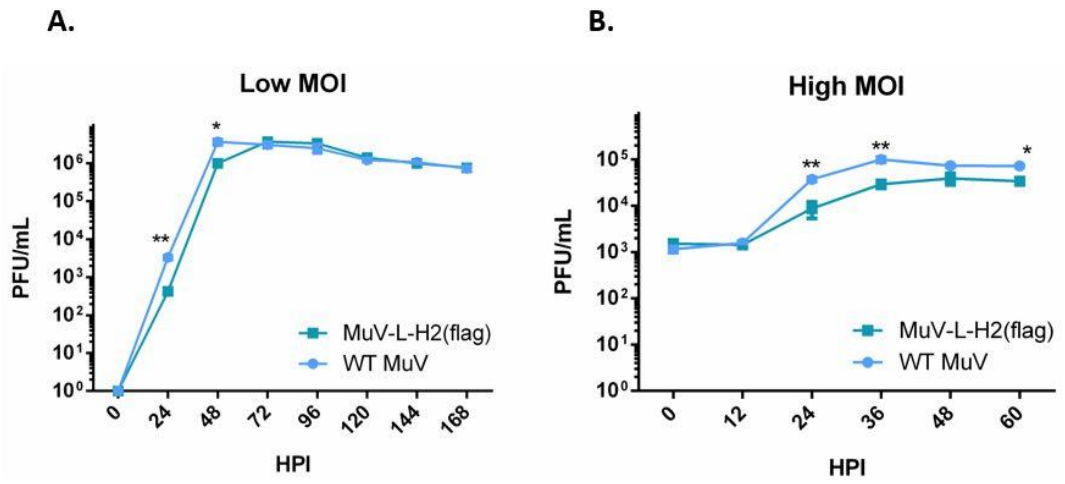


**Figure 4.5. Growth kinetics of recombinant MuV virus.** Vero cells were infected with WT MuV or MuV-L-H2(flag). Media was collected at various time points and titers were determined by plaque assay using Vero cells. **(A)** Multi-cycle growth curve, cells were infected at an MOI of 0.01 **(B)** Single-cycle growth curve, cells were infected at an MOI of 1. n=3; ANOVA with Dunnett's multiple comparison test; *, $p < 0.05$; **, $p < 0.01$.

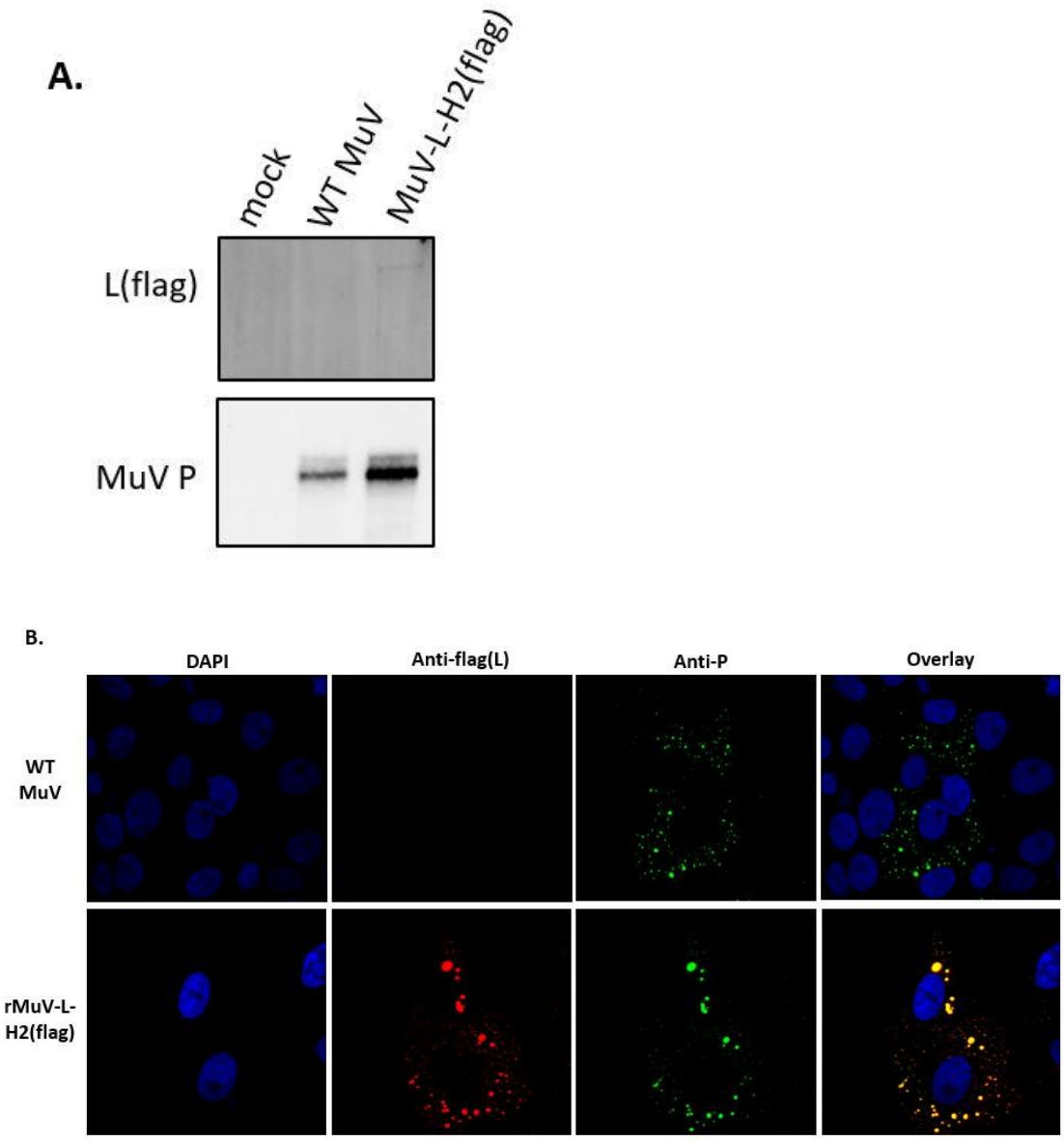


**Figure 4.6. Detection of MuV L in recombinant virus. (A)** MuV L expression during an infection was assessed by western blot. Vero cells were infected at a high MOI with either WT MuV or MuV-L-H2(flag). At 48 HPI, cells were lysed and resolved by SDS-PAGE. MuV P expression was used a control. An anti-flag antibody was used to detect L expression in the MuV-L-H2(flag) infected cells. **(B)** MuV L expression during an infection was assessed by IFA. Vero cells were

infected at a high MOI with either WT MuV or MuV-L-H2(flag). At 48 HPI, cells were fixed and stained with an anti-MuV P (green) and anti-flag antibody (red). An overlay of P and L protein expression (yellow) can be seen in the right bottom panel.

**A.**

MAGLNEILLPEVHLNSPIVRYKLFYYILHGQLPNDLEPDDLGPLANQNWKAIRAEESQVHARLKQIRVELIARIPSLRWTRSQREIAILIWPRIL
PILQAYDLRQSMQLPTVWEKLTQSTVNLISDGLERVVLHISNQLTGKPNLFTRSRTGQDTKDYSIPSTRELSQIWFNNEWSGSVKTWLMIKY
RMRQLITNQKTGELTDLVTIVDTRSTLCIITPELVALYSNEHKALTYLTFEMVLMVTDMLEGRLNVSSLCTASHYLSPLKKRIEILLTLVDDLALLM
GDKVYGVVSSLESFVYAQLQYGDPVVDIKGTFYGFICNEILDLLTEDNIFTEEEANKVLLDLTSQFDNLSPDLTAELLCIMRLWGHPTLTASQAA
SKVRESMCAPKVLDFQTIMKTLAFFHAILINGYRRSHNGIWPPTTLHGNAPKSLIEMRHDNSELKYEYVLKNWKSISMLRIHKCFDASPDED
LSIFMKDKAISCPKQDWMGVFRRSLIKQRYRDANRPLPQPFNRRLLLNFLEDDRFDPIKELEYVTSGEYLRDPEFCASYSLKEKEIKATGRIFAK
MTKRMRSCQVIAESLLANHAGKLMRENGVVLDQLKLTKSLLTMNQIGIISEHSRRSTADNMTLAHSGSNKHRINNSQFKKNKDNKHEMP
DDGFEIAACFLTTDLTKYCLNWRYQVIIPFARTLNSMYGIPHLFEWIHLRLMRSTLYVGDPFNPPSDPTQLDLDTALNDDIFIVSPRGGIEGLCQ
KLWTMISISTIILSATEANTRVMSMVQGDNQAIAITTRVVRSLSHSEKKEQAYKASKLFFERLRANNHGIGHHLKEQETILSSDFFIYSKRVFYK
GRILTQALKNVSKMCLTADILGDCSQASCSNLATTVMRLTENGVEKDLCYFLNAFMTIRQLCYDLVFPQTKSLSQDITNAYLNHPILISRLCLLP
SQLGGLNFLSCSRLFNRNIGDPLVSAIADVKRLIKAGCLDIWVLYNILGRRPGKGKWSTLAADPYTLNIDYLVPSTTFLKKHAQYTLMERSVNP
MLRGVFSENAAEEEEELAQYLLDREVVMPRVAHVILAQSSCGRRKQIQGYLDSTRTHRYSLEVRPLSAKKLNTVIEYNLLYLSYNLEIIEKPNIV
QPFLNAINVDTCSIDIARSLRKLSWATLLNGRPIEGLETPDPIELVHGCLIIGSDECEHCSSGDDKFTWFFLPKGIRLDNDPASNPPIRVPYIGSK
TDERRVASMAYIKGASVSLKSALRLAGVYIWAFGDTEESWQDAYELASTRVNLTLEQLQSLTPLPTSANLVHRLDDGTTQLKFTPASSYAFSSF
VHISNDCQVLEIDDQVKDSNLIYQQVMITGLALIETWNNPPINFSVYETTLHLHTGSSCCIRPVESCVVNPPLLPVPFINVPQMNKFVYDPEP
LSLLEMEKIEDIAYQTRIGGLDQIPLLEKIPLLAHLTAKQMVNSITGLDEATSIVNDAVVQADYTSNWISECCYTYIDSVFVYSGWALLLELSYQM
YYLRIQGIQGILDYVYMTLRRIPGMAITGISSTISHPRILRRCINLDVIAPINSPHIASLDYTKLSIDAVMWGTKQVLTNISQGIDYEIVVPSESQLT
LSDRVLNLVARKLSLLAIIWANYNYPPKVKGMSPEDKCQALTTHLIQTVEYVEHIQIEKTNIRRMILEPKLTAYPSNLFYLSRKLLNAIRDSEEGQ
FLIASYYNSFGFLEPILMESSGRDYKDDDDKAAAKIFNLNSSESASLTEFDFILNLELSEASLEKYSLPSLLMTAENMDNPFPQPPLHHVLRPLG
LSSTSWYKTISVLNYISHMKISDGAHLYLAEGSGASMSLIETFLPGETIWYNSLFNSGENPPQRNFAPLPTQFIESVPYRLIQAGIAAGSGVVQS
FYPLWNGNSDITDLSTKTSVEYIIHKVGADTCALVHVDLEGVPGSMNSMLERAQVHALLITVTVLKPGGLLILKASWEPFNRFSFLLTILWQFF
STIRILRSSYSDPNNHEVYIIATLAVDPTTSSFTTALNRARTLNEQGFSLIPPELVSEYWRRRVEQGQIIQDRIDKVISECVRDQYLTDNNIILQAG
GTPSTRKWLDLPDYPSFNELQSEMARLITIHLKEVIEILKGQSSDHDTLLFTSYNVGPLGKINTILRLIVERILMYTVRNWCILPTQTRLTLRQSIE
LGEFRLRDVITPMEILKLSPNRKYLKSALNQSTFNHLMGETSDILLNRAYQKRIWKAIGCVIYCFGLLTPDVEDSERIDIDNDIPDYDIHGDII*

**B.**

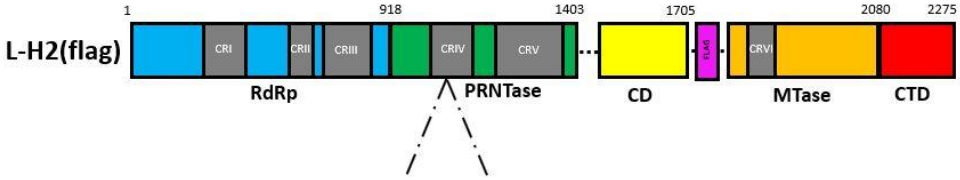


LISRLCLLPSQLGGLNFLSCSRLFNRNIGDPLVSAIADVKRLIKAGCLDIWVLYNILGRRPGKGKWSTLAADPYTLNIDYLVPSTTFLKKHAQ
YTLMERSVNPMLRGVFSENAAEEEEELAQYLLDREVVMPRVAHVILAQSSCGRRKQIQGYLDSTRTHRYSLEVRPLSAKK

**Figure 4.7. Analysis of L phosphorylation by mass spectrometry. (A)** Coverage of MuV L protein after anti-flag immunoprecipitation. The L band was excised for trypsin digest and analysis by LC-MS/MS Residues not detected by LC-MS/MS are struck through. The inserted flag tag is bolded. **(B)** Putative phosphorylation sites within L. The schematic of domains and conserved regions within MuV L illustrates the region the sites are located. The underlined amino acid sequence is the CRIV within the PRNTase domain. Phosphorylated residues are in red and bolded.

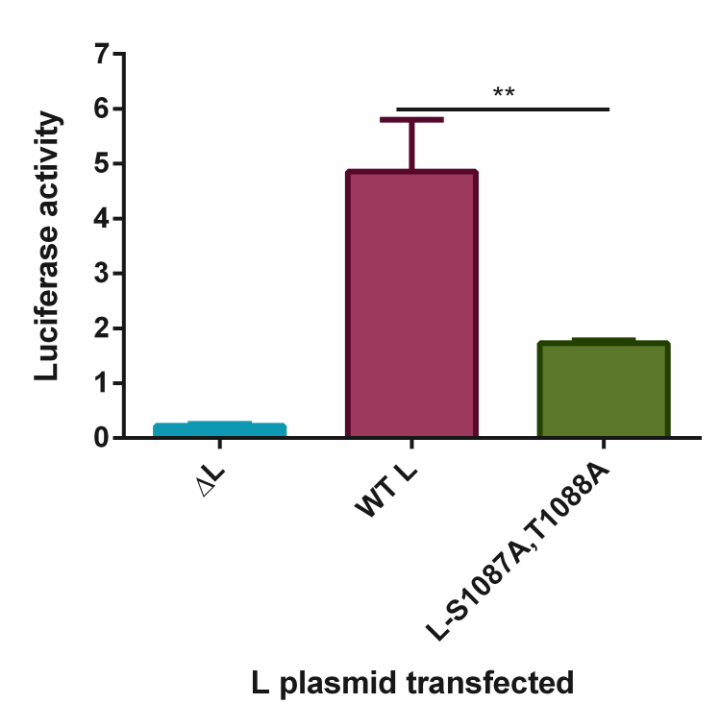


**Figure 4.8. Effects of L mutant on MuV minigenome system.** Peak minigenome activity of a L mutant was assessed. A MuV minigenome assay was performed using a plasmid encoding for L-S1087A,T1088A. The amount of L was 500 ng/well. A ΔL control used was a negative control. The ratio of renilla luciferase to firefly luciferase is reported. n=3; ANOVA with Dunnett's multiple comparison test; *, $p < 0.05$, **, $p < 0.01$, ***, $p < 0.001$. Individual experiments were performed 3 times.

| Residue in MuV L | LC-MS/MS Phosphosite probability score (%) | NetPhos 3.1 (*in silico* prediction) value | Mutation(s) | MG activity (percent of WT) |
|---|---|---|---|---|
| S1087, T1088 | 50/50 | 0.460, 0.515 | S1087A, T1088A | 31.92 |
| T1090 | 80.21 | 0.671 | T1090A | N/A |
| S1102 | 100.0 | 0.989 | S1102A | N/A |
| S1087, T1088, T1090, S1102 | N/A | N/A | S1087A, T1088A, T1090A, S1102A | N/A |

**Table 4.1. Summary of putative phosphorylation sites in MuV L.** Phosphorylation of MuV L was determined by mass spectrometry (LC-MS/MS) and *in silico* site prediction. The LC-MS/MS Phosphosite probability score is the probability that the serine/threonine residue in the peptide detected is phosphorylated. *In silico* prediction was performed using the NetPhos 3.1 server. The serine/threonine residues were mutated to an alanine in a plasmid containing WT L. The minigenome activity of the plasmids containing L-T1090A, L-S1102A, and L-S1087A/T1088A/T1090A/S1102A is not reported. The L mutants minigenome (MG) activity was assessed and calculated as a percent of the WT L control. Average MG activity of three independent experiments is reported. N/A = not applicable.

# CHAPTER 6

## IMMUNOGENICITY OF MUMPS VIRUS GENOTYPE G VACCINE CANDIDATES IN JERYL LYNN-IMMUNIZED MICE

Briggs K., Kirby, C., Beavis, A., Zengel, J., Patil, P., Sauder, C., He, B., Submitted to *Journal of Virology*, 11/2021

**Abstract**

Mumps virus (MuV) causes a highly contagious human disease characterized by the enlargement of the parotid glands. In severe cases, mumps can lead to neurological complications such as aseptic meningitis and encephalitis. Vaccination with the attenuated Jeryl Lynn (JL) MuV vaccine has dramatically reduced the incidence of MuV infection. Recently, large outbreaks have occurred in vaccinated populations. The vaccine strain JL was generated from genotype A, while most current circulating strains belong to genotype G. In this study, we examine the immunogenicity and longevity of genotype-G based vaccines. We found that our recombinant genotype-G based vaccines provide robust neutralizing titers toward genotype G for up to one year in mice. In addition, we demonstrate a third dose of a genotype G-based vaccine following two doses of JL immunization significantly increased neutralizing titers towards the genotype G strain. Our data suggests that after two doses of JL vaccination, which most people have received, a third dose of a genotype G-based vaccine can generate immunity against a genotype G strain.

**Importance**

At present, most individuals have received two doses of MMR, which contains genotype A mumps vaccine. One hurdle in developing a new mumps vaccine against circulating genotype G virus is whether the new genotype G vaccine can generate immunity in humans that are immunized against genotype A virus. This work demonstrates that a novel genotype G-based vaccine can be

effective in animals which received two doses of genotype A-based vaccine, suggesting that the lead genotype G vaccine may induce anti-G immunity in humans who have received two doses of the current vaccine, providing support for testing this vaccine in humans.

## Introduction

Mumps is a highly contagious human disease characterized by the enlargement of the parotid glands, fever, and other upper respiratory symptoms. Mumps virus (MuV) is transmitted through the respiratory tract and is present in saliva of patients with symptoms typically appearing 16-18 days post exposure (1, 2). While many cases are mild or asymptomatic, the highly neurotropic nature of the virus can lead to severe complications such as encephalitis, meningitis, and permanent deafness (250). Prior to mass vaccination, MuV was the leading cause of viral encephalitis and meningitis. It is estimated that a MuV infection invades the nervous system in roughly 50% of cases, however only 5-10% of patients will develop meningitis and <0.5% encephalitis (1). Before mass vaccination in the 1960's, mumps was considered a common childhood disease, resulting in seroconversion of >90% of the population before age 15 (6).

There is currently no treatment available for a MuV infection. The best preventative is the vaccine, as a component of the measles, mumps, and rubella (MMR) vaccine, given at 12-15 months and then boosted at 4-6 years. This vaccine strategy has been able to reduce MuV cases in the United States by 99%, but outbreaks still occur (2). In recent years, there has been an increase in the number

of reported mumps cases (2, 213). The MMR vaccine contains an attenuated version of MuV from genotype A (23). Since the implementation of the MMR vaccination program, the largest outbreak of mumps in the United States started in Iowa in 2006 (IA/06) due to a strain from genotype G. The resurgence resulted in more than 6,500 cases across the nation. At the university where the initial outbreak occurred, several individuals infected had been vaccinated with two doses of the MMR vaccine (222). Since then, the U.S. has had several years with greater than 500 cases, which was the yearly average prior to 2006. In 2016 and 2017, the U.S. had over 6000 cases and 2019 had roughly 3500 cases (2). Again, with a large proportion of cases being in vaccinated populations. Outbreaks in supposedly vaccinated populations have been observed in other countries including China, Canada, and India (24, 251, 252). In Europe, in late 2019 to early 2020, a school in Portugal with high vaccine coverage experienced an outbreak of a genotype G MuV virus (194, 253, 254).

The most widely used MuV vaccine is based on the Jeryl-Lynn (JL) strain, a genotype A virus. The virus was isolated from a patient and serial passaged in embryonated hen’s eggs and chicken embryo cell culture to achieve attenuation over fifty years ago (22, 23). While genotype A strains have circulated in the past, the most common strains in North America and many European countries are currently from genotype G (24). It is thought that genotype G viruses arose in the 1990’s when genotype A viruses were last observed in the human population (28). This drift away from genotype A MuV strains has brought into question the efficacy

of the MuV vaccine in recent years and called for a better understanding of genotype G viruses, like the IA/06 outbreak strain.

MuV is one of many human pathogens in the family *Paramyxoviridae*. It has a single-stranded, negative-sense RNA genome that encodes 7 genes that are transcribed into 9 viral proteins. The internal proteins include the nucleoprotein (N), phosphoprotein (P) and large protein (L), which are involved in RNA synthesis, and the matrix protein (M), which is involved in virion assembly and budding. The small hydrophobic (SH) and V proteins are accessory proteins involved in evasion of the host immune response (10). Preventing the expression of SH and V in the MuV genome resulted in attenuation *in vivo*, and the proteins were shown to play a role in TNF-α and interferon (IFN) signaling respectively (8, 61). The membrane proteins, fusion (F) and hemagglutinin-neuraminidase (HN), are responsible for entry and exit of the virion. They also play a role in virus to cell and cell to cell fusion causing syncytia among the cells (10). Of particular interest for vaccine development are the F and HN proteins because they are the major targets for antibody neutralization (213). Several studies have shown that epitopes found within the HN protein are targets for neutralization (255, 256). While F neutralization has been less studied, it has been implicated as a major determinant of neurovirulence (257, 258).

Previously our lab generated a MuV vaccine candidate based on the IA/06 outbreak strain, named rMuV(ΔVΔSH). It was attenuated by preventing transcription of the V mRNA and deleting the SH ORF and shown to be immunogenic *in vivo* and have an outstanding safety profile (22, 25, 61). In this

study, we used a MuV reverse genetics system based on the JL vaccine strain to create chimeric vaccine candidates using the circulating genotype G (IA/06) F and HN proteins. We tested their antigenicity and longevity in mice and examined a heterologous prime-boost strategy to enhance neutralization to genotype G MuV viruses.

## Materials and methods

### Plasmids and Cells

All plasmids were constructed using standard molecular cloning techniques. Plasmid sequences were based on virus isolated in Iowa from 2006 and the Jeryl-Lynn vaccine major component. MuV NP, P, and L from the IA/06 strain were previously cloned into the pCAGGS expression vector (8). The recombinant JL (rJL) was generated using RNA from the Jeryl Lynn vaccine strain as a template for RT-PCR as previously described (8). The genome was inserted into a rMuV vector containing a T7 promoter and hepatitis delta ribozyme (HDR), using natural restriction sites (PvuI, XmaI, NaeI, KpnI, and RsrII), in pieces to replace the rMuV sequence with rJL. The plasmid encoding the rMuV(ΔVΔSH) vaccine sequence was previously generated (8, 25, 61). The rJL(ΔSH, IA-F/HN) rescue plasmid was generated by replacing the F to HN region of rJL with the IA F to HN of rMuV(ΔVΔSH), while the rJL(ΔSH, IA-F), and rJL(ΔSH, IA-HN) constructs were generated by replacing only the F or HN, respectively, of rJL. Both, the rJL(ΔSH, IA-F), and rJL(ΔSH, IA-HN), were generated from a rJL(ΔSH) backbone by

replacing their open reading frames (ORF) with either IA-F or IA-HN. The corresponding untranslated regions (UTR) remained from JL.

HEK293T and Vero cells were maintained in DMEM supplemented with 10% fetal bovine serum (FBS) 1% penicillin/streptomycin (P/S). All cells were cultured at 37$^{o}$C and 5% $CO_2$.

**Virus rescue**

HEK293T cells were 60-80% confluent and then transfected with pCAGGS-NP (100 ng), pCAGGS-P (320 ng), pCAGGS-L (1250 ng), pCAGGS-T7 (200 ng), and full-length genome (2500 ng) using JetPRIME (Polyplus). After 48 hours, cells were co-cultured with Vero cells at a ratio of 1:5 in a 10-cm dish until CPE was observed around 5-7 days later. Single plaques were isolated and propagated in Vero cells. RNA extractions were performed on the media using Qiagen's Viral RNA extraction kit. Viral sequences were confirmed by RT-PCR and sequencing as previously described (8, 22, 25, 61). Primers are available upon request.

**Growth curves and immunoblotting**

Vero cells in 6-well plates were infected with MuV in 2% FBS, 1% P/S DMEM for 1 hr at a low (0.01) and high (5) multiplicity of infection (MOI). Cells were washed 3x with sterile PBS and 2 mL of 2% FBS 1% P/S was added to the cells. Samples were collected every 24 hours post-infection (HPI) for the low MOI and every 12 HPI for the high MOI infection. Virus titers were determined by plaque assay in Vero cells. Plaque assays were stained with crystal violet to assess plaque formation as previously described (8).

Vero cells were infected in a 24-well plate at a low MOI. At 48 HPI, cells were washed with PBS and lysed with 2x Laemmli buffer with 2-mercaptoethanol then heated at 95 $^{o}$C for 5 minutes. Samples were resolved by SDS-PAGE and transferred to a low fluorescence PVDF blot (Bio Rad). The samples were immunoblotted using a mouse anti-MuV-F (1:100) antibody and a rabbit anti-actin (1:2500) antibody (Sigma-Aldrich) followed by a Cy3-conjugated goat anti-mouse IgG secondary antibody and Cy3-conjuguated goat anti-rabbit IgG secondary antibody (1:2500; Jackson ImmunoResearch). The blots were imaged using a Bio Rad ChemiDoc™ MP imaging system.

**Mouse experiments**

6-8 week old BALB/c mice were used for the experiments. Mice were intranasally or intramuscularly infected with the various MuV vaccines at a PFU of $10^5$ or $10^6$. For the initial study, mice were boosted at 21 and 35 days post prime. Serum was collected at 42 days post prime at the time of termination. For the longevity study, mice were boosted 21 days post prime and monitored for up to 1 year. They were bled at day 56, and 364 days post prime vaccination (DPV). ELISAs and neutralization assays were performed. For the heterologous prime-boost, mice were boosted at 1 month post immunization, and then boosted again with the same or different vaccine candidate at 3 months. Mice were bled at 2.5, 3.5 and 6 months. All animal studies were conducted under guidelines approved by the Institutional Animal Care and Use Committee (IACUC) of the University of Georgia.

**ELISA**

MuV antigens were produced by infecting Vero cells with either IA or JL MuV strains. At 48 HPI, cells were lysed by freeze-thaw cycles and then sonicated. Diluted lysate was coated unto Immulon high binding polystyrene plates (Thermo scientific) in 100 ul overnight at 4$^{o}$C. Plates were then washed and blocked with 200 ul blotto (20X KPL wash solution concentrate, 2% BSA, 5% nonfat dry Milk, and distilled $H_2O$) for 1 hour at room temperature. Serum was diluted in blotto and diluted 1:2 starting at 1:50. It was added to the plates and incubated at room temperature for 1-2 hours. Secondary goat anti-mouse HRP antibody (SouthernBiotech) was used at 1:1000 for 1 hour at room temperature. Plates were developed using SureBlue Reserve TMB substrate (KPL). Absorbance at 450nm was determined by a BioTek Epoch plate reader. Background was calculated from the average absorbance obtained from the MuV antigens that received no serum and anti-mouse IgG-HRP antibody. Endpoint titers were based on the $OD_{450}$ value that was greater than 2 standard deviations above the mean of the naïve serum. Endpoint titers are the reciprocal of the highest positive dilution. The average endpoint titer is presented with SEM.

**Plaque reduction neutralization assay**

Mouse serum was heat inactivated at 56$^{o}$C for 45 minutes and then serially diluted in PBS. Diluted serum was incubated with 50 PFU virus in 2% FBS 1% P/S DMEM at a 1:1 ratio for 1 hour at 37$^{o}$C. The mixture was then used to infect Vero cells in a 12-well plate for 1-2 hours at 37$^{o}$C. Media was aspirated and overlaid with 2% FBS + 1% P/S + 1% low-melt agarose in DMEM. Plates were fixed and

stained 8 days post infection to allow the rJL(ΔSH, IA-F), and rJL(ΔSH, IA-HN) plaques to form more clearly. Every virus neutralized had a no serum control. The LOD is the lower limit of detection and is the reciprocal of the starting dilution. The plaque reduction neutralization titer (PRNT50) was determined based on the reciprocal of the dilution of serum that reduced the number of plaques by one half the input virus control. The average PRNT50 for each vaccine was presented as a bar. Individual samples showing SEM variation are plotted.

**Neurotoxicity test**

The neonate rat neurotoxicity test was performed as previously described (8, 61, 66, 67). The neurotoxicity of a given mumps virus strain is defined here by the severity of hydrocephalus induced by the virus. Per virus two to three litters of Lewis rats (Envigo) were used. Within 16 hours post-partum, neonates were inoculated intracranially with 10 ul of EMEM containing 100 PFU of the respective viruses. Remaining inocula of each virus were back-titered by plaque assay on Vero cells to confirm the target dose was administered. 29-30 days post infection animals were humanely euthanized by $CO_2$ asphyxiation. Brains were removed, divided into the brain hemispheres and fixed in 10% neutral buffered formalin for 5 days at 4° C. Brains were embedded in paraffin and two 10 um thick sagittal sections from each brain hemisphere, cut approximately 1 mm from the brain midline, were stained with hematoxylin and eosin. Brain sections were scanned and the cross-sectional area of the brain (without cerebellum) and the cross-sectional area of third lateral ventricle (that is enlarged following infection with neurotoxic mumps virus strains) was measured using the open-source image-

processing software Image J (NIH). The mean ratio (indicated in %) between these two measurements obtained from two brain sections each is the neurovirulence score for the individual rat. The neurovirulence score for each virus is calculated as the mean score for all brains of animals inoculated with the same respective virus. Animal studies were conducted under guidelines approved by the Institutional Animal Care and Use Committee (IACUC) of the FDA at Silver Spring, MD.

## Results

### Generation and analysis of recombinant viruses

Previously, we constructed a genotype G vaccine using a recombinant MuV-IA (rMuV) virus based on the MuV IA/06 outbreak strain and it will be referred to here as rMuV(ΔVΔSH) (8, 25). In this work, genotype G-based vaccines were generated in a rJL(ΔSH) backbone by replacing the open reading frames (ORFs) of JL F and/or HN with the IA F and/or HN as described in the materials and methods. We previously showed that rMuV-ΔSH was attenuated *in vivo*, so we chose the ΔSH backbone for our recombinant JL constructs (8) (Fig 5.1). We first generated a recombinant JL (rJL) from the Jeryl Lynn MuV vaccine strain. RNA from the JL vaccine strain was used as a template for RT-PCR as previously described (8). The genome was obtained, and sequentially cloned into a pMuV plasmid containing a T7 promotor and hepatitis delta ribozyme (HDR) using traditional cloning techniques.

A recombinant JL virus was rescued using the full-length genome of JL plasmid (pJL) and the MuV- NP, P, and L helper plasmids previously constructed (8). RNA extractions were performed on the plaque purified stock of virus and reverse transcribed into cDNA for sequencing (Fig 5.2A). The recombinant JL virus sequence matched to the JL major component, rather than the JL minor component. To confirm syncytia formation by the virus, we infected Vero cells at a low and high MOI with rJL. At 48 HPI, we observed extensive syncytia at both MOIs (Fig 5.2B).

After we confirmed that the rJL was comparable to the JL vaccine virus, we used the plasmid (pJL) to clone the rest of the plasmids as described in the materials and methods (Fig 1). The rJL(ΔSH, IA-F/HN), rJL(ΔSH, IA-F), and rJL(ΔSH, IA-HN) viruses were rescued, plaque purified, and the sequences were confirmed by RT-PCR (Fig 5.3A). Immunoblotting was performed to confirm F protein expression in lysates of Vero cells infected with the recombinant viruses (Fig 5.3B). A low (0.01) and high (5) multiplicity of infection (MOI) growth curve was performed in Vero cells to examine the virus growth *in vitro*. The rJL(ΔSH, IA-F/HN), rJL(ΔSH, IA-F), and rJL(ΔSH, IA-HN) had similar growth to both the IA and JL viruses at a low and high MOI (Fig 5.3C, 5.3D). The rJL(ΔSH, IA-F/HN) virus had peak titers very similar to JL at a low and high MOI, but it remained at a higher titer at 72, 96, and 120 HPI (Fig 5.3C). We observed different amounts of syncytia and plaque phenotypes between the chimera vaccines. JL, IA, and rJL(ΔSH, IA-F/HN) form large, fully cleared plaques, while the rJL(ΔSH, IA-F), and rJL(ΔSH, IA-HN) form smaller more opaque plaques (Fig 5.3E). This data demonstrates that

interchanging the F and/or HN does not drastically change the growth of the vaccine or protein expression, however plaque appearance is slightly altered.

**Humoral immune responses in mice immunized with vaccine candidates**

To examine the immunogenicity of the recombinant viruses, BALB/c mice were intranasally immunized with $10^5$ PFU of each virus and then boosted at 21- and 35-days post prime. Serum was collected at termination and plaque reduction neutralization assays were performed against genotype A and G viruses as described in the material and methods. All vaccine constructs elicited neutralizing antibody responses against both genotype A and G viruses (Fig 5.4A, 5.4B). JL-immunized mice had lower neutralization titers against the genotype G virus, with two samples being below the detection level. The IA and IA-based viruses had higher neutralizing titers towards genotype G (Fig 5.4B). The rJL(ΔSH, IA-HN) virus had significantly lower neutralizing titers compared to the other candidates. Serum from rJL(ΔSH, IA-F/HN) had the highest neutralization titers against genotype G, suggesting it would be a good vaccine candidate (Fig 5.4A, 5.4B).

To determine the longevity of antibodies in mice immunized with the recombinant vaccine constructs, a similar study was conducted. BALB/c mice were intranasally immunized with $10^5$ PFU and then boosted at 21 days post-vaccination (DPV). Mice were maintained and periodically bled for serum collection up to 364 DPV (Fig 5.5A). ELISAs were performed at day 56 and day 364 post-vaccination to determine if MuV antibodies decreased over time (Fig 5.5B). All immunization groups had detectable antibodies using ELISA at 56 and 364 DPV against both genotype A and G antigens. The level of ELISA antibody detected was comparable

between the two timepoints, suggesting total antibody amounts do not wane over a 1-year period. Serum from rJL(ΔSH, IA-HN) had notably lower antibody titers at both timepoints. Interestingly, its antibody titer increased at 1 year, but it was not significant (Fig 5.5B). This data corresponds with the low neutralizing antibody titers obtained after a prime and two boosts (Fig 5.4). Apart from the rJL(ΔSH, IA-HN) serum, all other vaccine constructs had similar ELISA titers at both time points. Taken together, this data shows that MuV antibodies are still present in mice 1-year post-vaccination and shows that the amount of total antibodies present is similar between constructs.

After detecting antibodies in mice 364 days post-vaccination, we tested the antibody neutralizing ability against genotype A and G viruses. We performed plaque reduction neutralization assays with 56 and 364 DPV serum to compare neutralizing ability over time. As expected, JL-immunized mice had higher neutralizing titers against genotype A at both time points. It is interesting to note that only JL-immunized sera had significantly higher neutralizing titers 364 DPV against genotype A, while the other constructs had little to no increase (Fig 5.5C). In contrast, the genotype G-based vaccines produced higher neutralizing titers than JL against genotype G. Interestingly, the titers significantly increased over time in the sera from rMuV(ΔVΔSH), rJL(ΔSH, IA-F/HN), and rJL(ΔSH, IA-F) (Fig 5.5C). Both rMuV(ΔVΔSH) and rJL(ΔSH, IA-F/HN) sera had high ELISA and neutralizing antibody titers against genotype G at 364 DPV suggesting they would provide long-term protection against genotype G MuV strains. This data shows the rJL(ΔSH) vaccine constructs are capable of generating neutralizing antibodies

towards both genotypes but having both IA F and HN creates a more robust humoral response against the circulating genotype G strain.

**Evaluation of a genotype G-based vaccine as a third dose immunization in mice**

To determine if a genotype G-based vaccine boost could increase MuV neutralization titers in mice previously vaccinated with JL, BALB/c mice were intramuscularly immunized with JL at $10^6$ PFU and then boosted with the same dose 1 month post prime (Fig 5.6A) and then at 2.5 months post prime, mice were bled and neutralization titers against genotype G and A were determined. JL-immunized mice neutralized genotype A virus significantly better than genotype G virus (Fig 5.6B). At 3 months post prime, mice were boosted with either JL, rMuV(ΔVΔSH), or rJL(ΔSH, IA-F/HN) by intranasal (IN) or intramuscular (IM) inoculation (Fig 5.6A). Mice were bled at 3.5- and 6-months post-prime, and neutralization titers were determined for genotype A and G viruses. At both time points, all vaccine groups had high neutralizing titers against genotype A suggesting a third dose of an IA-based vaccine does not affect neutralization against genotype A (Fig 5.6C, 5.6D). Neutralization titers against genotype G significantly increased post-boost with the IA-based vaccines, and the antibodies maintained neutralizing ability 6 months post prime (Fig 5.6C, 5.6D). Interestingly, a mouse that was given a third dose of rMuV(ΔVΔSH) intranasally did not have detectable neutralizing antibodies to JL or IA at 6 months post vaccination but did have them at 3.5 months (Fig 5.6C, 5.6D). Route of immunization did not play a major role in neutralization titer, which is consistent with previous observations in

mice (25). However, we observed that nAb titers trended higher with the IN route. These results suggest that a third dose of a genotype G-based vaccine would increase neutralizing ability to the circulating genotype G strains, while maintaining the ability to neutralize genotype A strains.

**Neurotoxicity of vaccine constructs**

Neurotoxicity is a major concern in developing new mumps vaccine candidates. To examine the neurovirulence phenotype of our vaccine constructs, the neonate rat neurotoxicity test was performed as previously described (8, 61, 66). The MuV-induced hydrocephalus, the major neuropathological outcome of MuV infection in this model, was assessed. We compared rJL(ΔSH, IA-F/HN) to our previously established low neurovirulent rMuV(ΔVΔSH) vaccine and used WT IA/06 as a positive control. Surprisingly, we found that the rJL(ΔSH, IA-F/HN) was relatively neurotoxic and that the JL ΔSH backbone was not enough to attenuate the neurovirulence of the IA F and HN proteins (Fig 5.7).

**Discussion**

Two doses of the MMR vaccine have dramatically decreased MuV cases in the United States, but outbreaks still occur in vaccinated populations. The continued outbreaks have been attributed mainly to waning immunity and antigenic variation, but failure of primary vaccine and lack of natural boosting may also play a role (24). A major challenge in developing a new MuV vaccine is the lack of immune correlates that assure protection from a mumps infection (1, 208, 213). However, the presence of neutralizing antibodies is thought to be essential in

preventing infection. A neutralization titer of >1:8 has been suggested, but there are several examples that negate that titer (199, 202, 208, 213).

In this study, we established a reverse genetics system based on the JL vaccine strain and tested the immunogenicity and longevity of immune responses following vaccination with chimeric MuV vaccine candidates. The JL vaccine, comprised of at least two well characterized virus strains, is an effective and safe vaccine, but its production through serial passaging can lead to variation between batches (23, 259). In addition, there are no standard markers for attenuation and neuroattenuation for MuV vaccines making the validation process more difficult (23, 257, 258, 260). Recombinant viruses offer an advantage over attenuated viruses by by-passing the need for serial passaging and offer higher homogeneity of the vaccine product. In addition, recombinant vaccine candidates can be continually generated from a cDNA plasmid with a defined sequence. Here we used reverse genetics to engineer three chimeric rJL vaccines with IA-F, IA-HN, or IA-F/HN in a ΔSH backbone (Fig 5.3).

The IA-based rJL(ΔSH, IA-F/HN) and rMuV(ΔVΔSH) immunized mice produced higher nAb titers than the JL immunized mice against genotype G, as expected (Fig 5.4). In addition, JL serum neutralized genotype A significantly better than genotype G at 2.5 months (Fig 5.6B). Genotype A and genotype G MuV viruses are phylogenetically different, which can lead to reduced cross-neutralization between the vaccine and circulating strains (22, 28). Sera from children immunized with 2 doses of MMR have been shown to have lower neutralizing titers towards non-genotype A virus strains, including genotype G and

H (208, 211, 213). Reduced cross neutralization of JL has also been observed in other mouse studies, which is consistent with our results (22, 25).

To the best of our knowledge, this is the first time a MuV vaccine has been tested for longevity of antibodies in mice. We compared ELISA antibody titers and neutralizing antibody titers at 56 and 364 DPV for our vaccine constructs. We found that there was little change between day 56 and day 364 suggesting that the total amount of antibodies produced by our vaccines do not wane in a 1-year period (Fig 5.5). We didn't observe differences in ELISA titers between genotype A and G antigens likely due to a large portion of the antigens being the NP protein. It is known that NP is the immunodominant antigen in a MuV infection and is fairly conserved between MuV strains (199). High NP antibody titers may mask the decrease in F and HN antibodies in an ELISA.

Neutralization assays were performed on the same serum samples to examine if neutralizing ability changed from 56 to 364 DPV. Surprisingly, all genotype G-based vaccines (except rJL(ΔSH, IA-HN)) had significantly increased neutralizing ability toward genotype G at 364 DPV. JL immunized mice titers increased, but it was not significant (Fig 5.5). Interestingly, only the JL vaccine had significantly higher nAbs when neutralized against genotype A. The increase in neutralization titers from day 56 to 364 could be indicative of antibody affinity maturation. While the level of total antibodies did not drastically change over time, the nAb ability increased in the IA-based vaccines against genotype G. In this study, we did not observe waning immunity in either total or neutralizing antibody titers. Waning immunity has been documented in several outbreaks, where it's

estimated that risk of developing clinical MuV increases 10-27% every year post vaccination (24, 208, 261, 262). One mathematical model found the MuV vaccine to wane about 27 years post vaccination, with a 25% loss of protection starting at 7.9 years post vaccination (210). However, other studies found no, or minimal antibody decline over time after two doses of the MMR vaccine (206, 263). The lifespan of a mouse is significantly shorter than a human, and it is possible that waning could have been observed if kept longer. It is also possible that, unlike humans, MuV antibodies do not wane in mice, which presents a limitation for the model.

A routine third dose of JL (MMR3) has been suggested to help reduce outbreaks. A study was conducted, in a non-outbreak setting, to determine if a third dose of JL would significantly increase MuV neutralizing antibodies. A plaque reduction neutralization assay was performed using the JL vaccine virus for neutralization. The serum was not tested against another MuV genotype. The results of the 656-person study showed a moderate increase at 1 month post MMR3, but nAb titers returned to baseline at 1 year (200, 264). Another study showed that the MMR3 vaccination campaign that took place in IA during the 2016 outbreak did help reduce cases, however 12% of the cases reported received 3 doses of the MMR vaccine (222). Taken together, these findings show boosting with MMR3 has limited success.

We compared nAb responses from mice immunized with either three doses of JL or two doses of JL and one dose of a genotype G-based vaccine. We observed a large increase in neutralization titer towards genotype G at 3.5 months

post-prime or two weeks post genotype G-based boost (Fig 5.6C). Neutralization titers toward genotype A or G were maintained at 6 months post prime (Fig 5.6D). These results suggest that a 3rd dose of a genotype G-based vaccine would increase nAb titers to the circulating strain, while maintaining a strong genotype A response. Additionally, the vaccines can overcome pre-existing immunity towards MuV and retain a high neutralizing titer 6 months post vaccination to another strain. Although route of administration didn't play a major role in nAb production, rMuV(ΔVΔSH) had a slightly better response by the IN route. Mucosal IgA nAbs have been implicated as an important means of protection against a MuV infection (159, 265, 266). Immunization by the route of natural infection could help create a localized IgA response and increase overall protection.

MuV is highly neurotropic disease. While JL has been shown to be very safe, other MuV vaccines have caused CNS complications in the past, resulting in their discontinuation (1, 25, 28). We assessed the neurotoxicity of our rJL(ΔSH, IA-F/HN) vaccine candidate compared to our previously tested rMuV(ΔVΔSH) candidate (Fig 5.7). A previous study by Sauder *et al.*, showed that replacing the F and HN of JL with the F and HN of the neurovirulent 88-1961 strain significantly increased its neurovirulence score, but did not completely rescue the neurovirulent phenotype (260). Based on that study and our own findings that rMuV(ΔSH) (IA/06 background) was partially attenuated, we reasoned that using a rJL ΔSH backbone would be sufficient to attenuate the IA/06 F and HN (8). Unfortunately, ΔSH used in conjunction with the rJL background was not sufficient to attenuate the virus. This data supports the proposed conclusion that the mechanism of neurovirulence

and neuroattenuation are not the same for different MuV strains, and that multiple proteins are involved (258, 260).

MuV vaccines have also been pulled from the market for having little to no effectiveness demonstrating the fine line between attenuation and effectiveness (267). The rJL(ΔSH, IA-F/HN) vaccine, although highly immunogenic, would likely cause CNS complications. Additional modification of the rJL backbone will be necessary to reduce the neurotoxicity score.

In this study, we created chimeric genotype G-based rJL vaccines to assess their immunogenicity and longevity towards MuV. We showed that rMuV(ΔVΔSH) and rJL(ΔSH, IA-F/HN) produced long lasting neutralizing antibodies towards genotype G. Although, rJL(ΔSH, IA-F/HN) was shown to be neurotoxic for human use, it illustrates the complex nature of the disease and the difficulties in developing a new vaccine. rMuV(ΔVΔSH), however, continues to be a safe and effective vaccine candidate for MuV. We propose that a 3$^{rd}$ dose, later in life, with a genotype G-based vaccine will be beneficial in preventing future MuV outbreaks.

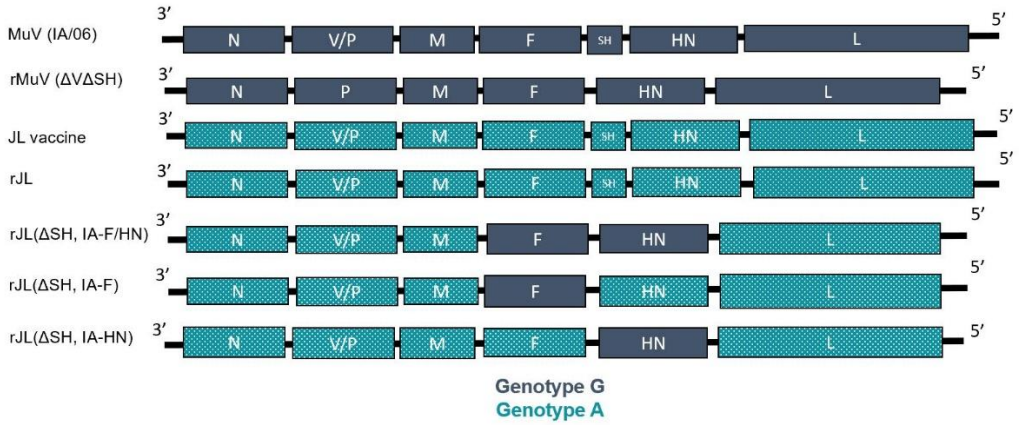


**Figure 5.1. Schematic of recombinant viruses**

Schematic of recombinant viruses. N, nucleoprotein; V, V protein; P, phosphoprotein; M, matrix protein; F, fusion protein; SH, small hydrophobic; HN, hemagglutinin-neuraminadase protein; L, large protein/RNA-dependent polymerase. Vaccine construct sequences are based on the JL vaccine (genotype A) and the IA, 06 isolate (genotype G). rMuV(ΔVΔSH) was generated by mutating the editing site of the V/P gene to only transcribe P and deleting the SH ORF. The recombinant JL (rJL) vaccines were generated by deleting the SH ORF and changing the JL F and/or HN with IA F and/or HN.

**A.**

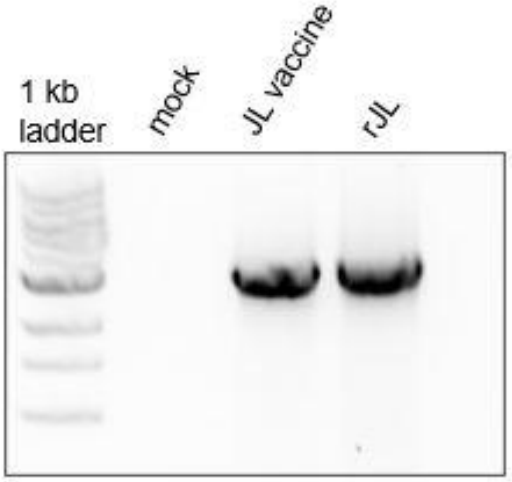


**B.**

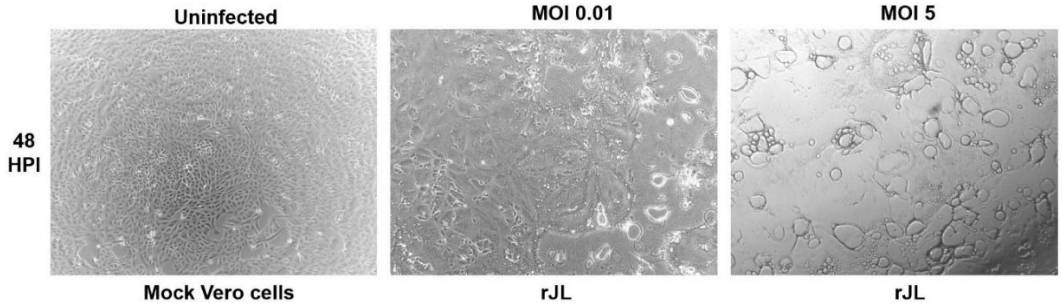


**Figure 5.2: Generation of an infectious recombinant JL**

**(A) Confirmation of rJL virus rescue.** After plaque purification, viral RNA was extracted from the media and subjected to RT-PCR. Primers flanking the NP gene and M gene region were used to amplify a 3.1 kilobase region of the viral genome. The JL vaccine and rJL viruses are shown along with a mock. The recovered virus matched to the JL major component. **(B) Syncytia formation after rJL infection.** Vero cells were infected at an MOI 0.01 and 5 with rJL. After, 48 hours post infection (HPI) syncytia formation was observed by microscopy.

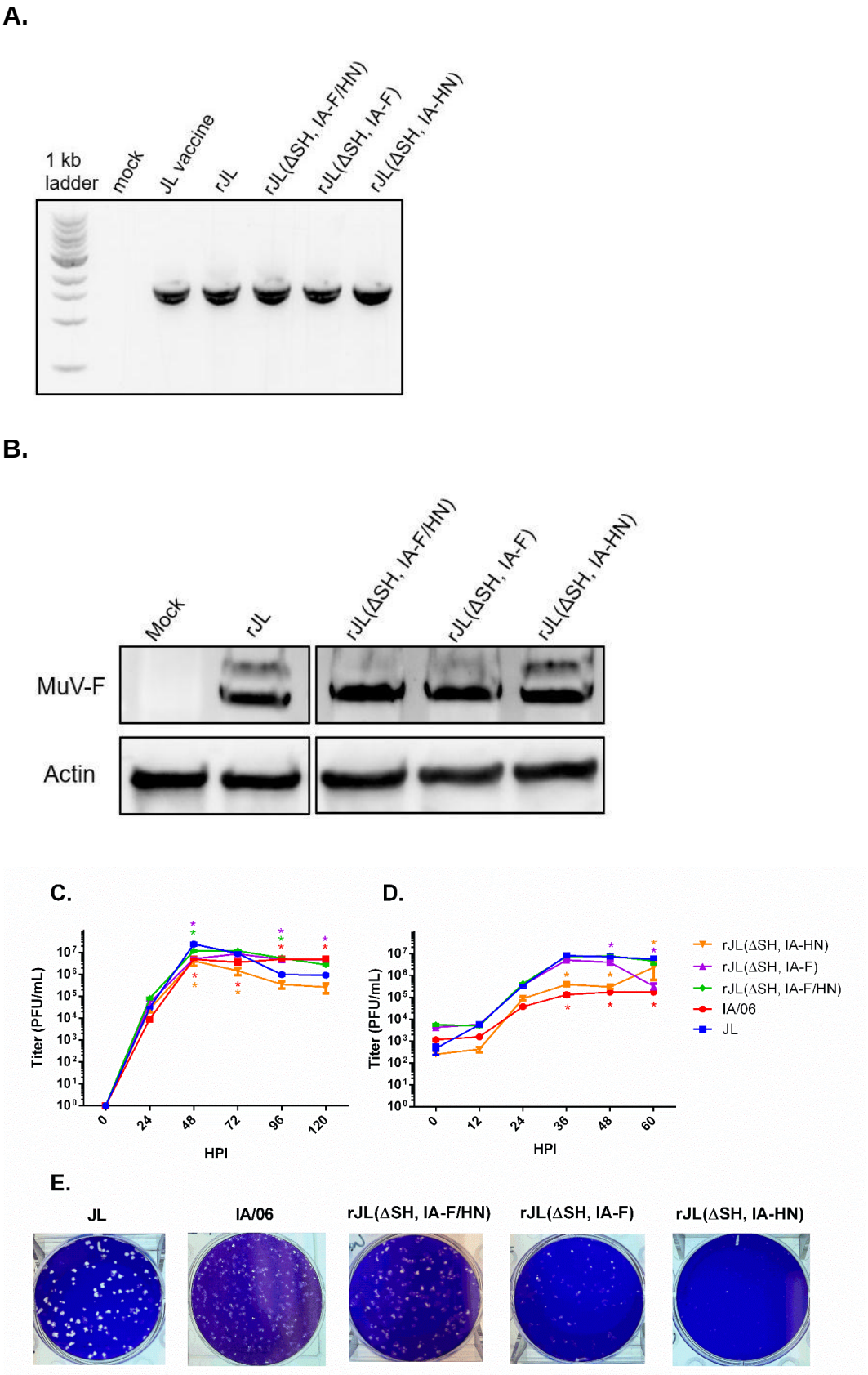
A.
1 kb ladder
mock
JL vaccine
rJL
rJL(ΔSH, IA-F/HN)
rJL(ΔSH, IA-F)
rJL(ΔSH, IA-HN)
B.
Mock
rJL
rJL(ΔSH, IA-F/HN)
rJL(ΔSH, IA-F)
rJL(ΔSH, IA-HN)
MuV-F
Actin
C.
Titer (PFU/mL)
HPI
D.
Titer (PFU/mL)
HPI
rJL(ΔSH, IA-HN)
rJL(ΔSH, IA-F)
rJL(ΔSH, IA-F/HN)
IA/06
JL
E.
JL
IA/06
rJL(ΔSH, IA-F/HN)
rJL(ΔSH, IA-F)
rJL(ΔSH, IA-HN)

**Figure 5.3: Characterization of recombinant viruses**

**(A) Confirmation of recombinant virus rescues.** After plaque purification, a stock was propagated, and viral RNA was extracted from the media and subjected to RT-PCR. Primers in the NP gene and P gene region were used to amplify a 1.6 kilobase region of the viral genome. **(B) Viral protein expression of recombinant viruses.** Vero cells were infected at a low MOI. Cells were lysed at 48 HPI and subjected to immunoblotting with an anti-MuV-F and anti-actin antibody**. (C) Growth kinetics at a low MOI.** Vero cells were infected with the recombinant viruses at MOI 0.01. Media was collected at 24-hour increments and titered by plaque assay. **(D) Growth kinetics at a high MOI**. Vero cells were infected at MOI 5 with the recombinant viruses and media was collected at 12-hour increments. Titers were determined by plaque assay. JL and IA were used as controls. The growth rate of each vaccine was compared to the JL vaccine strain. n=3; 2-way ANOVA with Dunnett's multiple comparison test to JL; (*) color corresponds to vaccine; * $P < 0.05$. **(E) Plaque formation in Vero cells**. The recombinant viruses were plaqued in Vero cells, grown for 8 days, and then stained with crystal violet.

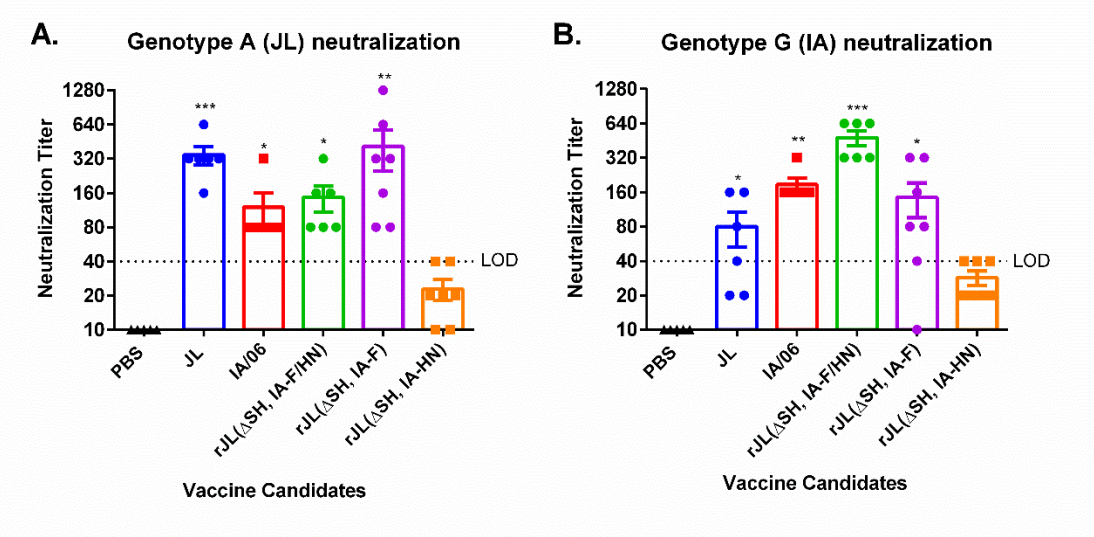


**Figure 5.4: Neutralization titers in mice immunized with vaccine candidates.** Neutralization titer in mice post immunization**.** Plaque reduction neutralization titers against genotype A (JL) virus **(A)** and genotype G (IA) virus **(B)**. The mean 50% plaque reduction neutralization titer and SEM are reported. Bars represent the mean plaque reduction neutralization titer, and individual samples are plotted as points within the bars to show SEM. Lower limit of detection (LOD) is defined at the lowest dilution of serum that was plaqued, negative samples are reported as below the detection level. n=5-7; 1-way ANOVA with comparison to PBS; * P<0.05, ** P<0.01, *** P<0.001.

**A.**

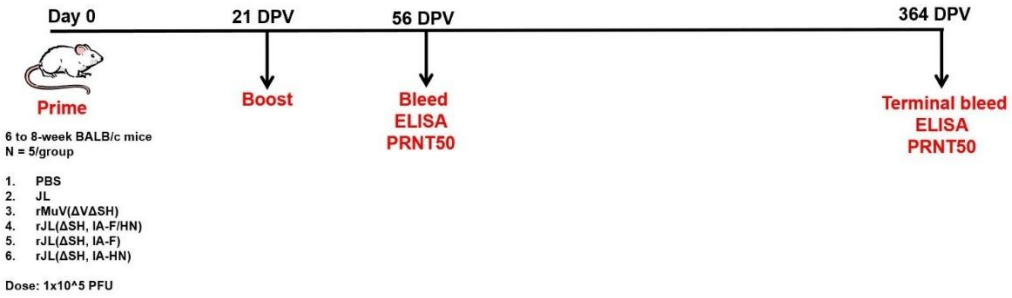
Day 0
21 DPV
56 DPV
364 DPV
Prime
Boost
Bleed
ELISA
PRNT50
Terminal bleed
ELISA
PRNT50
6 to 8-week BALB/c mice
N = 5/group
1. PBS
2. JL
3. rMuV(ΔVΔSH)
4. rJL(ΔSH, IA-F/HN)
5. rJL(ΔSH, IA-F)
6. rJL(ΔSH, IA-HN)
Dose: 1x10^5 PFU

**B.**

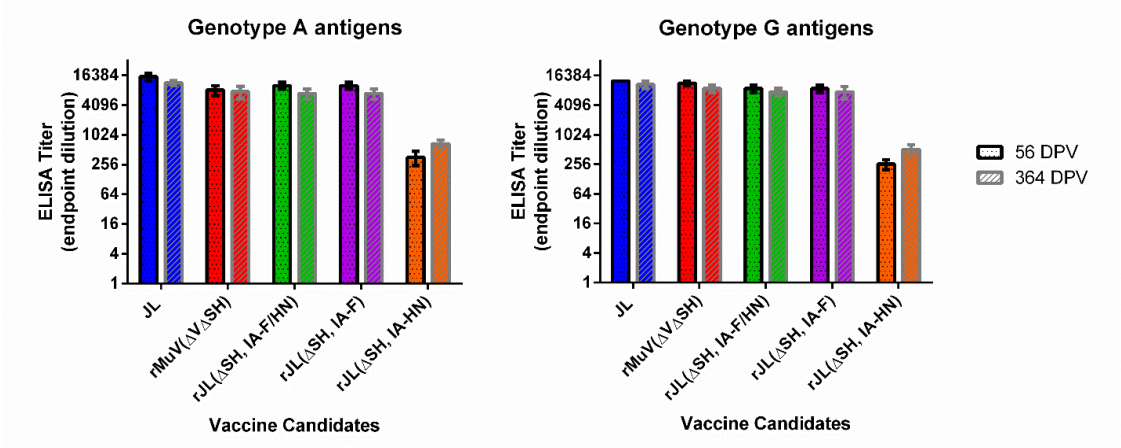
Genotype A antigens
Genotype G antigens
ELISA Titer
(endpoint dilution)
16384
4096
1024
256
64
16
4
1
JL
rMuV(ΔVΔSH)
rJL(ΔSH, IA-F/HN)
rJL(ΔSH, IA-F)
rJL(ΔSH, IA-HN)
Vaccine Candidates
56 DPV
364 DPV

**C.**

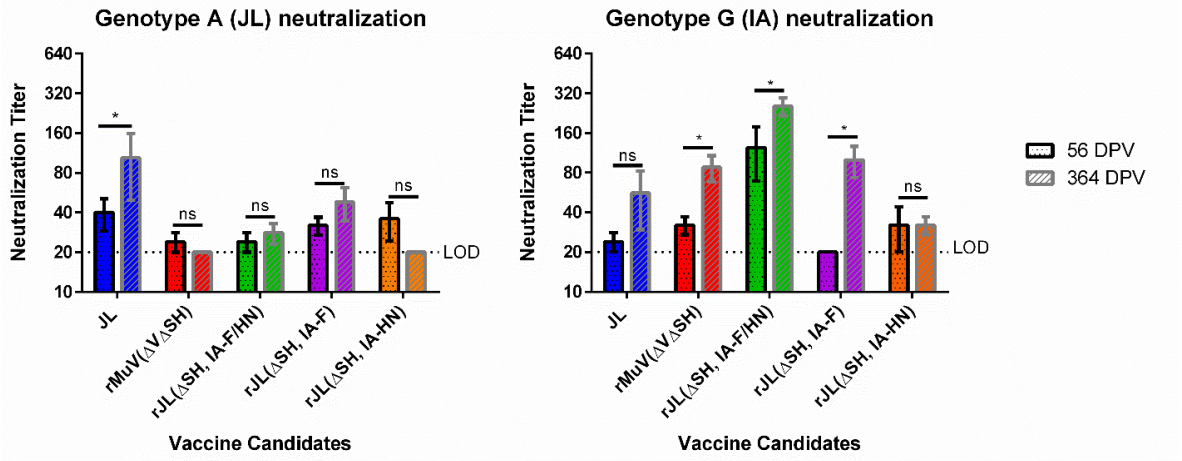
Genotype A (JL) neutralization
Genotype G (IA) neutralization
Neutralization Titer
640
320
160
80
40
20
10
LOD
*
ns
JL
rMuV(ΔVΔSH)
rJL(ΔSH, IA-F/HN)
rJL(ΔSH, IA-F)
rJL(ΔSH, IA-HN)
Vaccine Candidates
56 DPV
364 DPV

**Figure 5.5: Longevity of antibodies in mice immunized with vaccine candidates**

**(A) Timeline of BALB/c study.** BALB/c mice were intranasally immunized with $10^5$ PFU and then boosted with the same dose 21 days later. Mice were bled at 35, 56, 364 DPV. ELISAS and/or plaque reduction neutralization assays were performed. The study concluded 1 year post prime immunization. **(B) ELISA titers in mice post vaccination.** Mice were bled at day 56 and 364 post-prime immunization. Serum antibody titers were determined by ELISA. Endpoint titers were determined using serum from day 56 and day 364. Plates were coated in either genotype A **(left)** or genotype G **(right)** antigens. The reciprocal of the highest positive dilution and SEM of the average titer are reported. (n=5; 1-way ANOVA with comparison to the JL vaccine candidate was performed; *, $P<0.05$) **(C) Longevity of neutralization titers in mice post vaccination.** Plaque reduction assays were performed with day 56 and 364 serum to compare nAb levels over time. The mean 50% plaque reduction neutralization titer and SEM are reported. The bars represent the average plaque reduction neutralization titer. LOD is defined at the lowest dilution of serum that was plaqued, negative samples are reported as below the detection level. Neutralization against genotype A (JL) virus **(left)** Neutralization against genotype G (IA) virus **(right)**. n=5; Multiple T tests comparing 56 and 364 DPV was compared; * $P<0.05$.

A.

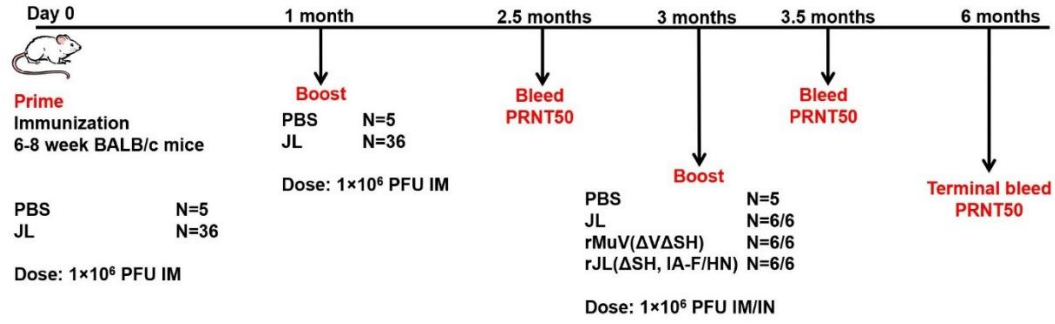
Day 0
1 month
2.5 months
3 months
3.5 months
6 months
Prime
Immunization
6-8 week BALB/c mice
PBS N=5
JL N=36
Dose: 1×10⁶ PFU IM
Boost
PBS N=5
JL N=36
Dose: 1×10⁶ PFU IM
Bleed
PRNT50
Boost
PBS N=5
JL N=6/6
rMuV(ΔVΔSH) N=6/6
rJL(ΔSH, IA-F/HN) N=6/6
Dose: 1×10⁶ PFU IM/IN
Bleed
PRNT50
Terminal bleed
PRNT50

B.

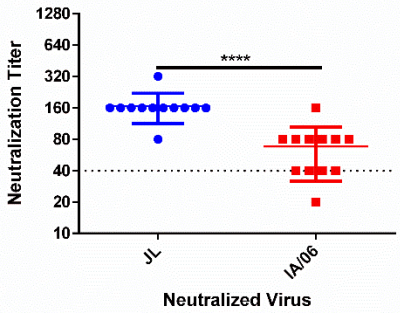
Neutralization Titer
1280
640
320
160
80
40
20
10
****
JL
IA/06
Neutralized Virus

C.

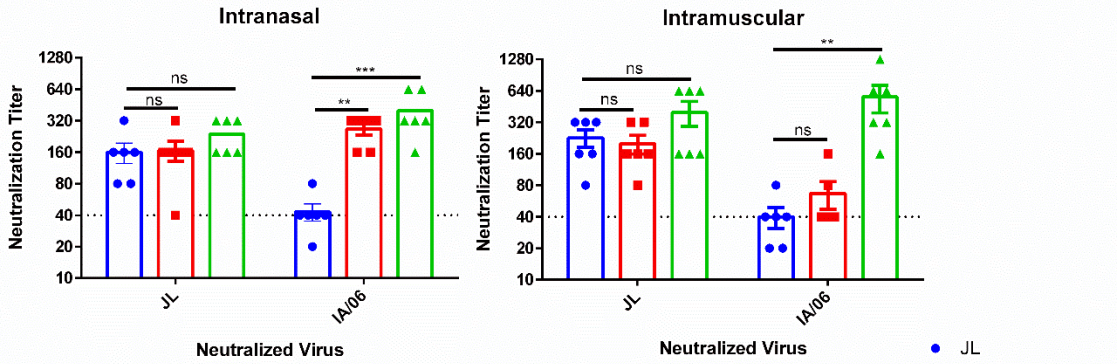
Intranasal
Intramuscular
Neutralization Titer
1280
640
320
160
80
40
20
10
ns
ns
***
**
**
ns
JL
IA/06
Neutralized Virus
JL
rMuV(dVdSH)
rJL(dSH, IA-F/HN)

D.

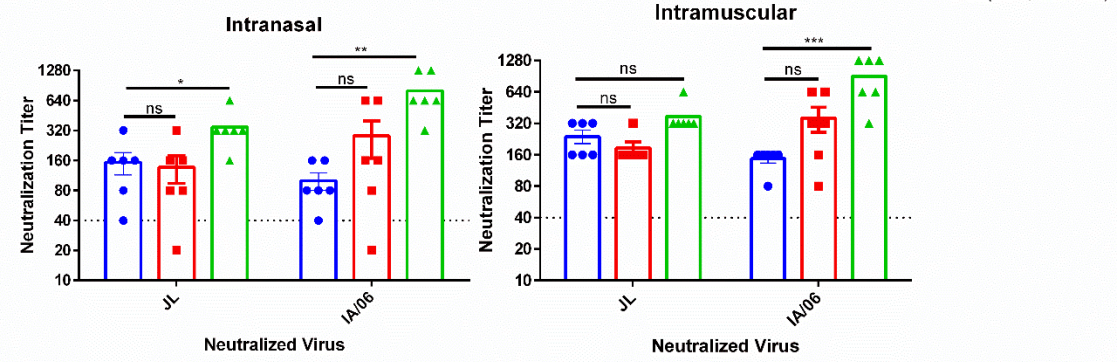
Intranasal
Intramuscular
Neutralization Titer
1280
640
320
160
80
40
20
10
*
ns
**
ns
ns
ns
***
ns
JL
IA/06
Neutralized Virus

**Figure 5.6: Neutralization titer in mice after a third dose of a genotype G-based vaccine.**

**(A) Timeline of BALB/c study.** BALB/c mice were intramuscularly immunized with $10^6$ PFU of JL and then boosted with the same dose at 1 month post prime. At 3 months post-prime mice were boosted intramuscularly or intranasally with $10^6$ PFU of JL, rMuV(ΔVΔSH), or rJL(ΔSH, IA-F/HN). Mice were bled at 2.5 and 3.5 months and then terminated at 6 months post prime. Serum was obtained for neutralization. **(B-D) Neutralization titers in mice post vaccination.** Plaque reduction assays were performed on serum collected from mice. The mean 50% plaque reduction neutralization titer and SEM are reported (n=6). Bars represent the average plaque reduction neutralization titer, and individual samples are plotted as points within the bars to show SEM. The dotted line represents the LOD, negative samples were plotted below the detection level. **(B)** Neutralization titers after prime-boost of JL given intramuscularly (2.5 months after prime). **(C)** Neutralization titers 3.5 months post prime, 2 weeks post IA-based immunization. **(D)** Neutralization 6 months post prime, 3 months post genotype G-based immunization. 1-way ANOVA with comparison to PBS; * $P<0.05$, ** $P<0.01$, *** $P<0.001$.

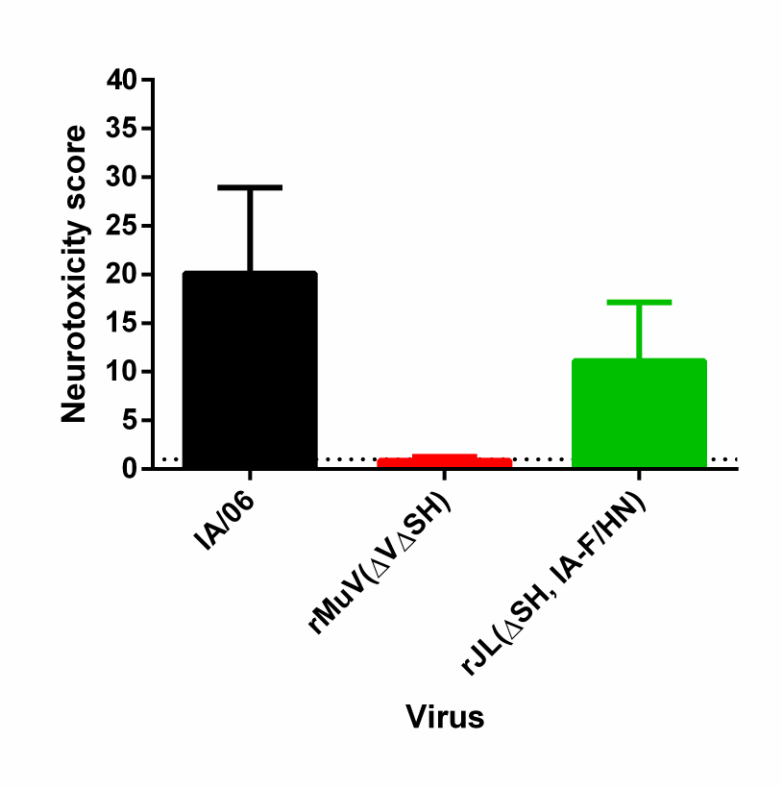


**Figure 5.7: Neurotoxicity of vaccine candidates**

The severity of hydrocephalus in rats inoculated with MuV (IA/06), rMuV(ΔVΔSH), and rJL(ΔSH, IA-F/HN) was measured as described in the Materials and Methods. Number of neonate rats per group: WT Iowa; n=10, rMuV(ΔVΔSH); n=26, and rJL(ΔSH, IA-F/HN); n=18. Mean score of neurotoxicity, and standard deviation (SD) is listed for each virus. The dotted line represents the neurotoxicity score of the JL vaccine that has been previously established.

# CHAPTER 6

## CONCLUSIONS

Mumps is a human pathogen that causes acute parotitis and is neurotropic with estimates of CNS infiltration in half of all clinical cases (1, 175, 268). Since the introduction of the MuV vaccine in 1967 the incidence of mumps has decreased by 99%. However, there has been a worldwide resurgence of mumps in the last two decades. Goals to eliminate mumps from the United States have failed due to increased cases (2). Several outbreaks have occurred in highly vaccinated populations and act as a reminder that mumps remains a global healthcare concern (2, 269). Even though mumps is an ancient disease, there are many gaps in our knowledge of its viral replication, pathogenesis, and immunity. Since the disease is rarely fatal, there have been few human autopsies which would provide valuable insight into its pathology. Animal models provide limited knowledge as humans are the only natural host of mumps (1). Additionally, the success of the vaccine has resulted in minimal continued research of the virus. A better understanding of mumps is required to develop therapeutics and better vaccines. This works seeks to provide insight into MuV viral RNA synthesis and advance the development of a next generation MuV vaccine.

**Specific Aim 1:** The goal of this aim was to identify and characterize a host kinase that effects the growth of MuV. Previous studies have shown that MuV P is highly phosphorylated by host kinases, so a large-scale siRNA screen was used to identify unknown host kinases that affect MuV genome replication and transcription (16, 17, 151). RPS6KB1, was shown to have an effect on MuV growth. Inhibition of this serine/threonine host kinase resulted in enhanced MuV growth. The hypothesis was that RPS6KB1 negatively regulates MuV replication and transcription through phosphorylation of MuV P. The results in chapter 3 validate RPS6KB1's role in negatively regulating MuV by using siRNA knockdown, an inhibitor, and RPS6KB1 knockout cells. This study detected an interaction between MuV P and RPS6KB1 suggesting that RPS6KB1 directly regulates MuV replication and transcription. This is the first report to identify an interaction between MuV P and RPS6KB1.

**Specific Aim 2:** The goal of this aim was to create an immunologically detectable MuV L protein to determine L's phosphorylation status. The L protein is essential for viral RNA synthesis, however the entirety of its function remains unclear (9, 11). In this study, a flag tagged MuV L (L-H2(flag)) was generated and tested in a minigenome assay. The insertion did not affect L function and it was rescued in a full-length virus. The phosphorylation status of paramyxovirus L proteins is debated, and MuV L has not been formally examined (140, 146-148). The hypothesis for this aim was that MuV L is phosphorylated, and its phosphorylation status plays a role in viral RNA synthesis. The results in chapter 4 validate the flag tag as tool for detecting MuV L and use it to identify four putative phosphorylation

sites in the protein. The L-S1087A/T1088A was found to have significantly reduced minigenome activity indicating it is a critical site for MuV L, however additional *in vitro* studies are required to validate this phenotype. The other sites identified, T1090A and S1102A, should be examined for a potential role in regulated mumps growth through phosphorylation. This is the first report to identify phosphorylation sites within MuV L.

**Specific Aim 3:** The goal of this aim was to evaluate the immunogenicity of genotype G-based vaccines. Vaccination with the attenuated Jeryl Lynn (JL) vaccine has dramatically reduced MuV cases, however large outbreaks are occurring in vaccinated populations (213, 218, 270). The vaccine strain was generated from genotype A, while most circulating strains belong to genotype G (2). The hypothesis for this aim is that a genotype G-based vaccine will protect against MuV infection better than the current vaccine. The results in chapter 5 show that the genotype G-based vaccines provide a robust humoral response for up to 1 year in mice. The study demonstrates that a third dose of a genotype G-based vaccine following two doses of JL increases neutralizing titers towards genotype G. In addition, it strengthens the notion that immunization with JL results in lower neutralizing titers towards a genotype G virus (22, 25, 213). This work proposes that a 3$^{rd}$ dose of a genotype G-based vaccine would be beneficial in preventing future mumps outbreaks.

Developing antiviral therapeutics and adjusting the current vaccine strategy are crucial to prevent future outbreaks. This body of work provides novel insights into MuV replication and transcription using a clinically relevant strain (IA, 06) and

advances the development of a next generation MuV vaccine. The discovery of the interaction between MuV P and RPS6KB1 can be exploited for the development of antivirals and the creation of the L-H2(flag) will aide in examining MuV L function. The development of recombinant MuV vaccine candidates offer an advantage over serial passaged attenuation because they offer higher homogeneity between batches and can be continually generated from a cDNA plasmid. The recombinant genotype G-based vaccines produced long-lasting neutralizing antibodies towards genotype G, the most prevalent of the circulating strains. This knowledge can aide in adjusting the current vaccine strategy. Taken together, these studies provide insight into MuV RNA synthesis, virus-host interactions, and aide in the development of a next generation MuV vaccine.

## REFERENCES


1. Rubin S, Eckhaus M, Rennick LJ, Bamford CG, Duprex WP. 2015. Molecular biology, pathogenesis and pathology of mumps virus. J Pathol 235:242-52.
2. Diseases NCfIaR. April 26th, 2019. Mumps cases and outbreaks *on* National Center for Immunization and Respiratory Diseases, Division of Viral Diseases, Centers for Disease Control and Prevenation https://www.cdc.gov/mumps/outbreaks.html. Accessed
3. Cox R, Plemper RK. 2015. The paramyxovirus polymerase complex as a target for next-generation anti-paramyxovirus therapeutics. Front Microbiol 6.
4. Pickar A, Xu P, Elson A, Li Z, Zengel J, He B. 2014. Roles of Serine and Threonine Residues of Mumps Virus P Protein in Viral Transcription and Replication. 88:4414-4422.
5. Zengel J, Pickar A, Xu P, Lin A, He B. 2015. Roles of Phosphorylation of the Nucleocapsid Protein of Mumps Virus in Regulating Viral RNA Transcription and Replication. 89:7338-7347.
6. Galazka AM, Robertson SE, Kraigher A. 1999. Mumps and mumps vaccine: a global review. Bull World Health Organ 77:3-14.

7. Marin M, Quinlisk P, Shimabukuro T, Sawhney C, Brown C, Lebaron CW. 2008. Mumps vaccination coverage and vaccine effectiveness in a large outbreak among college students--Iowa, 2006. Vaccine 26:3601-7.

8. Xu P, Li Z, Sun D, Lin Y, Wu J, Rota PA, He B. 2011. Rescue of wild-type mumps virus from a strain associated with recent outbreaks helps to define the role of the SH ORF in the pathogenesis of mumps virus. Virology 417:126-36.

9. Lamb RA, Parks GD. 2013. Paramyxoviridae, p 957-995. *In* Knipe DM, Howley PM (ed), Fields Virology, 6 ed, vol 1. Lippincott Williams & Wilkins, Philadelphia, PA.

10. Lamb RA, Parks GD. 2013. Mumps Virus. *In* Knipe DM, Howley PM (ed), Fields Virology, vol 1. Lippincott Williams & Wilkins, Philadelphia, PA.

11. Lamb RA KD. 2001. Paramyxoviridae: The viruses and their replication, 4 ed. Lippincott Williams and Wilkins, Philadelphia.

12. Asenjo A, Calvo E, Villanueva N. 2006. Phosphorylation of human respiratory syncytial virus P protein at threonine 108 controls its interaction with the M2-1 protein in the viral RNA polymerase complex. J Gen Virol 87:3637-42.

13. Timani KA, Sun D, Sun M, Keim C, Lin Y, Schmitt PT, Schmitt AP, He B. 2008. A single amino acid residue change in the P protein of parainfluenza virus 5 elevates viral gene expression. J Virol 82:9123-33.

14. Lenard J. 1999. Host cell protein kinases in nonsegmented negative-strand virus (mononegavirales) infection. Pharmacol Ther 83:39-48.

15. Sun M, Fuentes SM, Timani K, Sun D, Murphy C, Lin Y, August A, Teng MN, He B. 2008. Akt Plays a Critical Role in Replication of Nonsegmented Negative-Stranded RNA Viruses ▿ , p 105-14, J Virol, vol 82.

16. Pickar A, Zengel J, Xu P, Li Z, He B. 2016. Mumps Virus Nucleoprotein Enhances Phosphorylation of the Phosphoprotein by Polo-Like Kinase 1. Journal of virology 90:1588-1598.

17. Sun D, Luthra P, Li Z, He B. 2009. PLK1 Down-Regulates Parainfluenza Virus 5 Gene Expression. PLOS Pathogens 5:e1000525.

18. Villanueva N, Navarro J, Mendez E, Garcia-Albert I. 1994. Identification of a protein kinase involved in the phosphorylation of the C-terminal region of human respiratory syncytial virus P protein. J Gen Virol 75 ( Pt 3):555-65.

19. Sidhu MS, Menonna JP, Cook SD, Dowling PC, Udem SA. 1993. Canine distemper virus L gene: sequence and comparison with related viruses. Virology 193:50-65.

20. Duprex WP, Collins FM, Rima BK. 2002. Modulating the function of the measles virus RNA-dependent RNA polymerase by insertion of green fluorescent protein into the open reading frame. Journal of virology 76:7322-7328.

21. Cox R, Green TJ, Purushotham S, Deivanayagam C, Bedwell GJ, Prevelige PE, Luo M. 2013. Structural and Functional Characterization of the Mumps Virus Phosphoprotein. 87:7558-7568.

22. Zengel J, Phan SI, Pickar A, Xu P, He B. 2017. Immunogenicity of mumps virus vaccine candidates matching circulating genotypes in the United States and China. Vaccine 35:3988-3994.

23. Buynak EB, Hilleman MR. 1966. Live attenuated mumps virus vaccine. 1. Vaccine development. Proc Soc Exp Biol Med 123:768-75.

24. Connell AR, Connell J, Leahy TR, Hassan J. 2020. Mumps Outbreaks in Vaccinated Populations-Is It Time to Re-assess the Clinical Efficacy of Vaccines? Frontiers in immunology 11:2089-2089.

25. Xu P, Chen Z, Phan S, Pickar A, He B. 2014. Immunogenicity of novel mumps vaccine candidates generated by genetic modification. Journal of virology 88:2600-2610.

26. C. TE. 1967. HIPPOCRATES DESCRIBES MUMPS FOLLOWED BY ORCHITIS. Pediatrics 40:420-420.

27. C. TE. 1970. THE FIRST DETAILED DESCRIPTION OF MUMPS BY ROBERT HAMILTON, M.D. (1721-1793), PUBLISHED IN 1790. Pediatrics 45:253-253.

28. Jin L, Örvell C, Myers R, Rota PA, Nakayama T, Forcic D, Hiebert J, Brown KE. 2015. Genomic diversity of mumps virus and global distribution of the 12 genotypes. Rev Med Virol 25:85-101.

29. Johnson CD, Goodpasture EW. 1934. AN INVESTIGATION OF THE ETIOLOGY OF MUMPS. The Journal of experimental medicine 59:1-19.

30. Enders JF, Levens JH, *et al.* 1946. Attenuation of virulence with retention of antigenicity of mumps virus after passage in the embryonated egg. J Immunol 54:283-91.

31. Levens JH, Enders JF. 1945. THE HEMOAGGLUTINATIVE PROPERTIES OF AMNIOTIC FLUID FROM EMBRYONATED EGGS INFECTED WITH MUMPS VIRUS. Science 102:117-20.

32. Habel K. 1946. Preparation of Mumps Vaccines and Immunization of Monkeys against Experimental Mumps Infection. Public Health Reports (1896-1970) 61:1655-1664.

33. Elango N, Varsanyi TM, Kövamees J, Norrby E. 1988. Molecular Cloning and Characterization of Six Genes, Determination of Gene Order and Intergenic Sequences and Leader Sequence of Mumps Virus. Journal of General Virology 69:2893-2900.

34. Anonymous. 2021. International Commitee on Taxonmy of Viruses (ICTV), *on* 2021. https://ictv.global/taxonomy/. Accessed 9/14/21.

35. Jin L, Rima B, Brown D, Örvell C, Tecle T, Afzal M, Uchida K, Nakayama T, Song JW, Kang C, Rota PA, Xu W, Featherstone D. 2005. Proposal for genetic characterisation of wild-type mumps strains: Preliminary standardisation of the nomenclature. Archives of Virology 150:1903-1909.

36. Noton SL, Fearns R. 2015. Initiation and regulation of paramyxovirus transcription and replication. Virology 479-480:545-54.

37. Paterson RG, Lamb RA. 1990. RNA editing by G-nucleotide insertion in mumps virus P-gene mRNA transcripts. J Virol 64:4137-45.

38. Wignall-Fleming EB, Hughes DJ, Vattipally S, Modha S, Goodbourn S, Davison AJ, Randall RE. 2019. Analysis of Paramyxovirus Transcription and Replication by High-Throughput Sequencing. Journal of virology 93:e00571-19.

39. Douglas J, Drummond AJ, Kingston RL. 2021. Evolutionary history of cotranscriptional editing in the paramyxoviral phosphoprotein gene. Virus Evolution 7.

40. Douglas J, Drummond AJ, Kingston RL. 2021. Evolutionary history of cotranscriptional editing in the paramyxoviral phosphoprotein gene. Virus Evol 7:veab028.

41. Kingston RL, Baase WA, Gay LS. 2004. Characterization of nucleocapsid binding by the measles virus and mumps virus phosphoproteins. J Virol 78:8630-40.

42. Kingston RL, Gay LS, Baase WS, Matthews BW. 2008. Structure of the nucleocapsid-binding domain from the mumps virus polymerase; an example of protein folding induced by crystallization. J Mol Biol 379:719-31.

43. Precious B, Young DF, Bermingham A, Fearns R, Ryan M, Randall RE. 1995. Inducible expression of the P, V, and NP genes of the paramyxovirus simian virus 5 in cell lines and an examination of NP-P and NP-V interactions. J Virol 69:8001-10.

44. Masters PS, Banerjee AK. 1988. Complex formation with vesicular stomatitis virus phosphoprotein NS prevents binding of nucleocapsid protein N to nonspecific RNA. Journal of virology 62:2658-2664.

45. Peluso RW, Moyer SA. 1988. Viral proteins required for the in vitro replication of vesicular stomatitis virus defective interfering particle genome RNA. Virology 162:369-76.

46. Kolakofsky D, Roux L, Garcin D, Ruigrok RWH. 2005. Paramyxovirus mRNA editing, the ‘rule of six’ and error catastrophe: a hypothesis. 86:1869-1877.

47. Matsumoto Y, Ohta K, Kolakofsky D, Nishio M. 2018. The control of paramyxovirus genome hexamer length and mRNA editing. RNA (New York, NY) 24:461-467.

48. Iseni F, Baudin F, Garcin D, Marq JB, Ruigrok RW, Kolakofsky D. 2002. Chemical modification of nucleotide bases and mRNA editing depend on hexamer or nucleoprotein phase in Sendai virus nucleocapsids. Rna 8:1056-67.

49. Bourhis JM, Johansson K, Receveur-Bréchot V, Oldfield CJ, Dunker KA, Canard B, Longhi S. 2004. The C-terminal domain of measles virus nucleoprotein belongs to the class of intrinsically disordered proteins that fold upon binding to their physiological partner. Virus Res 99:157-67.

50. Cox R, Pickar A, Qiu S, Tsao J, Rodenburg C, Dokland T, Elson A, He B, Luo M. 2014. Structural studies on the authentic mumps virus nucleocapsid showing uncoiling by the phosphoprotein. Proc Natl Acad Sci U S A 111:15208-13.

51. Kingston RL, Hamel DJ, Gay LS, Dahlquist FW, Matthews BW. 2004. Structural basis for the attachment of a paramyxoviral polymerase to its template. Proc Natl Acad Sci U S A 101:8301-6.

52. Sugai A, Sato H, Yoneda M, Kai C. 2013. Phosphorylation of measles virus nucleoprotein affects viral growth by changing gene expression and genomic RNA stability. J Virol 87:11684-92.

53. Cox R, Green TJ, Qiu S, Kang J, Tsao J, Prevelige PE, He B, Luo M. 2009. Characterization of a mumps virus nucleocapsidlike particle. Journal of virology 83:11402-11406.

54. Briggs K, Wang L, Nagashima K, Zengel J, Tripp RA, He B. 2020. Regulation of Mumps Virus Replication and Transcription by Kinase RPS6KB1. Journal of Virology 94:e00387-20.

55. Pickar A, Elson A, Yang Y, Xu P, Luo M, He B. 2015. Oligomerization of Mumps Virus Phosphoprotein. J Virol 89:11002-10.

56. Takeuchi K, Tanabayashi K, Hishiyama M, Yamada YK, Yamada A, Sugiura A. 1990. Detection and characterization of mumps virus V protein. Virology 178:247-53.

57. Nishio M, Ohtsuka J, Tsurudome M, Nosaka T, Kolakofsky D. 2008. Human Parainfluenza Virus Type 2 V Protein Inhibits Genome Replication by Binding to the L Protein: Possible Role in Promoting Viral Fitness. Journal of Virology 82:6130-6138.

58. Yang Y, Zengel J, Sun M, Sleeman K, Timani KA, Aligo J, Rota P, Wu J, He B. 2015. Regulation of Viral RNA Synthesis by the V Protein of Parainfluenza Virus 5. Journal of virology 89:11845-11857.

59. Luthra P, Sun D, Silverman RH, He B. 2011. Activation of IFN-β expression by a viral mRNA through RNase L and MDA5. Proceedings of the National Academy of Sciences 108:2118-2123.

60. Motz C, Schuhmann KM, Kirchhofer A, Moldt M, Witte G, Conzelmann K-K, Hopfner K-P. 2013. Paramyxovirus V Proteins Disrupt the Fold of the RNA Sensor MDA5 to Inhibit Antiviral Signaling. Science doi:10.1126/science.1230949:1230949.

61. Xu P, Luthra P, Li Z, Fuentes S, D'Andrea JA, Wu J, Rubin S, Rota PA, He B. 2012. The V Protein of Mumps Virus Plays a Critical Role in Pathogenesis, p 1768-76, J Virol, vol 86.

62. Andrejeva J, Childs KS, Young DF, Carlos TS, Stock N, Goodbourn S, Randall RE. 2004. The V proteins of paramyxoviruses bind the IFN-inducible RNA helicase, mda-5, and inhibit its activation of the IFN-β promoter. Proceedings of the National Academy of Sciences of the United States of America 101:17264-17269.

63. Kubota T, Yokosawa N, Yokota S, Fujii N. 2001. C terminal CYS-RICH region of mumps virus structural V protein correlates with block of interferon alpha and gamma signal transduction pathway through decrease of STAT 1-alpha. Biochem Biophys Res Commun 283:255-9.

64. Lin Y, Sun M, Fuentes SM, Keim CD, Rothermel T, He B. 2007. Inhibition of interleukin-6 expression by the V protein of parainfluenza virus 5. Virology 368:262-272.

65. Lin Y, Horvath F, Aligo JA, Wilson R, He B. 2005. The role of simian virus 5 V protein on viral RNA synthesis. Virology 338:270-80.

66. Rubin SA, Afzal MA, Powell CL, Bentley ML, Auda GR, Taffs RE, Carbone KM. 2005. The rat-based neurovirulence safety test for the assessment of mumps virus neurovirulence in humans: an international collaborative study. J Infect Dis 191:1123-8.

67. Rubin SA, Pletnikov M, Taffs R, Snoy PJ, Kobasa D, Brown EG, Wright KE, Carbone KM. 2000. Evaluation of a neonatal rat model for prediction of mumps virus neurovirulence in humans. J Virol 74:5382-4.

68. Elango N. 1989. Complete nucleotide sequence of the matrix protein mRNA of mumps virus. Virology 168:426-8.

69. Li M, Schmitt PT, Li Z, McCrory TS, He B, Schmitt AP. 2009. Mumps virus matrix, fusion, and nucleocapsid proteins cooperate for efficient production of virus-like particles. J Virol 83:7261-72.

70. Mottet-Osman G, Miazza V, Vidalain PO, Roux L. 2014. Patchwork structure-function analysis of the Sendai virus matrix protein. Virology 464-465:330-340.

71. Naim HY, Ehler E, Billeter MA. 2000. Measles virus matrix protein specifies apical virus release and glycoprotein sorting in epithelial cells. The EMBO journal 19:3576-3585.

72. Udem SA, Cook KA. 1984. Isolation and characterization of measles virus intracellular nucleocapsid RNA. J Virol 49:57-65.

73. Takimoto T, Bousse T, Coronel EC, Scroggs RA, Portner A. 1998. Cytoplasmic domain of Sendai virus HN protein contains a specific sequence required for its incorporation into virions. Journal of virology 72:9747-9754.

74. Schmitt AP, Leser GP, Morita E, Sundquist WI, Lamb RA. 2005. Evidence for a new viral late-domain core sequence, FPIV, necessary for budding of a paramyxovirus. Journal of virology 79:2988-2997.

75. Pei Z, Bai Y, Schmitt AP. 2010. PIV5 M protein interaction with host protein angiomotin-like 1. Virology 397:155-66.

76. Waxham MN, Server AC, Goodman HM, Wolinsky JS. 1987. Cloning and sequencing of the mumps virus fusion protein gene. Virology 159:381-8.

77. Waxham MN, Merz DC, Wolinsky JS. 1986. Intracellular maturation of mumps virus hemagglutinin-neuraminidase glycoprotein: conformational changes detected with monoclonal antibodies. Journal of virology 59:392-400.

78. Merz DC, Server AC, Waxham MN, Wolinsky JS. 1983. Biosynthesis of mumps virus F glycoprotein: non-fusing strains efficiently cleave the F glycoprotein precursor. J Gen Virol 64 (Pt 7):1457-67.

79. Chang A, Dutch RE. 2012. Paramyxovirus fusion and entry: multiple paths to a common end. Viruses 4:613-636.

80. Liu Y, Xu Y, Lou Z, Zhu J, Hu X, Gao GF, Qiu B, Rao Z, Tien P. 2006. Structural characterization of mumps virus fusion protein core. Biochem Biophys Res Commun 348:916-22.

81. Liu Y, Xu Y, Zhu J, Qiu B, Rao Z, Gao GF, Tien P. 2005. Crystallization and preliminary X-ray diffraction analysis of central structure domains from mumps virus F protein. Acta crystallographica Section F, Structural biology and crystallization communications 61:855-857.

82. Liu Y, Zhu J, Feng MG, Tien P, Gao GF. 2004. Six-helix bundle assembly and analysis of the central core of mumps virus fusion protein. Arch Biochem Biophys 421:143-8.

83. Elango N, Kövamees J, Varsanyi TM, Norrby E. 1989. mRNA sequence and deduced amino acid sequence of the mumps virus small hydrophobic protein gene. J Virol 63:1413-5.

84. Hiebert SW, Richardson CD, Lamb RA. 1988. Cell surface expression and orientation in membranes of the 44-amino-acid SH protein of simian virus 5. J Virol 62:2347-57.

85. Künkel U, Driesel G, Henning U, Gerike E, Schreier E, Willers H. 1995. Differentiation of vaccine and wild mumps viruses by polymerase chain reaction and nucleotide sequencing of the SH gene: Brief report. Journal of Medical Virology 45:121-126.

86. Takeuchi K, Tanabayashi K, Hishiyama M, Yamada A. 1996. The mumps virus SH protein is a membrane protein and not essential for virus growth. Virology 225:156-62.

87. Wilson RL, Fuentes SM, Wang P, Taddeo EC, Klatt A, Henderson AJ, He B. 2006. Function of small hydrophobic proteins of paramyxovirus. Journal of virology 80:1700-1709.

88. Abraham M, Arroyo-Diaz NM, Li Z, Zengel J, Sakamoto K, He B. 2018. Role of Small Hydrophobic Protein of J Paramyxovirus in Virulence. Journal of virology 92:e00653-18.

89. Luthra P, Sun D, Wolfgang M, He B. 2008. AKT1-Dependent Activation of NF-κB by the L Protein of Parainfluenza Virus 5. 82:10887-10895.

90. Colman PM, Hoyne PA, Lawrence MC. 1993. Sequence and structure alignment of paramyxovirus hemagglutinin-neuraminidase with influenza virus neuraminidase. J Virol 67:2972-80.

91. Crennell S, Takimoto T, Portner A, Taylor G. 2000. Crystal structure of the multifunctional paramyxovirus hemagglutinin-neuraminidase. Nat Struct Biol 7:1068-74.

92. Lawrence MC, Borg NA, Streltsov VA, Pilling PA, Epa VC, Varghese JN, McKimm-Breschkin JL, Colman PM. 2004. Structure of the haemagglutinin-neuraminidase from human parainfluenza virus type III. J Mol Biol 335:1343-57.

93. Choppin PW, Scheid A. 1980. The role of viral glycoproteins in adsorption, penetration, and pathogenicity of viruses. Rev Infect Dis 2:40-61.

94. Yuan P, Thompson TB, Wurzburg BA, Paterson RG, Lamb RA, Jardetzky TS. 2005. Structural studies of the parainfluenza virus 5 hemagglutinin-

neuraminidase tetramer in complex with its receptor, sialyllactose. Structure 13:803-15.

95. Scheid A, Hsu M, Choppin PW. 1980. Role of paramyxovirus glycoproteins in the interactions between viral and cell membranes. Soc Gen Physiol Ser 34:119-30.

96. Cevik B, Holmes DE, Vrotsos E, Feller JA, Smallwood S, Moyer SA. 2004. The phosphoprotein (P) and L binding sites reside in the N-terminus of the L subunit of the measles virus RNA polymerase. Virology 327:297-306.

97. Cevik B, Smallwood S, Moyer SA. 2003. The L-L oligomerization domain resides at the very N-terminus of the sendai virus L RNA polymerase protein. Virology 313:525-36.

98. Emerson SU. 1982. Reconstitution studies detect a single polymerase entry site on the vesicular stomatitis virus genome. Cell 31:635-42.

99. Emerson SU, Yu Y. 1975. Both NS and L proteins are required for in vitro RNA synthesis by vesicular stomatitis virus. J Virol 15:1348-56.

100. Li Z, Xu J, Chen Z, Gao X, Wang L-F, Basler C, Sakamoto K, He B. 2013. The L gene of J paramyxovirus plays a critical role in viral pathogenesis. Journal of virology 87:12990-12998.

101. Abdella R, Aggarwal M, Okura T, Lamb RA, He Y. 2020. Structure of a paramyxovirus polymerase complex reveals a unique methyltransferase-CTD conformation. Proceedings of the National Academy of Sciences 117:4931-4941.

102. Poch O, Blumberg BM, Bougueleret L, Tordo N. 1990. Sequence comparison of five polymerases (L proteins) of unsegmented negative-strand RNA viruses: theoretical assignment of functional domains. J Gen Virol 71 ( Pt 5):1153-62.

103. Poch O, Sauvaget I, Delarue M, Tordo N. 1989. Identification of four conserved motifs among the RNA-dependent polymerase encoding elements. Embo j 8:3867-74.

104. Gilman MSA, Liu C, Fung A, Behera I, Jordan P, Rigaux P, Ysebaert N, Tcherniuk S, Sourimant J, Eléouët JF, Sutto-Ortiz P, Decroly E, Roymans D, Jin Z, McLellan JS. 2019. Structure of the Respiratory Syncytial Virus Polymerase Complex. Cell 179:193-204.e14.

105. Masters PS, Banerjee AK. 1988. Resolution of multiple complexes of phosphoprotein NS with nucleocapsid protein N of vesicular stomatitis virus. J Virol 62:2651-7.

106. Ruedas JB, Perrault J. 2014. Putative domain-domain interactions in the vesicular stomatitis virus L polymerase protein appendage region. Journal of virology 88:14458-14466.

107. Liang B, Lowen AC. 2020. Structures of the Mononegavirales Polymerases. Journal of Virology 94:e00175-20.

108. Li J, Rahmeh A, Morelli M, Whelan SP. 2008. A conserved motif in region v of the large polymerase proteins of nonsegmented negative-sense RNA viruses that is essential for mRNA capping. J Virol 82:775-84.

109. Feller JA, Smallwood S, Horikami SM, Moyer SA. 2000. Mutations in conserved domains IV and VI of the large (L) subunit of the sendai virus RNA polymerase give a spectrum of defective RNA synthesis phenotypes. Virology 269:426-39.

110. Sutto-Ortiz P, Tcherniuk S, Ysebaert N, Abeywickrema P, Noël M, Decombe A, Debart F, Vasseur J-J, Canard B, Roymans D, Rigaux P, Eléouët J-F, Decroly E. 2021. The methyltransferase domain of the Respiratory Syncytial Virus L protein catalyzes cap N7 and 2'-O-methylation. PLOS Pathogens 17:e1009562.

111. Hao X, Wang Y, Zhu M, Zhou D, Liu R, Wang B, Huang YW, Zhao Z. 2020. Development of Improved Mumps Vaccine Candidates by Mutating Viral mRNA Cap Methyltransferase Sites in the Large Polymerase Protein. Virol Sin doi:10.1007/s12250-020-00326-y:1-16.

112. Kubota M, Takeuchi K, Watanabe S, Ohno S, Matsuoka R, Kohda D, Nakakita S-I, Hiramatsu H, Suzuki Y, Nakayama T, Terada T, Shimizu K, Shimizu N, Shiroishi M, Yanagi Y, Hashiguchi T. 2016. Trisaccharide containing α2,3-linked sialic acid is a receptor for mumps virus. Proceedings of the National Academy of Sciences of the United States of America 113:11579-11584.

113. Reyes-Leyva J, Baños R, Borraz-Argüello M, Santos-López G, Rosas N, Alvarado G, Herrera I, Vallejo V, Tapia-Ramírez J. 2007. Amino acid change 335 E to K affects the sialic-acid-binding and neuraminidase

activities of Urabe AM9 mumps virus hemagglutinin-neuraminidase glycoprotein. Microbes Infect 9:234-40.

114. Sauder CJ, Zhang CX, Link MA, Duprex WP, Carbone KM, Rubin SA. 2009. Presence of lysine at aa 335 of the hemagglutinin-neuraminidase protein of mumps virus vaccine strain Urabe AM9 is not a requirement for neurovirulence. Vaccine 27:5822-9.

115. Lamb RA, Paterson RG, Jardetzky TS. 2006. Paramyxovirus membrane fusion: lessons from the F and HN atomic structures. Virology 344:30-7.

116. Smith EC, Popa A, Chang A, Masante C, Dutch RE. 2009. Viral entry mechanisms: the increasing diversity of paramyxovirus entry. The FEBS journal 276:7217-7227.

117. Afzal MA, Dussupt V, Minor PD, Pipkin PA, Fleck R, Hockley DJ, Stacey GN. 2005. Assessment of mumps virus growth on various continuous cell lines by virological, immunological, molecular and morphological investigations. J Virol Methods 126:149-56.

118. Gresser I, Enders JF. 1961. Cytopathogenicity of mumps virus in cultures of chick embryo and human amnion cells. Proc Soc Exp Biol Med 107:804-7.

119. McCarthy M, Johnson RT. 1980. Morphological heterogeneity in relation to structural and functional properties of mumps virus. J Gen Virol 48:395-9.

120. Ogino T, Kobayashi M, Iwama M, Mizumoto K. 2005. Sendai Virus RNA-dependent RNA Polymerase L Protein Catalyzes Cap Methylation of Virus-specific mRNA*. Journal of Biological Chemistry 280:4429-4435.

121. Stillman EA, Whitt MA. 1999. Transcript initiation and 5'-end modifications are separable events during vesicular stomatitis virus transcription. J Virol 73:7199-209.

122. Wang JT, McElvain LE, Whelan SPJ. 2007. Vesicular Stomatitis Virus mRNA Capping Machinery Requires Specific cis-Acting Signals in the RNA. Journal of Virology 81:11499-11506.

123. Abraham G, Banerjee AK. 1976. Sequential transcription of the genes of vesicular stomatitis virus. Proc Natl Acad Sci U S A 73:1504-8.

124. Ball LA, White CN. 1976. Order of transcription of genes of vesicular stomatitis virus. Proc Natl Acad Sci U S A 73:442-6.

125. Collins PL, Wertz GW. 1983. cDNA cloning and transcriptional mapping of nine polyadenylylated RNAs encoded by the genome of human respiratory syncytial virus. Proceedings of the National Academy of Sciences 80:3208-3212.

126. Vidal S, Kolakofsky D. 1989. Modified model for the switch from Sendai virus transcription to replication. Journal of virology 63:1951-1958.

127. Qanungo KR, Shaji D, Mathur M, Banerjee AK. 2004. Two RNA polymerase complexes from vesicular stomatitis virus-infected cells that carry out transcription and replication of genome RNA. Proceedings of the National Academy of Sciences of the United States of America 101:5952-5957.

128. Howard M, Wertz G. 1989. Vesicular stomatitis virus RNA replication: a role for the NS protein. J Gen Virol 70 ( Pt 10):2683-94.

129. Patton JT, Davis NL, Wertz GW. 1984. N protein alone satisfies the requirement for protein synthesis during RNA replication of vesicular stomatitis virus. J Virol 49:303-9.

130. Schmitt AP, Lamb RA. 2004. Escaping from the cell: assembly and budding of negative-strand RNA viruses. Curr Top Microbiol Immunol 283:145-96.

131. Hagiwara K, Sato H, Inoue Y, Watanabe A, Yoneda M, Ikeda F, Fujita K, Fukuda H, Takamura C, Kozuka-Hata H, Oyama M, Sugano S, Ohmi S, Kai C. 2008. Phosphorylation of measles virus nucleoprotein upregulates the transcriptional activity of minigenomic RNA. PROTEOMICS 8:1871-1879.

132. Sugai A, Sato H, Yoneda M, Kai C. 2012. Phosphorylation of measles virus phosphoprotein at S86 and/or S151 downregulates viral transcriptional activity. FEBS Lett 586:3900-7.

133. Yang J, Koprowski H, Dietzschold B, Fu ZF. 1999. Phosphorylation of rabies virus nucleoprotein regulates viral RNA transcription and replication by modulating leader RNA encapsidation. J Virol 73:1661-4.

134. Becker S, Huppertz S, Klenk HD, Feldmann H. 1994. The nucleoprotein of Marburg virus is phosphorylated. J Gen Virol 75 ( Pt 4):809-18.

135. Naruse H, Nagai Y, Yoshida T, Hamaguchi M, Matsumoto T, Isomura S, Suzuki S. 1981. The polypeptides of mumps virus and their synthesis in infected chick embryo cells. Virology 112:119-30.

136. Das T, Schuster A, Schneider-Schaulies S, Banerjee AK. 1995. Involvement of cellular casein kinase II in the phosphorylation of measles virus P protein: identification of phosphorylation sites. Virology 211:218-26.

137. Liu Z, Huntley CC, De BP, Das T, Banerjee AK, Oglesbee MJ. 1997. Phosphorylation of canine distemper virus P protein by protein kinase C-zeta and casein kinase II. Virology 232:198-206.

138. Sánchez-Seco MP, Navarro J, Martínez R, Villanueva N. 1995. C-terminal phosphorylation of human respiratory syncytial virus P protein occurs mainly at serine residue 232. J Gen Virol 76 ( Pt 2):425-30.

139. Navarro J, López-Otín C, Villanueva N. 1991. Location of phosphorylated residues in human respiratory syncytial virus phosphoprotein. J Gen Virol 72 ( Pt 6):1455-9.

140. Barik S, McLean T, Dupuy LC. 1995. Phosphorylation of Ser232 directly regulates the transcriptional activity of the P protein of human respiratory syncytial virus: phosphorylation of Ser237 may play an accessory role. Virology 213:405-12.

141. Lu B, Ma C-H, Brazas R, Jin H. 2002. The major phosphorylation sites of the respiratory syncytial virus phosphoprotein are dispensable for virus replication in vitro. Journal of virology 76:10776-10784.

142. Beavis AC, Tran KC, Barrozo ER, Phan SI, Teng MN, He B. 2021. Respiratory Syncytial Virus Phosphoprotein Residue S156 Plays a Role in Regulating Genome Transcription and Replication. J Virol doi:10.1128/jvi.01206-21:Jvi0120621.

143. Mazumder B, Adhikary G, Barik S. 1994. Bacterial expression of human respiratory syncytial viral phosphoprotein P and identification of Ser237 as the site of phosphorylation by cellular casein kinase II. Virology 205:93-103.

144. Mazumder B, Barik S. 1994. Requirement of casein kinase II-mediated phosphorylation for the transcriptional activity of human respiratory syncytial viral phosphoprotein P: transdominant negative phenotype of phosphorylation-defective P mutants. Virology 205:104-11.

145. Sun D, Luthra P, Xu P, Yoon H, He B. 2011. Identification of a Phosphorylation Site within the P Protein Important for mRNA Transcription and Growth of Parainfluenza Virus 5. Journal of Virology 85:8376-8385.

146. Hammond DC, Haley BE, Lesnaw JA. 1992. Identification and characterization of serine/threonine protein kinase activity intrinsic to the L protein of vesicular stomatitis virus New Jersey. J Gen Virol 73 ( Pt 1):67-75.

147. Massey DM, Deans N, Lenard J. 1990. Phosphorylation of NS protein by vesicular stomatitis virus nucleocapsids: lack of effect during RNA synthesis and separation of kinase from L protein. J Virol 64:3259-64.

148. Einberger H, Mertz R, Hofschneider PH, Neubert WJ. 1990. Purification, renaturation, and reconstituted protein kinase activity of the Sendai virus large (L) protein: L protein phosphorylates the NP and P proteins in vitro. Journal of virology 64:4274-4280.

149. Eden J-S, Sharpe LJ, White PA, Brown AJ. 2011. Norovirus RNA-dependent RNA polymerase is phosphorylated by an important survival kinase, Akt. Journal of virology 85:10894-10898.

150. Bagchi P, Nandi S, Nayak MK, Chawla-Sarkar M. 2013. Molecular Mechanism behind Rotavirus NSP1-Mediated PI3 Kinase Activation:

Interaction between NSP1 and the p85 Subunit of PI3 Kinase. 87:2358-2362.

151. Fuentes SM, Sun D, Schmitt AP, He B. 2010. Phosphorylation of paramyxovirus phosphoprotein and its role in viral gene expression. Future Microbiol 5:9-13.

152. Liu J, Wang H, Wang B, Chen T, Wang X, Huang P, Xu L, Guo Z. 2016. Microcystin-LR promotes proliferation by activating Akt/S6K1 pathway and disordering apoptosis and cell cycle associated proteins phosphorylation in HL7702 cells. Toxicol Lett 240:214-25.

153. Henle G, Henle W, *et al.* 1948. Isolation of mumps virus from human beings with induced apparent or inapparent infections. J Exp Med 88:223-32.

154. Utz JP, Kasel JA, Cramblett HG, Szwed CF, Parrott RH. 1957. Clinical and laboratory studies of mumps. I. Laboratory diagnosis by tissue-culture technics. N Engl J Med 257:497-502.

155. Utz JP, Szwed CF, Kasel JA. 1958. Clinical and laboratory studies of mumps. II. Detection and duration of excretion of virus in urine. Proc Soc Exp Biol Med 99:259-61.

156. Jin L, Brown DWG, Litton PA, White JM. 2004. Genetic Diversity of Mumps Virus in Oral Fluid Specimens: Application to Mumps Epidemiological Study. The Journal of Infectious Diseases 189:1001-1008.

157. Jin L, Vyse A, Brown DW. 2002. The role of RT-PCR assay of oral fluid for diagnosis and surveillance of measles, mumps and rubella. Bull World Health Organ 80:76-7.

158. Katoh H, Kubota T, Ihara T, Maeda K, Takeda M, Kidokoro M. 2016. Cross-Neutralization between Human and African Bat Mumps Viruses. Emerging infectious diseases 22:703-706.

159. Xu P, Huang Z, Gao X, Michel FJ, Hirsch G, Hogan RJ, Sakamoto K, Ho W, Wu J, He B. 2013. Infection of Mice, Ferrets, and Rhesus Macaques with a Clinical Mumps Virus Isolate. Journal of Virology 87:8158-8168.

160. Lin CY, Chen WP, Chiang H. 1990. Mumps associated with nephritis. Child Nephrol Urol 10:68-71.

161. Kabakuş N, Aydinoğlu H, Bakkaloğlu SA, Yekeler H. 1999. Mumps interstitial nephritis: a case report. Pediatr Nephrol 13:930-1.

162. Hughes WT, Steigman AJ, Delong HF. 1966. Some implications of fatal nephritis associated with mumps. Am J Dis Child 111:297-301.

163. Brown NJ, Richmond SJ. 1980. Fatal mumps myocarditis in an 8-month-old child. Br Med J 281:356-7.

164. Nishino H, Engel AG, Rima BK. 1989. Inclusion body myositis: the mumps virus hypothesis. Ann Neurol 25:260-4.

165. Maynard JE, Shramek G, Noble GR, Deinhardt F, Clark P. 1970. Use of attenuated live mumps virus vaccine during a "virgin soil" epidemic of mumps on St. Paul Island, Alaska. Am J Epidemiol 92:301-6.

166. Prinz W, Taubert HD. 1969. Mumps in pubescent females and its effect on later reproductive function. Gynaecologia 167:23-7.

167. Morrison JC, Givens JR, Wiser WL, Fish SA. 1975. Mumps oophoritis: a cause of premature menopause. Fertil Steril 26:655-9.

168. Bjorvatn B. 1973. Mumps virus recovered from testicles by fine-needle aspiration biopsy in cases of mumps orchitis. Scand J Infect Dis 5:3-5.

169. Jalal H, Bahadur G, Knowles W, Jin L, Brink N. 2004. Mumps epididymo-orchitis with prolonged detection of virus in semen and the development of anti-sperm antibodies. J Med Virol 73:147-50.

170. Clifford V, Wadsley J, Jenner B, Buttery JP. 2010. Mumps vaccine associated orchitis: Evidence supporting a potential immune-mediated mechanism. Vaccine 28:2671-3.

171. St Geme JW, Jr., Peralta H, Van Pelt LF. 1972. Intrauterine infection of the rhesus monkey with mumps virus: abbreviated viral replication in the immature fetus as an explanation for split immunologic recognition after birth. J Infect Dis 126:249-56.

172. Kurtz JB, Tomlinson AH, Pearson J. 1982. Mumps virus isolated from a fetus. Br Med J (Clin Res Ed) 284:471.

173. Ylinen O, Jarvinen PA. 1953. Parotitis during pregnancy. Acta Obstet Gynecol Scand 32:121-32.

174. Yamauchi T, Wilson C, Geme JW, Jr. 1974. Transmission of live, attenuated mumps virus to the human placenta. N Engl J Med 290:710-2.

175. Brown JW, Kirkland HB, Hein GE. 1948. Central nervous system involvement during mumps. Am J Med Sci 215:434-41.

176. Bruyn HB, Sexton HM, Brainerd HD. 1957. Mumps meningoencephalitis; a clinical review of 119 cases with one death. Calif Med 86:153-60.

177. Kilham L. 1949. Mumps meningoencephalitis with and without parotitis. Am J Dis Child 78:324-33.

178. Watson JC, Hadler SC, Dykewicz CA, Reef S, Phillips L. 1998. Measles, mumps, and rubella--vaccine use and strategies for elimination of measles, rubella, and congenital rubella syndrome and control of mumps: recommendations of the Advisory Committee on Immunization Practices (ACIP). MMWR Recomm Rep 47:1-57.

179. Hall R, Richards H. 1987. Hearing loss due to mumps. Arch Dis Child 62:189-91.

180. Okamoto M, Shitara T, Nakayama M, Takamiya H, Nishiyama K, Ono Y, Sano H. 1994. Sudden deafness accompanied by asymptomatic mumps. Acta Otolaryngol Suppl 514:45-8.

181. Mizushima N, Murakami Y. 1986. Deafness following mumps: the possible pathogenesis and incidence of deafness. Auris Nasus Larynx 13 Suppl 1:S55-7.

182. Vuori M, Lahikainen EA, Peltonen T. 1962. Perceptive deafness in connectionwith mumps. A study of 298 servicemen suffering from mumps. Acta Otolaryngol 55:231-6.

183. Copelovici Y, Strulovici D, Cristea AL, Tudor V, Armaşu V. 1979. Data on the efficiency of specific antimumps immunoglobulins in the prevention of mumps and of its complications. Virologie 30:171-7.

184. Afzal MA, Buchanan J, Heath AB, Minor PD. 1997. Clustering of mumps virus isolates by SH gene sequence only partially reflects geographical origin. Arch Virol 142:227-38.

185. Chambers P, Rima BK, Duprex WP. 2009. Molecular differences between two Jeryl Lynn mumps virus vaccine component strains, JL5 and JL2. The Journal of general virology 90:2973-2981.

186. Smorodintsev AA, Nasibov MN, Jakovleva NV. 1970. Experience with live rubella virus vaccine combined with live vaccines against measles and mumps. Bull World Health Organ 42:283-9.

187. Beck M, Welsz-Malecek R, Mesko-Prejac M, Radman V, Juzbasic M, Rajninger-Miholic M, Prislin-Musklic M, Dobrovsak-Sourek V, Smerdel S, Stainer DW. 1989. Mumps vaccine L-Zagreb, prepared in chick fibroblasts. I. Production and field trials. J Biol Stand 17:85-90.

188. Cizman M, Mozetic M, Radescek-Rakar R, Pleterski-Rigler D, Susec-Michieli M. 1989. Aseptic meningitis after vaccination against measles and mumps. Pediatr Infect Dis J 8:302-8.

189. Tesović G, Begovac J, Baće A. 1993. Aseptic meningitis after measles, mumps, and rubella vaccine. Lancet 341:1541.

190. Black S, Shinefield H, Ray P, Lewis E, Chen R, Glasser J, Hadler S, Hardy J, Rhodes P, Swint E, Davis R, Thompson R, Mullooly J, Marcy M, Vadheim C, Ward J, Rastogi S, Wise R. 1997. Risk of hospitalization because of aseptic meningitis after measles-mumps-rubella vaccination in one- to two-

year-old children: an analysis of the Vaccine Safety Datalink (VSD) Project. Pediatr Infect Dis J 16:500-3.

191. Sugiura A, Yamada A. 1991. Aseptic meningitis as a complication of mumps vaccination. Pediatr Infect Dis J 10:209-13.

192. Glück R, Hoskins JM, Wegmann A, Just M, Germanier R. 1986. Rubini, a new live attenuated mumps vaccine virus strain for human diploid cells. Dev Biol Stand 65:29-35.

193. Palacios G, Jabado O, Cisterna D, de Ory F, Renwick N, Echevarria JE, Castellanos A, Mosquera M, Freire MC, Campos RH, Lipkin WI. 2005. Molecular identification of mumps virus genotypes from clinical samples: standardized method of analysis. J Clin Microbiol 43:1869-78.

194. Park SH. 2015. Resurgence of mumps in Korea. Infect Chemother 47:1-11.

195. Cui A, Zhu Z, Chen M, Zheng H, Liu L, Wang Y, Ma Y, Wang C, Fang X, Li P, Guan R, Wang S, Zhou J, Zheng L, Gao H, Ding Z, Li L, Bo F, Sun Z, Zhang Z, Feng D, He J, Chen H, Jin L, Rota PA, Xu W. 2014. Epidemiologic and genetic characteristics of mumps viruses isolated in China from 1995 to 2010. Infect Genet Evol 21:384-90.

196. Liu Y, Hu Y, Deng X, Wang Z, Lu P, Ma F, Zhou M, Liu P, Min J. 2015. Seroepidemiology of mumps in the general population of Jiangsu province, China after introduction of a one-dose measles-mumps-rubella vaccine. Scientific Reports 5:14660.

197. Ong G, Goh KT, Ma S, Chew SK. 2005. Comparative efficacy of Rubini, Jeryl-Lynn and Urabe mumps vaccine in an Asian population. J Infect 51:294-8.

198. Gouma S, Ten Hulscher HI, Schurink-van 't Klooster TM, de Melker HE, Boland GJ, Kaaijk P, van Els C, Koopmans MPG, van Binnendijk RS. 2016. Mumps-specific cross-neutralization by MMR vaccine-induced antibodies predicts protection against mumps virus infection. Vaccine 34:4166-4171.

199. Latner DR, McGrew M, Williams NJ, Sowers SB, Bellini WJ, Hickman CJ. 2014. Estimates of mumps seroprevalence may be influenced by antibody specificity and serologic method. Clinical and vaccine immunology : CVI 21:286-297.

200. Latner DR, Parker Fiebelkorn A, McGrew M, Williams NJ, Coleman LA, McLean HQ, Rubin S, Hickman CJ. 2017. Mumps Virus Nucleoprotein and Hemagglutinin-Specific Antibody Response Following a Third Dose of Measles Mumps Rubella Vaccine. Open forum infectious diseases 4:ofx263-ofx263.

201. Hanna-Wakim R, Yasukawa LL, Sung P, Arvin AM, Gans HA. 2008. Immune responses to mumps vaccine in adults who were vaccinated in childhood. The Journal of infectious diseases 197:1669-1675.

202. Jokinen S, Osterlund P, Julkunen I, Davidkin I. 2007. Cellular immunity to mumps virus in young adults 21 years after measles-mumps-rubella vaccination. J Infect Dis 196:861-7.

203. de Wit J, Emmelot ME, Meiring H, van Gaans-van den Brink JAM, van Els C, Kaaijk P. 2020. Identification of Naturally Processed Mumps Virus Epitopes by Mass Spectrometry: Confirmation of Multiple CD8+ T-Cell Responses in Mumps Patients. J Infect Dis 221:474-482.

204. Kaaijk P, Emmelot ME, Meiring HD, van Els CACM, de Wit J. 2021. Novel mumps virus epitopes reveal robust cytotoxic T cell responses after natural infection but not after vaccination. Scientific reports 11:13664-13664.

205. Carr MJ, Moss E, Waters A, Dean J, Jin L, Coughlan S, Connell J, Hall WW, Hassan J. 2010. Molecular epidemiological evaluation of the recent resurgence in mumps virus infections in Ireland. J Clin Microbiol 48:3288-94.

206. Cohen C, White JM, Savage EJ, Glynn JR, Choi Y, Andrews N, Brown D, Ramsay ME. 2007. Vaccine effectiveness estimates, 2004-2005 mumps outbreak, England. Emerging infectious diseases 13:12-17.

207. Cortese MM, Jordan HT, Curns AT, Quinlan PA, Ens KA, Denning PM, Dayan GH. 2008. Mumps vaccine performance among university students during a mumps outbreak. Clin Infect Dis 46:1172-80.

208. Rubin SA, Qi L, Audet SA, Sullivan B, Carbone KM, Bellini WJ, Rota PA, Sirota L, Beeler J. 2008. Antibody induced by immunization with the Jeryl Lynn mumps vaccine strain effectively neutralizes a heterologous wild-type mumps virus associated with a large outbreak. J Infect Dis 198:508-15.

209. Vygen S, Fischer A, Meurice L, Mounchetrou Njoya I, Gregoris M, Ndiaye B, Ghenassia A, Poujol I, Stahl JP, Antona D, Le Strat Y, Levy-Bruhl D,

Rolland P. 2016. Waning immunity against mumps in vaccinated young adults, France 2013. Euro Surveill 21:30156.

210. Lewnard JA, Grad YH. 2018. Vaccine waning and mumps re-emergence in the United States. Sci Transl Med 10.

211. Nöjd J, Tecle T, Samuelsson A, Orvell C. 2001. Mumps virus neutralizing antibodies do not protect against reinfection with a heterologous mumps virus genotype. Vaccine 19:1727-31.

212. Kaaijk P, van der Zeijst B, Boog M, Hoitink C. 2008. Increased mumps incidence in the Netherlands: review on the possible role of vaccine strain and genotype. Euro Surveill 13.

213. Rubin SA, Link MA, Sauder CJ, Zhang C, Ngo L, Rima BK, Duprex WP. 2012. Recent mumps outbreaks in vaccinated populations: no evidence of immune escape. J Virol 86:615-20.

214. Gouma S, Hahné SJ, Gijselaar DB, Koopmans MP, van Binnendijk RS. 2016. Severity of mumps disease is related to MMR vaccination status and viral shedding. Vaccine 34:1868-73.

215. El Najjar F, Schmitt A, Dutch R. 2014. Paramyxovirus Glycoprotein Incorporation, Assembly and Budding: A Three Way Dance for Infectious Particle Production. Viruses 6:3019-3054.

216. Zengel J. 2017. The roles of phosphorylation in mumps virus RNA synthesis and replication. PhD. University of Georgia

217. Liang B, Li Z, Jenni S, Rahmeh AA, Morin BM, Grant T, Grigorieff N, Harrison SC, Whelan SPJ. 2015. Structure of the L Protein of Vesicular Stomatitis Virus from Electron Cryomicroscopy. Cell 162:314-327.

218. Dayan GH, Rubin S. 2008. Mumps outbreaks in vaccinated populations: are available mumps vaccines effective enough to prevent outbreaks? Clin Infect Dis 47:1458-67.

219. Dayan GH, Quinlisk MP, Parker AA, Barskey AE, Harris ML, Schwartz JM, Hunt K, Finley CG, Leschinsky DP, O'Keefe AL, Clayton J, Kightlinger LK, Dietle EG, Berg J, Kenyon CL, Goldstein ST, Stokley SK, Redd SB, Rota PA, Rota J, Bi D, Roush SW, Bridges CB, Santibanez TA, Parashar U, Bellini WJ, Seward JF. 2008. Recent resurgence of mumps in the United States. N Engl J Med 358:1580-9.

220. Nelson GE, Aguon A, Valencia E, Oliva R, Guerrero ML, Reyes R, Lizama A, Diras D, Mathew A, Camacho EJ, Monforte M-N, Chen T-H, Mahamud A, Kutty PK, Hickman C, Bellini WJ, Seward JF, Gallagher K, Fiebelkorn AP. 2012. Epidemiology of a mumps outbreak in a highly vaccinated island population and use of a third dose of measles-mumps-rubella vaccine for outbreak control--Guam 2009 to 2010. The Pediatric infectious disease journal 32:374-80.

221. Barskey AE, Schulte C, Rosen JB, Handschur EF, Rausch-Phung E, Doll MK, Cummings KP, Alleyne EO, High P, Lawler J, Apostolou A, Blog D, Zimmerman CM, Montana B, Harpaz R, Hickman CJ, Rota PA, Rota JS,

Bellini WJ, Gallagher KM. 2012. Mumps outbreak in Orthodox Jewish communities in the United States. N Engl J Med 367:1704-13.

222. Shah M, Quinlisk P, Weigel A, Riley J, James L, Patterson J, Hickman C, Rota PA, Stewart R, Clemmons N, Kalas N, Cardemil C, Iowa Mumps Outbreak Response T. 2018. Mumps Outbreak in a Highly Vaccinated University-Affiliated Setting Before and After a Measles-Mumps-Rubella Vaccination Campaign-Iowa, July 2015-May 2016. Clinical infectious diseases : an official publication of the Infectious Diseases Society of America 66:81-88.

223. Fields VS, Safi H, Waters C, Dillaha J, Capelle L, Riklon S, Wheeler JG, Haselow DT. 2019. Mumps in a highly vaccinated Marshallese community in Arkansas, USA: an outbreak report. The Lancet Infectious Diseases 19:185-192.

224. Donahue M HB, Julian D, *et al.* 2019. Multistate Mumps Outbreak Originating from Asymptomatic Transmission at a Nebraska Wedding — Six States, August–October 2019., CDC.

225. Bahrami BF, Ataie-Kachoie P, Pourgholami MH, Morris DL. 2014. p70 Ribosomal protein S6 kinase (Rps6kb1): an update. J Clin Pathol 67:1019-25.

226. Hanks SK, Hunter T. 1995. Protein kinases 6. The eukaryotic protein kinase superfamily: kinase (catalytic) domain structure and classification. Faseb j 9:576-96.

227. Jeno P, Ballou LM, Novak-Hofer I, Thomas G. 1988. Identification and characterization of a mitogen-activated S6 kinase. Proc Natl Acad Sci U S A 85:406-10.

228. Shima H, Pende M, Chen Y, Fumagalli S, Thomas G, Kozma SC. 1998. Disruption of the p70(s6k)/p85(s6k) gene reveals a small mouse phenotype and a new functional S6 kinase. Embo j 17:6649-59.

229. Chen B, Yang L, Zhang R, Gan Y, Zhang W, Liu D, Chen H, Tang H. 2017. Hyperphosphorylation of RPS6KB1, rather than overexpression, predicts worse prognosis in non-small cell lung cancer patients. PLoS One 12:e0182891.

230. Heinonen H, Nieminen A, Saarela M, Kallioniemi A, Klefstrom J, Hautaniemi S, Monni O. 2008. Deciphering downstream gene targets of PI3K/mTOR/p70S6K pathway in breast cancer. BMC Genomics 9:348.

231. Wiredja DD, Tabler CO, Schlatzer DM, Li M, Chance MR, Tilton JC. 2018. Global phosphoproteomics of CCR5-tropic HIV-1 signaling reveals reprogramming of cellular protein production pathways and identifies p70-S6K1 and MK2 as HIV-responsive kinases required for optimal infection of CD4+ T cells. Retrovirology 15:44.

232. Bhatt AP, Wong JP, Weinberg MS, Host KM, Giffin LC, Buijnink J, van Dijk E, Izumiya Y, Kung H, Temple BRS, Damania B. 2016. A viral kinase mimics S6 kinase to enhance cell proliferation, p 7876-81, Proc Natl Acad Sci U S A, vol 113.

233. Bell TM, Espina V, Senina S, Woodson C, Brahms A, Carey B, Lin SC, Lundberg L, Pinkham C, Baer A, Mueller C, Chlipala EA, Sharman F, de la Fuente C, Liotta L, Kehn-Hall K. 2017. Rapamycin modulation of p70 S6 kinase signaling inhibits Rift Valley fever virus pathogenesis. Antiviral Res 143:162-75.

234. Pearce LR, Komander D, Alessi DR. 2010. The nuts and bolts of AGC protein kinases. Nat Rev Mol Cell Biol 11:9-22.

235. Young DF, Galiano MC, Lemon K, Chen YH, Andrejeva J, Duprex WP, Rima BK, Randall RE. 2009. Mumps virus Enders strain is sensitive to interferon (IFN) despite encoding a functional IFN antagonist, p 2731-8, J Gen Virol, vol 90.

236. Davis NL, Wertz GW. 1982. Synthesis of vesicular stomatitis virus negative-strand RNA in vitro: dependence on viral protein synthesis. J Virol 41:821-32.

237. Baker SC, Moyer SA. 1988. Encapsidation of Sendai virus genome RNAs by purified NP protein during in vitro replication. J Virol 62:834-8.

238. Matsumoto Y, Ohta K, Yumine N, Goto H, Nishio M. 2015. Identification of two essential aspartates for polymerase activity in parainfluenza virus L protein by a minireplicon system expressing secretory luciferase. Microbiol Immunol 59:676-83.

239. Malur AG, Gupta NK, De Bishnu P, Banerjee AK. 2002. Analysis of the mutations in the active site of the RNA-dependent RNA polymerase of human parainfluenza virus type 3 (HPIV3). Gene Expr 10:93-100.

240. Ogino T, Banerjee AK. 2007. Unconventional mechanism of mRNA capping by the RNA-dependent RNA polymerase of vesicular stomatitis virus. Mol Cell 25:85-97.

241. Paesen GC, Collet A, Sallamand C, Debart F, Vasseur J-J, Canard B, Decroly E, Grimes JM. 2015. X-ray structure and activities of an essential Mononegavirales L-protein domain. Nature Communications 6:8749.

242. Ferron F, Longhi S, Henrissat B, Canard B. 2002. Viral RNA-polymerases -- a predicted 2'-O-ribose methyltransferase domain shared by all Mononegavirales. Trends Biochem Sci 27:222-4.

243. Dortmans JC, Rottier PJ, Koch G, Peeters BP. 2010. The viral replication complex is associated with the virulence of Newcastle disease virus. J Virol 84:10113-20.

244. Dortmans JC, Rottier PJ, Koch G, Peeters BP. 2011. Passaging of a Newcastle disease virus pigeon variant in chickens results in selection of viruses with mutations in the polymerase complex enhancing virus replication and virulence. J Gen Virol 92:336-45.

245. Jenni S, Bloyet L-M, Diaz-Avalos R, Liang B, Whelan SPJ, Grigorieff N, Harrison SC. 2020. Structure of the Vesicular Stomatitis Virus L Protein in Complex with Its Phosphoprotein Cofactor. Cell Reports 30:53-60.e5.

246. Munday DC, Wu W, Smith N, Fix J, Noton SL, Galloux M, Touzelet O, Armstrong SD, Dawson JM, Aljabr W, Easton AJ, Rameix-Welti MA, de Oliveira AP, Simabuco FM, Ventura AM, Hughes DJ, Barr JN, Fearns R, Digard P, Eléouët JF, Hiscox JA. 2015. Interactome analysis of the human

respiratory syncytial virus RNA polymerase complex identifies protein chaperones as important cofactors that promote L-protein stability and RNA synthesis. J Virol 89:917-30.

247. Brown DD, Rima BK, Allen IV, Baron MD, Banyard AC, Barrett T, Duprex WP. 2005. Rational attenuation of a morbillivirus by modulating the activity of the RNA-dependent RNA polymerase. Journal of virology 79:14330-14338.

248. Calain P, Roux L. 1993. The rule of six, a basic feature for efficient replication of Sendai virus defective interfering RNA. Journal of virology 67:4822-4830.

249. Parks GD. 1994. Mapping of a region of the paramyxovirus L protein required for the formation of a stable complex with the viral phosphoprotein P. J Virol 68:4862-72.

250. Dewar RS. 1950. Mumps meningitis and orchitis without parotitis. Lancet 1:256.

251. Wang D, Nie T, Pan F, Wang Y, Wang J, Qin W. 2021. Loss of protective immunity of two-dose mumps-containing vaccine over time: concerns with the new strategy of the mumps immunization program in China. Hum Vaccin Immunother doi:10.1080/21645515.2020.1861877:1-6.

252. H ASA, Shamila H, Khan I, Hamdani ZA. 2013. PATTERN OF MINI OUTBREAKS OF MUMPS AT SOUTH KASHMIR, PULWAMA, INDIA 2007-2011. Journal of Health and Allied Sciences NU 03:52-55.

253. Zamir CS, Schroeder H, Shoob H, Abramson N, Zentner G. 2015. Characteristics of a large mumps outbreak: Clinical severity, complications and association with vaccination status of mumps outbreak cases. Hum Vaccin Immunother 11:1413-7.

254. Duque MP, San-Bento A, Léon L, Custódio P, Esperança MA, Albuquerque MJ, Nascimento M, Balasegaram S, R SM. 2021. Mumps Outbreak affecting fully-vaccinated school-age children and young adults, Portugal 2019/2020. Epidemiol Infect doi:10.1017/s0950268821002028:1-9.

255. Wolinsky JS, Waxham MN, Server AC. 1985. Protective effects of glycoprotein-specific monoclonal antibodies on the course of experimental mumps virus meningoencephalitis. Journal of Virology 53:727-734.

256. Cusi MG, Fischer S, Sedlmeier R, Valassina M, Valensin PE, Donati M, Neubert WJ. 2001. Localization of a new neutralizing epitope on the mumps virus hemagglutinin-neuraminidase protein. Virus Res 74:133-7.

257. Rubin SA, Amexis G, Pletnikov M, Vanderzanden J, Mauldin J, Sauder C, Malik T, Chumakov K, Carbone KM. 2003. Changes in Mumps Virus Gene Sequence Associated with Variability in Neurovirulent Phenotype. Journal of Virology 77:11616-11624.

258. Lemon K, Rima BK, McQuaid S, Allen IV, Duprex WP. 2007. The F Gene of Rodent Brain-Adapted Mumps Virus Is a Major Determinant of Neurovirulence. Journal of Virology 81:8293-8302.

259. Goodpasture EW, Woodruff AM, Buddingh GJ. 1931. THE CULTIVATION OF VACCINE AND OTHER VIRUSES IN THE CHORIOALLANTOIC MEMBRANE OF CHICK EMBRYOS. Science 74:371-2.

260. Sauder CJ, Zhang CX, Ngo L, Werner K, Lemon K, Duprex WP, Malik T, Carbone K, Rubin SA. 2011. Gene-Specific Contributions to Mumps Virus Neurovirulence and Neuroattenuation. Journal of Virology 85:7059-7069.

261. Ramanathan R, Voigt EA, Kennedy RB, Poland GA. 2018. Knowledge gaps persist and hinder progress in eliminating mumps. Vaccine 36:3721-3726.

262. Davidkin I, Valle M, Julkunen I. 1995. Persistence of anti-mumps virus antibodies after a two-dose MMR vaccination. A nine-year follow-up. Vaccine 13:1617-22.

263. LeBaron CW, Forghani B, Beck C, Brown C, Bi D, Cossen C, Sullivan BJ. 2009. Persistence of mumps antibodies after 2 doses of measles-mumps-rubella vaccine. J Infect Dis 199:552-60.

264. Fiebelkorn AP, Coleman LA, Belongia EA, Freeman SK, York D, Bi D, Zhang C, Ngo L, Rubin S. 2014. Mumps antibody response in young adults after a third dose of measles-mumps-rubella vaccine. Open Forum Infect Dis 1:ofu094.

265. Tanaka K, Baba K, Okada S, Okuno Y, Yamanishi K, Ueda S, Takahashi M, Yamada A. 1992. Nasal antibody response to mumps virus after vaccination and natural infection. Vaccine 10:824-827.

266. Cusi MG, Correale P, Valassina M, Sabatino M, Valensin PE, Donati M, Glück R. 2001. Comparative study of the immune response in mice

immunized with four live attenuated strains of mumps virus by intranasal or intramuscular route. Arch Virol 146:1241-8.

267. Almansour I. 2020. Mumps Vaccines: Current Challenges and Future Prospects. Frontiers in microbiology 11:1999-1999.

268. Brown EG, Wright KE. 1998. Genetic studies on a mumps vaccine strain associated with meningitis. Rev Med Virol 8:129-142.

269. Barskey AE, Glasser JW, LeBaron CW. 2009. Mumps resurgences in the United States: A historical perspective on unexpected elements. Vaccine 27:6186-6195.

270. Dayan GH, Rubin S, Plotkin S. 2008. Mumps Outbreaks in Vaccinated Populations: Are Available Mumps Vaccines Effective Enough to Prevent Outbreaks? Clinical Infectious Diseases 47:1458-1467.